INVESTIGATION OF THE EFFECTS OF PULSATING FLOW ON THE THERMAL PERFORMANCE OF A SOLAR AIR HEATER USING NUMERICAL METHODS

2022
MASTER THESIS
MECHANICAL ENGINEERING

ALAA RAAD RADIE NEDAWI

Thesis Advisors

Assist. Prof. Dr. Erhan KAYABAŞI

Assist. Prof. Dr. Ali L. EKAID

INVESTIGATION OF THE EFFECTS OF PULSATING FLOW ON THE THERMAL PERFORMANCE OF A SOLAR AIR HEATER USING NUMERICAL METHODS

Alaa Raad Radie NEDAWI

T.C.

Karabuk University

Institute of Graduate Programs

Department of Mechanical Engineering

Prepared as

Master Thesis

Thesis Advisors

Assist. Prof. Dr. Erhan KAYABAŞI

Assist. Prof. Dr. Ali L. EKAID

KARABUK

September 2022

I certify that in my opinion the thesis submitted by Alaa Raad Radie NEDAWI titled "INVESTIGATION OF THE EFFECTS OF PULSATING FLOW ON THE THERMAL PERFORMANCE OF A SOLAR AIR HEATER USING NUMERICAL METHODS" is fully adequate in scope and quality as a thesis for the degree of Master of Science.

Assist.Prof.Dr. Erhan KAYABAŞI .....
Thesis Advisor, Department of Mechanical Engineering
Assist.Prof.Dr. Ali Lafta EKAID .....
Thesis Advisor, Department of Mechanical Engineering, U.O.T -IRAQ

This thesis is accepted by the examining committee with a unanimous vote in the Department of Mechanical Engineering as a Master of Science thesis. September 16, 2022

Examining Committee Members (Institutions)	Signature
Chairman: Prof. Dr. Kamil ARSLAN (KBU)	.....
Member: Assist. Prof. Dr. Abdulrazzak AKROOT (KBU)	.....
Member : Assist. Prof. Dr. Erhan KAYABAŞI (KBU)	.....
Member: Assist. Prof. Dr. Ali L. EKAID (UOT ,Iraq)	.....
Membe : Prof. Dr. Khudheyer S. Mushatet (Uni of Thiqar-Iraq)	.....

The degree of Master of Science by the thesis submitted is approved by the Administrative Board of the Institute of Graduate Programs, Karabuk University.

Prof. Dr. Hasan SOLMAZ..... .....
Director of the Institute of Graduate Programs

"I declare that all the information within this thesis has been gathered and presented in accordance with academic regulations and ethical principles and I have according to the requirements of these regulations and principles cited all those which do not originate in this work as well."

Alaa Raad Radie NEDAWI

ABSTRACT

M. Sc. Thesis

INVESTIGATION OF THE EFFECTS OF PULSATING FLOW ON THE THERMAL PERFORMANCE OF A SOLAR AIR HEATER USING NUMERICAL METHODS

Alaa Raad Radie NEDAWI

Karabük University
Institute of Graduate Programs
The Department of Mechanical Engineering

Thesis Advisor:
Assist. Prof. Dr Erhan KAYABAŞI
September 2022, 99 pages

Solar energy has become a reliable source in meeting energy needs, as it can be used in various applications depending on the radiation intensity. One of these applications is the solar air heater model for a single-pass solar air collector using a pulsed flow, which is also the subject of this study. In this study, numerical computational calculation methods were used to learn more about the thermal properties of the SAC. Besides the pulse frequency, different values of the pulse amplitude were modeled, and the dimensions of the collector were determined as follows (2x1x0.04 m) and the study was carried out according to the Iraqi climate. Numerical analysis was performed using the finite volume approach (SIMPLE) algorithm (FORTRAN90, CFD programming, Tecplot 9.0) using the turbulence model of the continuity equations (K-ε) for the two-dimensional system, Navier-stokes, and energy. Three values of the pulse amplitude Amp (0.25, 0.5 and 0.75) and four pulse frequency St values (0.2, 0.4,

0.6 and 0.8) were applied. The results proved that the increase of the frequency values has a positive effect on the solar collector, but at low values of the pulse amplitude, four values of the Reynolds number were taken (7.5x10^3, 10x10^3, 12.5 x 10^3, and 15 x 10^3). As a result, it was observed that the performance of the collector improved significantly when the Re value increased. In addition, since the Wave is sinusoidal, it would be better to improve the positive field of the wave, because it was observed that the increase in Re values and St values increased the area at the positive peak of the wave, thus achieving the desired result.

Key Word **:** Solar Air Collector, Pulsating Flow and Finite Volume Scheme.

Science Code : 914.08

ÖZET

Yüksek Lisans Tezi

INVESTIGATION OF THE EFFECTS OF PULSATING FLOW ON THE THERMAL PERFORMANCE OF A SOLAR AIR HEATER USING NUMERICAL METHODS

Alaa Raad Radie NEDAWI

Karabük Üniversitesi
Lisansüstü Eğitim Enstitüsü
Makina Mühendisliği Anabilim Dalı

Tez Danışmanı:
Dr.Öğr.Üyesi Erhan KAYABAŞI
Eylül 2022, 99 sayfa

Güneş enerjisi, radyasyon şiddetine bağlı olarak çeşitli uygulamalardan yararlanılabildiğinden, enerji ihtiyacını karşılamada güvenilir bir kaynak haline gelmiştir. Bu uygulamalardan biri, bu çalışmanın da konusu olan darbeli bir akış kullanan tek geçişli güneş hava kolektörü için güneş enerjili hava ısıtıcısı modelidir. Bu çalışmada güneş kollektörünün termal davranışını belirlemek için sayısal hesaplama hesaplama yöntemleri kullanıldı. Darbe frekansının yanı sıra darbe genliğinin farklı değerleri modellenerek kollektörün boyutları aşağıdaki gibi (2x1x0.04 m) belirlenmiş ve Irak iklimine göre inceleme yapılmıştır. Sayısal analiz, sonlu hacim yaklaşımı (SIMPLE) algoritması kullanılarak (FORTRAN90, CFD programlama, Tecplot 9.0) iki boyutlu sistem, Navier-stokes ve enerji için süreklilik denklemlerini (K- ε) türbülans modeli kullanılarak gerçekleştirilmiştir. Darbe

genliğinin üç değeri Amp (0,25, 0,5 ve 0,75) ve dört darbe frekansı St değeri (0,2, 0,4, 0,6 ve 0,8) uygulanmıştır. Sonuçlar, frekans değerlerinin artmasının güneş kollektörü üzerinde olumlu bir etkiye sahip olduğunu kanıtladı, ancak darbe genliğinin düşük değerlerinde, akış türbülanslı olduğundan, Reynolds sayısının dört değeri alındı (7.5x10^3 ,10x10^3, 12,5 x 10^3 ve 15 x 10^3). Souç olarak, Re değeri yükseldiğinde, kollektörün performansı önemli ölçüde iyileştiği gözlemlenmeiştir. BUna ek olarak, Dalga sinüzoidal olduğundan, dalganın pozitif alanını iyileştirmek daha iyi olacaktır, çünkü Re değerleri ile St değerlerindeki artışın dalganın pozitif zirvesindeki alanı arttırdığı fark gözlemlenmiştir ve böylece hedeflenen sonuç elde edilmiştir.

Anahtar Kelimeler : Solar Hava Kollektörü, Titreşimli Akış ve Sonlu Hacim Yaklaşımı.

Bilim Kodu : 914.08

ACKNOWLEDGMENT

Foremost, I praise Allaah almighty for giving me the motivation and ability to accomplish this thesis and its success.

I Would like to express my sincere gratitude and thanks to my supervisors, Assist. Prof. Dr. Erhan KAYABASI and Assist. Prof. Dr. Ali L. EKAID for the continuous support of my MS study through their scientific suggestions, guidance and assistance in carrying out the present research.

My deepest gratitude goes to my parents, to whom I will be grateful forever to my wife, brothers, and sisters have always been so close to me.

In the end, I would also like to offer my special thanks to the department of mechanical engineering at Karabuk University, and the Department of Mechanical Engineering at the University of Technology-Iraq

CONTENTS

Page

Page

Page

LIST OF FIGURES

Page

Page

Page

LIST OF TABLES

Page

SYMBOLS AND ABBREVIATIONS

SYMBOLS

T_g		Glass cover temarature
T_{ab}	:	Absorber temperature
T_{SKY}	:	Sky temperature
U	:	velocity of (x) component
V	:	velocity of (y) component
X, y, z	:	Cartesian coordinate
I_s	:	Solar irradiance
ε	:	Dissipation rate of turbulent kinetic energy
σ	:	Stefan-Boltzmann constant
ϵ	:	Emissivity
α	:	Absorptivity
ρ	:	Density of air
δ	:	Distance between absorber plate and glass
μ	:	Dynamic viscosity
v	:	Kinematic viscosity
Γ	:	Diffusion coefficient, = $\frac{v}{\sigma}$
Γ_e	:	Effective diffusion coefficient
k	:	Von Karman's constant
λ	:	General dependent variable
τ	:	Time
η_{th}	:	Thermal Efficiency
c_p	:	Specific heat
Ac	:	Area collector channel surface
Ra		Rayleight numbers
a_n, a_s, a_e	:	The coefficient in general finite volume

a_w, a_t, a_b	:	Equations
$C_{\varepsilon 1}, C_{\varepsilon 2}, C_\mu$	:	Constants in the turbulence model
D_h	:	Hydraulic diameter
h	:	averaged heat transfer coefficient
h_r	:	Radiation heat transfer coefficient
h_c	:	Convection heat transfer coefficient
i, j, k	:	Indices which indicate positions in the (x, y, z) direction
K	:	thermal conductivity
$\dot{m}$	:	Mass flow rate
$\bar{Nu}$		Average nusselt number
Nu_p	:	Nusselt number with pulsating flow
Nu_o		Nusselt number without pulsating flow
P	:	mean static pressure
L	:	Length
W	:	Width
H	:	Height
P_r	:	Prandtl number
Re	:	Reynolds number
$\bar{q}$	:	Average heat generation
Q	:	thermal energy transfer
r	:	relaxation factor
T_{in}	:	Inlet air temperature
T_{out}	:	Outlet air temperature
St	:	Strohal number
T_{amb}	:	Ambient air temperature
$\bar{f}$		Average friction factor
f_p		Friction factor with pulsating flow
f_o		Friction factor without pulsating flow

ABBREVIATIONS

SAC	:	Solar Air Collector
SAH	:	Solar Air Heater
CFD	:	Computational Fluid Dynamic
PDEs	:	Partial Differential Equations
NSEs	:	Navier stokes Equations
SIMPLE	:	Semi-implicit Momentum and Pressure Linked Equation.
TPF	:	Thermal Performance Factor
FVM		Finite-volume method

PART 1

INTRODUCTION

1.1. GENERAL

Solar energy is a reliable source of energy that is also ecologically friendly, since it contributes greatly to reducing dependency on fossil fuel sources of energy, which cause serious environmental harm. Many renewable energy systems and technologies have been produced and implemented in the last decade, although many are still under inquiry, analysis, and development.

As shown in Figure 1.1, the demand for renewable energy consumption has increased in recent years as a result of the Corona pandemic and the difficulty of transporting and importing fossil fuel materials, as the percentage of solar energy consumption has increased significantly since before the year 2020.

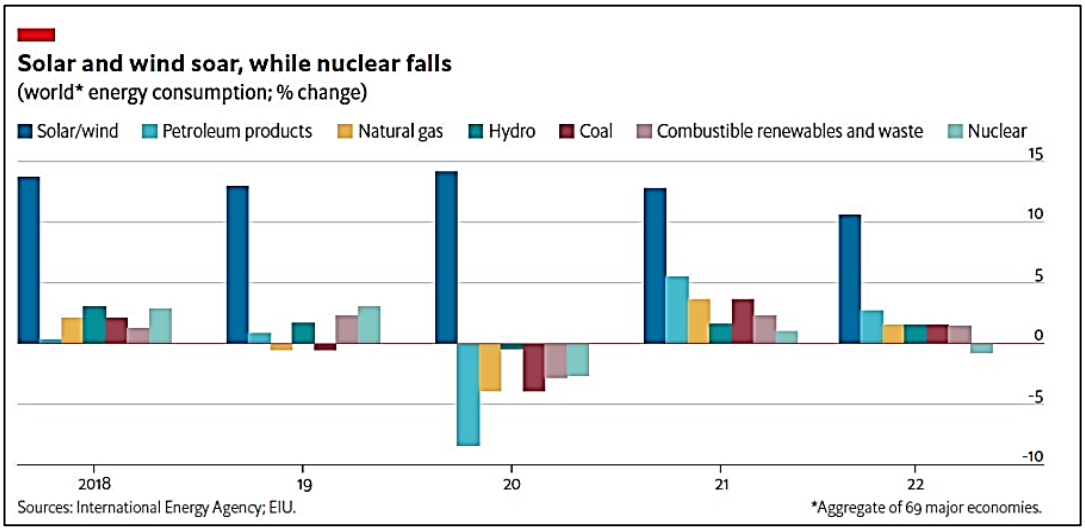

Figure 1.1. World energy consumption [1].

`

1.2. SOLAR RADIATION

Nuclear fusion events at the sun's core produce solar radiation, resulting in the release of a significant amount of electromagnetic radiation's latent energy. In visible and near-infrared light, the degree of heat radiated by a surface is proportional to the fourth power of its temperature. When the temperature of the Earth rises, it quickly emits, sending an increasing proportion of its energy into space. The surface temperature of the Sun is around 5500 degrees Celsius [1].

According to NASA satellite data, average sun irradiation is roughly 1360 W/m2, which is enough to power 14 ordinary 100-watt light bulbs across a one-meter square area when the SAC is pointing straight at the Sun and the sky is clear. The solar constant is a measurement of the sun's energy output. Every day, the sun emits millions of watts of energy, which the earth absorbs., which is around 150 million kilometers from the Sun. Almost half of all solar radiation is projected to reach Earth.

As illustrated in Figure 1.2, the remaining about half is scattered back into space, where nature can absorb it. Solar energy's price must be reduced if it is to become a viable alternative, and it must also become more responsive to market needs. Many governments currently have long-term strategies in place to promote the usage of renewable energy.

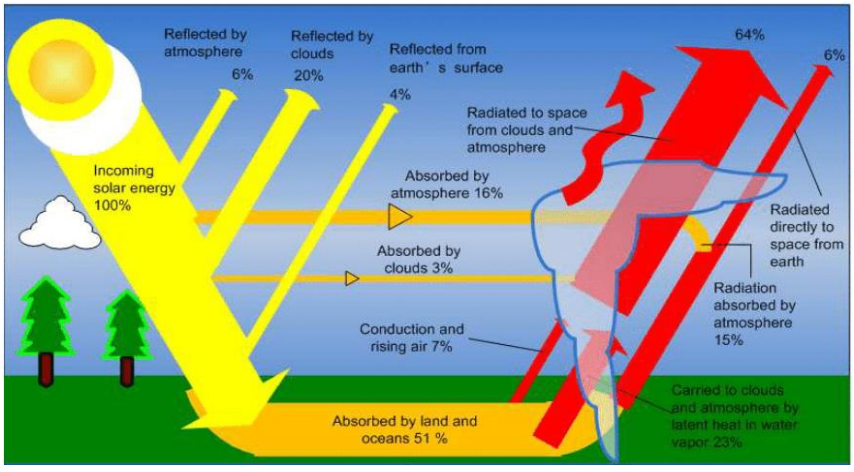

Figure 1.2. The earth’s energy deposit .

`

1.3. SOLAR AIR HEATER (SAH)

Solar air heaters are commonly abbreviated as SAH. SAHs were frequently utilized and invested in as heat exchangers [2]. Air heating benefits water desalination, agricultural drying, and home drying, making it one of the most important solar thermal applications. Using solar energy to heat air is an efficient technique to reduce traditional energy use and maintenance expenses [3].

The main components of the solar heater, which is otherwise a simple instrument for converting solar radiation into usable heat, are one or more layers of glass the cover, absorbent plate, airflow ducts (channels), and thermal insulation layers to reduce heat loss via the walls and bottom of the SAH. In general, the SAH generates electricity with relatively low operational costs. Its periodic maintenance requirements are quite modest, and may be restricted to cleaning the clear cover that lets light to enter through.

Because of the lack of various difficulties that might occur with solar water heaters, such as freezing and leaking, SAH offer numerous benefits over SWH. Due to the variety of designs and experimental constructions, classifying solar air heaters into distinct kinds is complex and challenging. SAH were characterized in the prior literature based on the number of transparent collecting covers, the kind of absorbent plate material, the form of the absorbing surface, and the style (pattern) of air flow.

Tyagia [4] classified solar air heaters based on the presence of an energy store and the presence of expanded plates, as well as the number of covers, as indicated in the picture below.

`

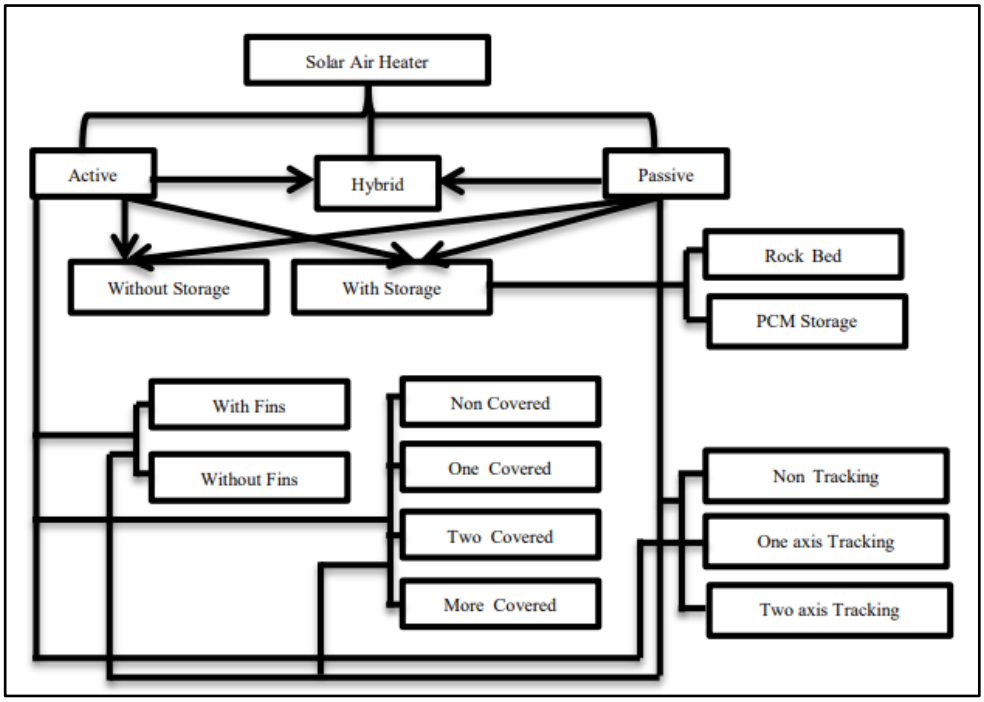

Figure 1.3. Classification of SAHs based on Tyagia [4].

Furthermore, solar air collectors were classified based on [5, 6] according to the number of air passages, it can be single or double, and also according to the presence or absence of energy storage.

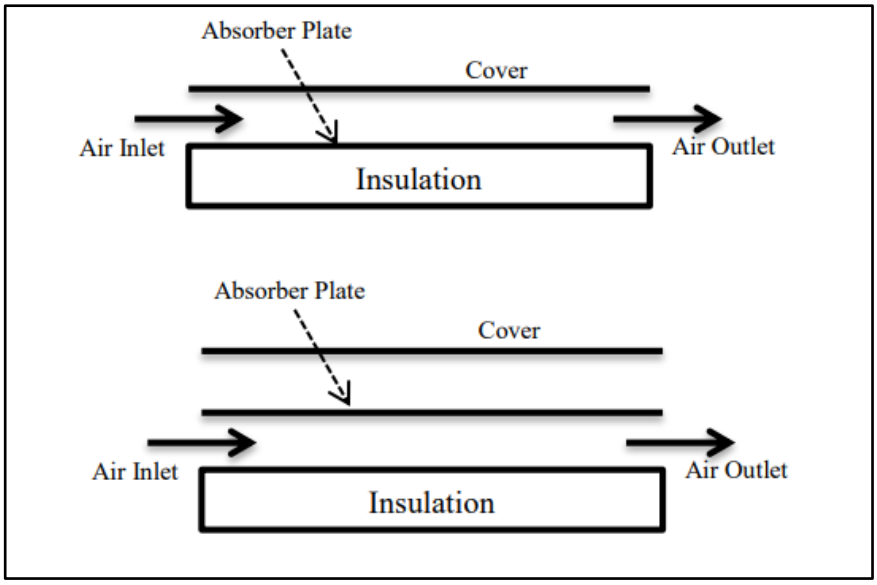

Figure 1.4. Single pass SAH sorts.

`

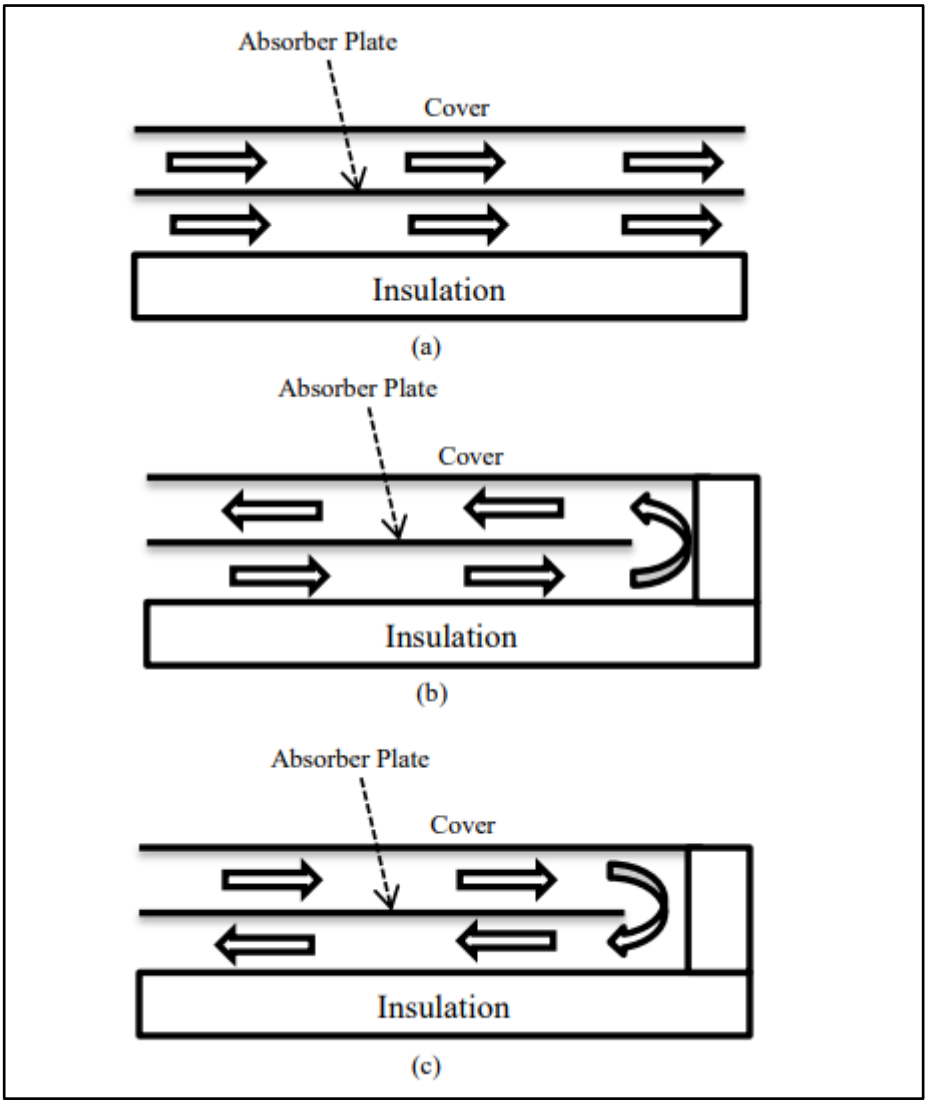

Figure 1.5. Double Pass SAH flow patterns.

1.3.1. Flat Plate Solar Air Heater (SAHs)

Solar-powered air warmers may exist in a number of configurations. SAHs are made up of three major components: the top cover, the black absorbent plate, and the insulation. In this part, we'll look at a variety of SAHs, including those with absorber plates above and below that utilize air as the working fluid rather than water. The area between the absorbent surface and the glass cover serves as an airflow conduit.

The absorbent plate was directly exposed to sunshine. The air stream warms up as energy is absorbed along the collecting tube. This warmed air may be used for a variety of purposes, including crop drying, home heating, and industrial heating. SAC is

`

becoming more popular due to the following advantages over extra solar water heaters (SWHs):

1) Safer and less expensive than SWHs, solar air heater technology also has less complicated maintenance and operation systems.
2) When compared to SWHs, this system has fewer corrosion and leakage issues.
3) The working fluid (air) does not freeze and its leakage is not hazardous.
4) The pressure rise in this design is relatively low.
5) Solar air heaters (SAHs) have the advantage over sun water heaters (SWHs) since they can produce usable energy at low solar irradiation intensities.

Though a solar air heater made with little or no material. However, solar air collectors have the following drawbacks:

1) When compared to SWHs,the thermal qualities of the working fluid (air) are poor, including its conductivity and heat capacity. .
2) Exchange of Thermal Energy requires higher mass or volumetric flows than SWHs due to low air density.
3) Auxiliary energy usage can be reduced by careful planning and installation of this system. .
4) In order to keep the application running at night, solar air heaters need a thermal storage unit. .

The main drawbacks of solar air heaters are their sluggish rate of heat transmission and limited efficiency owing to the different losses that might occur. As a result, numerous studies in the literature, which we will describe later, have investigated the possibilities and potential for improving the efficiency of solar power collectors and increasing their efficiency through changes and upgrades. Furthermore, the experimental test was used to monitor and enhance the thermodynamic efficacy of solar air heaters, as well as numerical analysis to model the thermal interpretation of solar heaters and simulate their performance using a computer. The use of CFD techniques provided many capabilities to raise the performance of SAH and analyze the strengths and weaknesses of the proposed and approved designs of solar heaters,

`

and as a result these designs were improved based on the results of CFD and this is shown in the reference studies below. Mentioning few improvements in literature:

- The addition of extended planes to the lower and/or upper channels.
- Connecting baffles to the absorbent plate surface.
- The investment of corrugated absorbent plate.
- Taking advantage of the additional heat energy over sunset.

1.3.2. Solar Air Heater Application

Solar air collectors are commonly utilized in a wide range of thermal engineering applications. An absorber plate is used to collect solar radiation, and heated air is produced as a result of the extra energy being transmitted to the air in the channel. As a result, this heated air has a variety of applications:

1) Domestic purposes: space heating in commercial, residential, and industrial settings;
2) Agricultural purposes; For example ,Solar crop drying (paddy grains, fruit, etc.). Directly growing the crop and dehydrating it with sun radiation to protect it from rodents and other harm is an efficient way to reduce energy use. Heating for greenhouses, storage buildings, and livestock pens
3) Modern methods of heating in industry : Heating air for combustion, a process that includes many steps. .

1.4. OBJECTIVES

1) With the help of pulsing flow under transient conditions, dynamical mathematical modeling of a single-pass active flat-plate SAC will be developed.
2) Create a technique of solving the derived model that can calculate transient temperature distributions at the collector for any cross section.
3) Modeling and simulation (CFD) by means of FORTRAN90 program. A mathematical model that based on the Finite-Volume method (SIMPLE-Algorithm) to be used in order to analyze the governing equations in 2-Dimensional forced convection, solar air collector with turbulent flow to

`

understand the thermal and fluid behavior and compare the numerical results with literature survey data.

1.5. THESIS ARRANGEMENT

The thesis consists of six parts:

Part one**:** Displays a brief summary of the thesis and highlights information about the solar air collector, as well as its main purpose.

Part two**:** This part is interested in studying previous research on the SAH, and knowing the improvements that previous produced by the research community.

Part three**:** The mathematical model is presented, together with a proposed method for solving it, that explains the behavior of a flat-plate SAC under transient circumstances. The mathematical model is presented, together with a proposed method for solving it, that describes the behavior of a flat-plate SAH under transient conditions. .

Part four**:** Present the numerical analysis based upon Computational Fluid Dynamic (CFD) by means of FORTRAN 90 program as the governing two-dimensional partial differential equations (PDE) were resolved for predicting heat transfer and air behavior.

Part five**:** this part discusses the results and figures obtained of the solar air collector using different values for amplitude and frequency,

Part six**:** This part provides a summary of the results obtained from the program, and clarify what the researcher has come to, as well as give some conclusions to new researchers.

`

PART 2

LITERATURE REVIEW

2.1. INTRODUCTION

Numerous varieties of Air Solar Heaters (SAHs) having been the subject of academic research, and the thermic efficiency of these heaters has also been investigated. New designs for these heaters have been proposed within different sectors in it, whether in the inlet or outlet or in the channels of the solar heater. The purpose of these designs is to attempt in order to boost the thermal performance and efficiency of the SAH. While studying and analyzing the thermal accomplishment of solar heaters and comparing them with each other or with different types, the numerical study and CFD simulation were frequently relied upon. The fact that this type of simulation allows for a deeper study and with a higher accuracy of the studied system, and based on that and relying on the results of the simulation, appropriate measures were taken in order to boost the solar heater's efficiency , and these measures often depended on modifying the internal design of the solar heater and its components. So far, a wide variety of techniques and methodologies have found work with the purpose of numerically improving solar collector thermal efficiency , analytical, and experimentally. Moreover, the numerical analysis based on CFD methods has been given a significant consideration in solar air heaters domain.

2.2. LITERATURE REVIEW

2.2.1. Previous Studies About Pulsating Frequency

Van Quan Hoang, et al., 2021 [7] presented The LES numerical technique was utilized to study the effects of pulsating intake conditions on heat transfer and pressure loss in a V-shaped Corrugated channel with the convective flow.

`

To avoid flow reversal, the amplitude of the forced pulsation did not go beyond 100% of the average speed (A 1.0), whereas the St dimensionless frequency varied from 0.0 to 0.79. The effects of the pulsing parameters (St, A) and Re are investigated. Flow structures are encouraged in pulsating conditions, and heat transmission is boosted due to the enforced unsteadiness. It is clear from the 3D flow patterns that coherent structures are being driven during the pulse time. ; everything happens as though the inlet pulsating circumstances allowed for a constant ebb and flow of laminar and turbulent flow. The results showed that pulsating flow has better thermal efficiency as a whole increased greatly when compared to continuous flow.

For this reason , It's been shown that the TPF improves under pulsating conditions. , with values ranging from 1.3 to 1.4 for pulsating corrugated channel and just 0.9 to 1.17 while maintaining a steady flow.

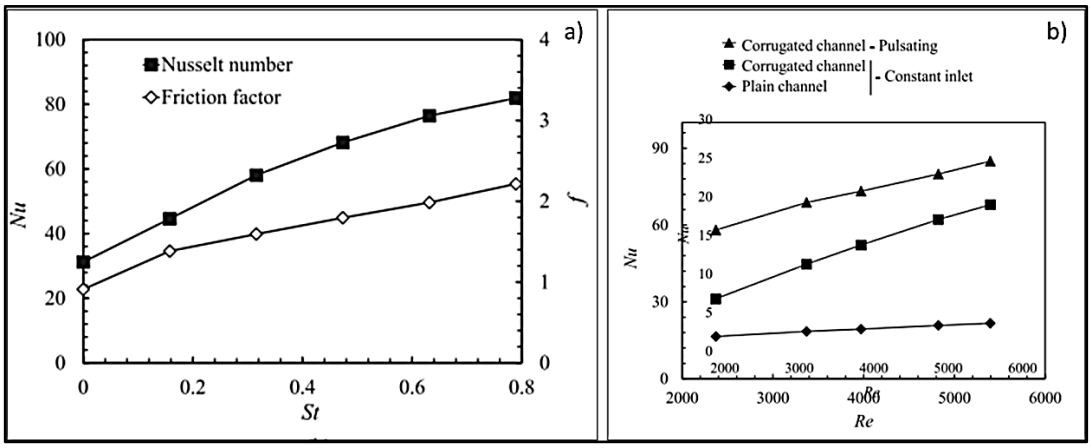

Figure 2.1. Variation heat transfer properties, a) average Nusselt number with friction factor, b) frequency and Reynolds number.

Nerkar, et al, .2015 [8] studied the dynamics of fluid motion were simulated using the Numerical Method. and thermal exchange in a two-dimensional channel subject to pulsating flow conditions . The flow in a duct developed thermally and hydro dynamically while the temperature of the channel wall remained constant. The two-dimensional Navier-Stokes equations has been solved by using the ANSYS fluent program. An (UDF) user defined functions a new file was presented in all circumstances to indicate the Inlet pulsating velocities.

`

The primary regulating parameter was the Reynold number (Re), which varying from (200 to 2000). To look into the impact of this change in temperature properties and heat transfer for fully developed flow, the temporal average local Nusselt number (Nu av) was utilized. Analyzing the data collected by the simulation yields the findings. There is evidence that the time average Nu grows with increasing Re and becomes constant beyond a certain value of Re, and that the axial velocity changes with pipe length in the developing area, hence enhancing the rate of thermal conduction through the wall.

Nandi, et al. (2017) [9] published It is done a numerical inquiry on generating unstable Regarding heat transfer in laminar flows within 2D wavy micro channel owing to a sinusoidal variable velocity constituent at the intake .As the micro channel walls were held at a steady invariant temperature, the thermo hydraulic flow developed. The SIMPLE method with momentum interpolation was used to solve the transient solution of the 2D -Navier-Stokes equation. The working fluid is deionized water with a range of 0.1 to 100 for the Reynolds number. The simulation findings compare the heat transmission and pressure drop for wavy micro channels with straight micro channels while maintaining the cross sectional area constant. When compared to constant flow in a wavy channel, it was shown that imposing sin wave velocity at the intake can enhance heat transfer accomplishment at varied Amplitudes (0.2, 0.5, 0.8) and frequencies (1, 5, 10) while keeping the friction factor within tolerable ranges.

Akdag, et al. (2014) [10] Investigated The thermal conductivity of Al2O3 - water based The motion of nanofluids in a waved mini-channel subject to a pulsing input flow are explored numerically in this work. The simulations are carried out for small volumes of nanofluids , pulsing frequency, and Amp while keeping volume-based control to hold the other variables CFD solver While the temperature along the channel walls is maintained , the flow develops thermally and hydro dynamically. The results show that employing nanoparticles under pulsing flow has a high potential for improving thermal performance. Pulsation in nanofluids is a novel approach to improving heat transmission. Furthermore, the pulsing flow has the benefit of preventing nanoparticle deposition in the base fluid. The results demonstrate that increasing the nanoparticle volume percentage and Amp of pulsation improves heat

`

transfer performance factor substantially, but pulsation frequencies have a minor influence. Unlike the steady-state flow condition, , the combined impact of pulsation and nanoparticles under pulsing flow circumstances is favorable for raising Nusselt number. The findings are presented as dimensionless parameters.

Chattopadhyay et al. (2006) [11] developed in the laminar regime, Investigation of pulsing flow and heat transfer in a circular tube circumstances was conducted numerically.The flow at the intake is composed of a constant component and a pulsing component that fluctuates sinusoidal over time. While the tube wall was held at a constant temperature, the flow developed thermally and hydro-dynamically. The SIMPLE method due to the momentum interpolation approach of Rhie and Chow had been used to solve the two-dimensional Navier-Stokes equation. By analyzing the simulation results, it is discovered that pulsation has no influence averaged throughout time heat transfer in the current research range (freq : 0 - 20 Hz , Amp: b1.0), despite the fact that the Nu distribution fluctuates in time in the pipe's near-entry area.

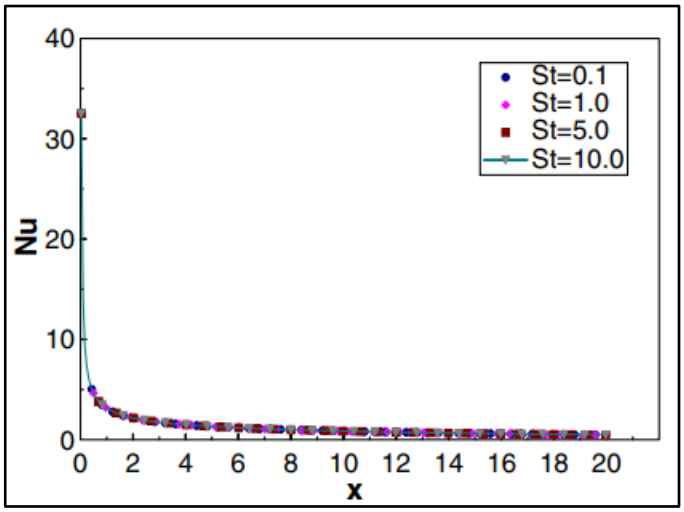

Figure 2.2. Distribution of Nu at different St (A=0.5).

Hemida, et al. (2002) [12] investigated Modifications to heat transfer due to pulsations in laminar incompressible flow, which has previously yielded contradicting results, is theoretically addressed in this paper beginning with basic concepts in an attempt to dispel current misunderstanding at many levels. The numerical solution for the fully developed thermal and-hydraulic profiles under constant wall heat flux is derived first.

`

It clears up the misunderstanding caused by article that has been printed before incorrect answer.

The physical effects of the proposed solution are investigated. . In addition, a novel temporal average heat transfer factor for pulsing flow is carefully established to obtain findings that are both engineering valuable and energy balance compliant. This logically calculated average is contrasted to simple averages found in the literature. Numerical results for the thermally developing area with a fully formed velocity profile are produced. boundary conditions of various sorts are studied, as well as the influence of wall thermal inertia. Heat transport is explored using Reynolds number and Prandtl values, as well as pulsation amplitude and frequency. The method which pulsation impacts the developing area by causing damped oscillations of the time Nu_{av} throughout the tube length is discussed.

Jackson et al. (2009) [13] has already shown a laser Doppler that consists of two parts An anemometer was used to measure the speed of the fluid at that instant in an experimental study of pulsating turbulent flow in a pipe. The data provided radial and axial components of the root-mean-square of the turbulent velocity fluctuation, as well as local values of the ensemble-averaged axial velocity. Forced flow rate pulsation frequency was systematically varied across a broad range, from 0.004 to 0.04, as measured by the dimensionless frequency v/u2. Equivalent values for the outer scale frequency D/u were found between (1.8 to 18) In addition, we looked at what would happen if we changed both the average flow rate and the Amp of the flow rate pulsation. Ensemble-averaged axial velocity, axial and radial components of root-mean-squared turbulent fluctuation, and radial distributions of amplitude of modulation, as well as their phase shifts relative to the imposed flow pulsation, are presented for conditions in the low, intermediate, and high frequency ranges. These add to and strengthen the existing body of information from prior experimental investigations, paving the way for useful advancements in evaluating and validating techniques used for data correlation. By connecting the dots between the data and the basic mechanisms of turbulence production, redistribution of turbulence energy among its components, and radial propagation, a thorough knowledge of the phenomena has been achieved.

`

G.Li, et al. (2015) [14] studied In this study, they examine and analyze experimental data on the fluid stream and heat transfer away from a flat rectangular plane subjected to a continuous invariant heat flux in laminar pulsating flows. . Quantitatively precise, second order systems for time, space, momentum, and energy are used, as well as fine meshes. There is agreement among the numerical findings and the experimental data. The results show that the relative low temperature gradient in the thermal boundary layer, as well as the lower surface temperature in pulsing flows, promote heat transfer increase. Furthermore, heat transfer impedance is substantially lower during the invert flow time than it is during the forward flow period. The flow turnabout time follows the pulsing pressure waves by roughly 180 degrees. Furthermore, conclusion based on spectral analysis of the simulated averaged surface temperature showed that when the Amp of the imposed pulsations is large, the temperature fluctuates in multiple-peaked modes, Nevertheless, when the amplitude of the externally applied pulsations is low , temperature changes follow a single peak.

Nandi,et al. (2013) [15] The investigation of the concurrently evolving unstable laminar fluid flow and heat transfer within a 2-Dimensional wavy micro channel due to sinusoidal variable input velocity component . The flow was growing thermally and hydro dynamically while the channel walls were held at a constant temperature. Combining the (SIMPLE) method with Rhie and Chow's momentum interpolation technique was used to derive the transient solution of the two-dimensional Navier-Stokes equation. The simulation was run in the laminar regime with Various Prandtl numbers, from (7 to 100) and Re numbers between (0.1 to 100). Based on a comparability with steady flow in a sinusoidal channel, it was discovered that forced sinusoidal velocity at the intake can increase TPF at various amplitudes (0.2, 0.5, 0.8) and frequencies (1, 5, 10).

`

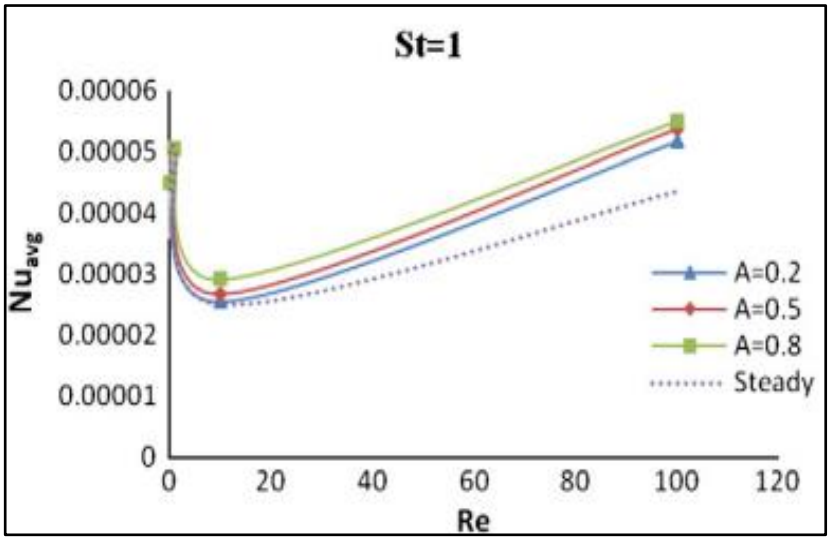

Figure 2.3. Comparison of time average Nu number with Re number with different amplitude.

Wang, et al. 2005 [16] presented The numerical study for Pulsating turbulent flow and convective heat transfer with huge velocity fluctuating amplitudes in a pipe at constant wall temperature. Turbulence modeling employs a Low-Re Number (LRN) k-ε turbulent model. According to the model analysis, the Womersley number is a critical quantity in the study of pulsating flow and heat transmission. The velocity and temperature characteristics of the flow are revealed by investigating fluid dynamics and thermal conduction over a broad spectrum of operating conditions. The numerical calculations indicate that there is an optimal womersley number in a pulsation turbulent flow where heat transmission is maximized. In pulsating turbulent flow, increased amplitudes of velocity fluctuation and flow reversal both considerably boost heat transfer enhancement.

Yu Wang et al. (2014) [17] developed A thorough model for fluid dynamics and thermal transfer in three dimensions, with transient states in a channel with LVG is described in this study. In comparison to previous research on pulsing flow for heat transfer enhancement, the present study details and analyzes the overall and local dynamic reaction performance of velocity and vortices, heat transfer and flow resistance, field synergy and channel dissipation at the entry with Lvg. Following model validation, the pulsing flow is numerically examined using four different instances. results show that amplitude and period are the two most important

`

determinants that influence flow and heat transfer performance. Cases 1-4 raise the total j-factor by 19.15 percent, 1.47 percent, 24.96 percent, and 1.51 percent, respectively. Furthermore, the total f-coefficient is enhanced by 17.61%, 17.58%, and 16%, respectively. All of the data were plotted in an energy-saving performance assessment plot and assessed using the field synergy and entrance extreme principles.

Jie-Cheng Yu. et al,. (2004) [18] studied the dynamics of heat convection in a pulsing laminar flow along a circular tube with a fixed wall heat flux. Dimensionless pulsation frequency w*, Amp y, and Prandtl number all influence the size of the temperature profile and Nusselt number fluctuations about the solution for continuous laminar convection. It is further shown that pulsation has no effect on the time-average Nu numbers for pulsating convection heat transfer in a circular tube with a constant wall heat flux.

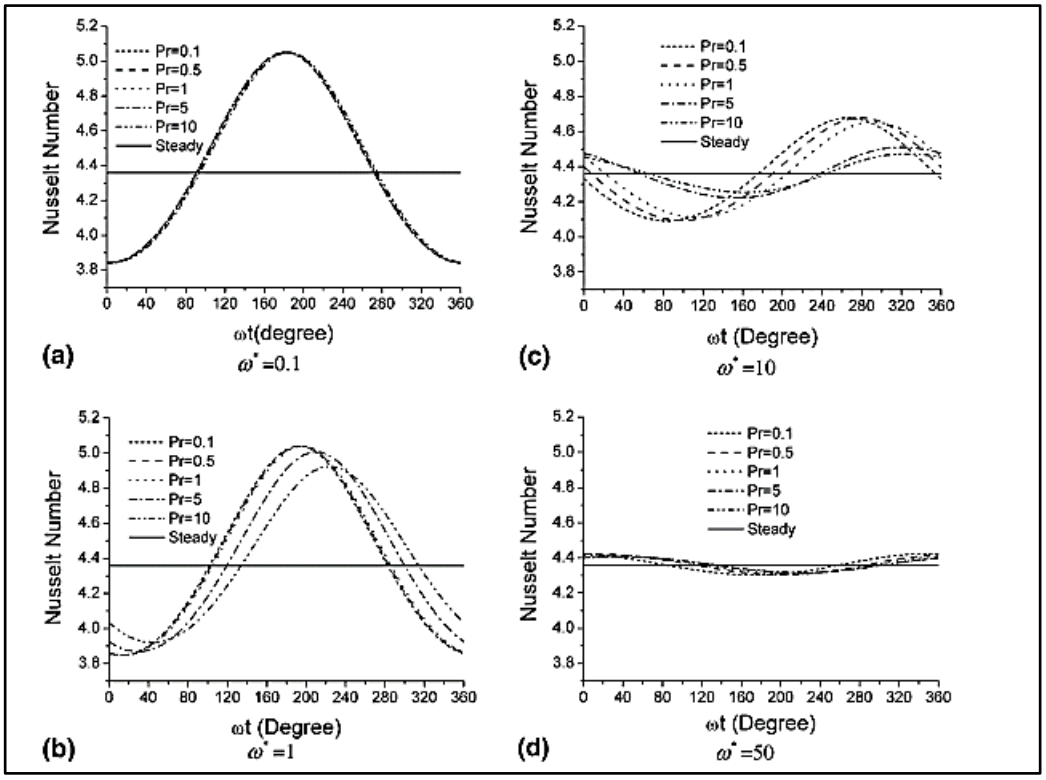

Figure 2.4. Transient Nu numbers for different prandtl number and dimensionless pulsation frequency w.

Zohir, et al. (2006) [19] heat transfer properties of laminar and turbulent pulsing pipe flows were explored experimentally under various parameters of Re Number, pulsate

`

frequency, pulsator position, and tube diameter. In both situations, the tube wall with homogeneous heat flow was examined. The Re- number ranged from (750 to 12320), as long as the pulsation frequency ranged among (1 to 10 Hz). The findings of positioning the pulsator upstream of the entrance of the test section tube revealed an raise in heat transfer rate owing to pulsate of as far as 30% with flow Re number of 1643 and pulse frequency of (1 Hz), depends while looking upstream placement of the pulsator valve. The closer the valve is to the tested section intake, the greater the improvement in heat transfer coefficient. When the results of heat transmission in the upstream and down stream pulsations were compared, the upstream pulsation produced small values for the relative mean Nusselt Number at Reynold Number of 1366 and 1643, respectively. Analyzing the heat transfer findings of the two examined tubes with test sections for Re numbers ranging from($8x10^3$ to $12x10^3$) and pulsation frequencies ranging from (1.0 to 10 Hz), revealed that a bigger tube diameter resulted in greater improvement in heat transfer rate. For Reynolds numbers ranging from $8x10^3$ to$12x10^3$ and pulsation frequencies of 10 Hz, mean value in relation to other variables Value of the Nusselt improvement on the order of around 50% was found at Reynolds number 8,000 for the big examination subsection diameter of 50 mm. At the same Reynold Number and frequency, a drop in the relative mean Nu number of up to 10% was recorded considering the 15 mm diameter of the test portion.

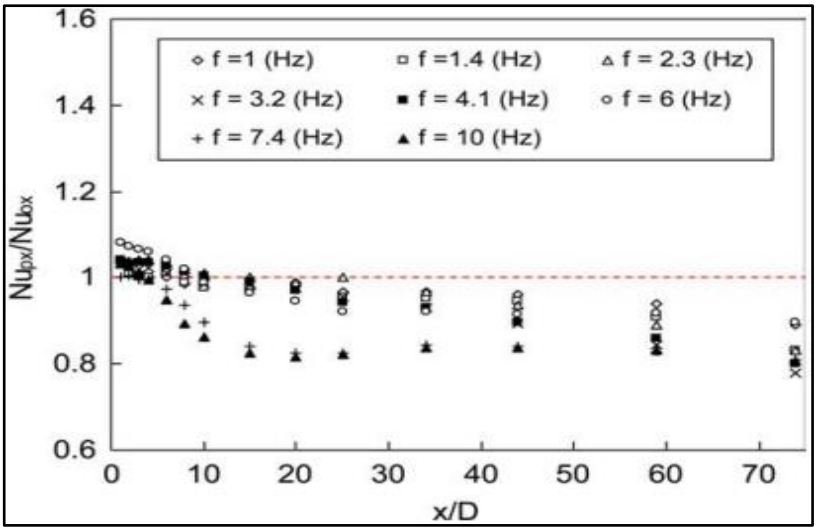

Figure 2.5. Relative Local Nu for different pulsate frequencies with (A=2, Re=1643).

`

2.2.2. Previous Improvements Made to Solar Air Collector

The study of V.S. Korpale, et al. (2020) [20] was concentrated on the formulating of empirical formulas and assessment of the highest thermo-hydraulic response of a rectangular section rib used in SAH with taking into account the entire combinations of design within the provided range of the parameters of input. Based on the design of experiment algorithms It was tested specifically with "response surface" methodology the same as four input variables were considered. Then CFD simulations were utilized to verify values of the related parameters of design. Eventually, errors were ranging within allowed limit. Therefore, the accuracy of empirical relations employed solar artificial air heater design is satisfactory.

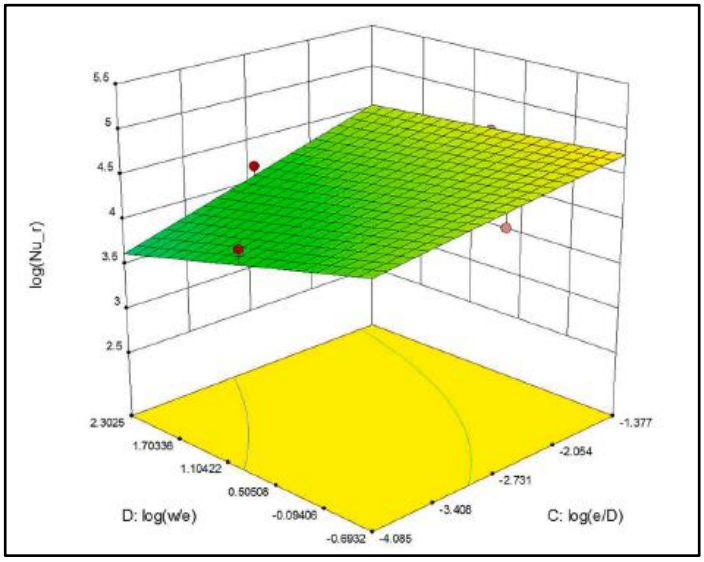

Figure 2.6. Variation of Nusselt number with the variation in e/D and w/e at Re = 8944 and P/e = 17.32.

Singh et al. (2019) [21] evaluated and compared in their study several performance properties of both solar air heater , curved and flat under various ambient conditions relying on numerical model validated experimentally. To begin with, the optimal curve angle for curved SAH that provides optimized thermal performance has been identified also important parameters have been determined such as the enhancement factor (i.e., Nu_{curved} /Nu_{flat}). Based on used parameters range, SAH was observed to be increased productivity in comparison with conventionally flat SAH. It is recommended to deploy

`

the data reported in the paper by the scientific society in order to obtain improved SAHs for harnessing sun's energy in effective methods.

Yadav et al. (2020) [22] conducted a numerical analysis on heat transfer behavior of a solar air collector possessing Absorber plate along with impinging Jet. Modeling fluid dynamics in three dimensions using (ANSYS software 18.1) has been implemented with RNG(k–**ε**) turbulence model, as well as the upwind scheme is used for the purpose of discretization of governing equations. The effect of non-dimensional parameters, such as jet diameter ratio and jet height ratio had research done on them considering Reynolds number varying from (3500 to 17500). There was a comparison between the conclusion reached from solar air collector with jet impingement and customary SAH,under same conditions. Mentioning few conclusions, the maximum enhancement of heat transfers of (7.58) with the Coefficient of Friction punishment for 9.01 times is recorded at jet diameter factor in 0.065 and jet height ratio of 0.216 considering 17,500 for Reynold number. The parameters of thermal-hydraulic performance that have the highest value of 3.66 are the jet height ratio of 0.216 and the jet diameter ratio of 0.065 for a Reynolds number of 15500.

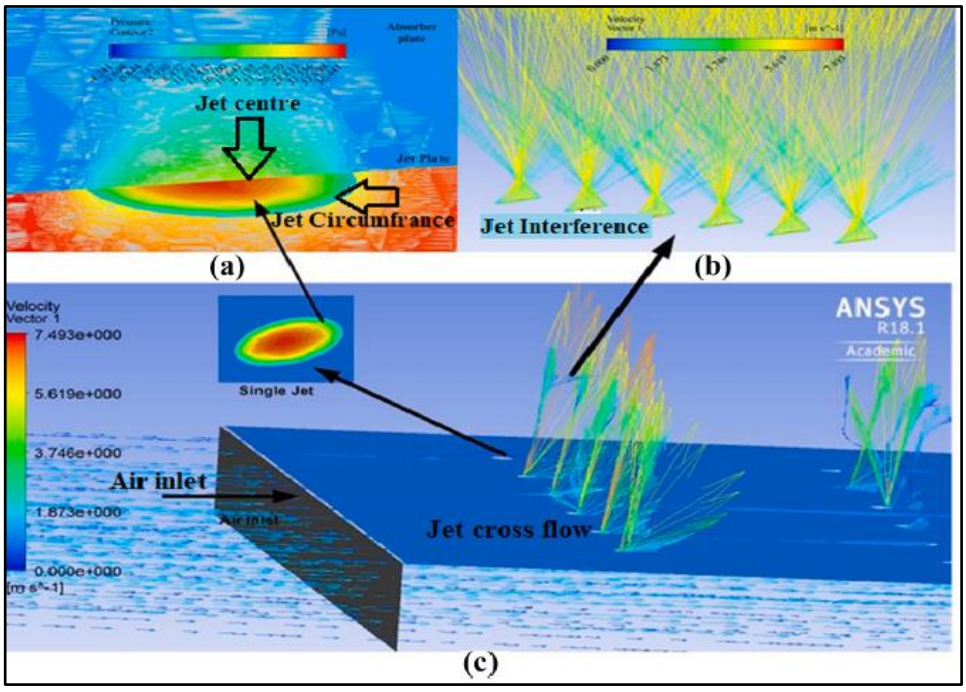

Figure 2.7. (a) Contour for the pressure of a jet on the jet plate (b) Streamlines showing jet interference between impinging jet (c) contour for air flow inside SAHJI.

`

Masoumi, et al. (2020) [23] presented in their paper a numerical simulation, improvement, and also experimental substantiation of an Asphalt Solar Collector (ASC). In the subsequent stage, Artificial Neural Networks were used to create the ASC's model (ANN) . In addition to this, several experiments were conducted in both hot and cold months of the year considering dissimilar rates of water flow from (9:00 to 17:00). The ANN inputs involve the parameters of the design, while the output was the outlet water temperature. It was evident that those models were capable of assessing the performance of the ASC in hourly basis over the day and under various boundary conditions. The conclusions demonstrated that the development of surface absorptivity plus asphalt's thermal conductivity results in a raises of the daily efficiency in August. It is recommended in future studies to carry out the consistent with prior research on the ASC; parameters of structure (pipe radius, pipe depth, etc.) modelled using both CFD and ANN techniques. Algorithms for optimal performance can be invested to ameliorate the proposed ASC performance.

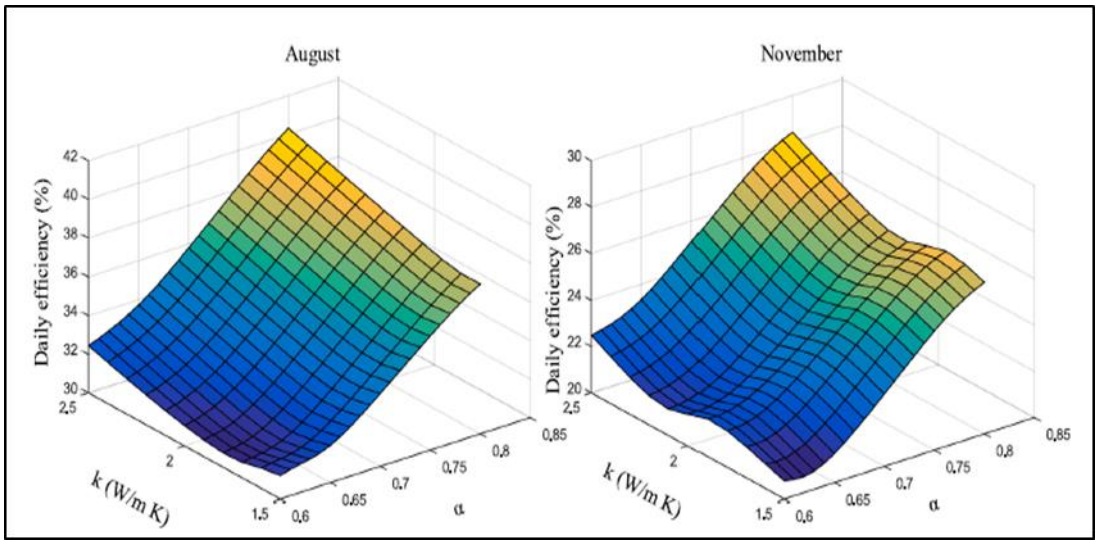

Figure 2.8. The daily efficiency as a function of thermal conductivity and surface absorptivity (Tin = 9 °C).

Rajarajeswari et al. (2018) [24] introduced comparing the heat transfer and friction coefficient properties of porous (wire screen) and non-porous solar air heaters through controlled laboratory experiments. The suggested research looked at how the mass flow rate affected the air temperature increase, thermal efficiency, and pressure

`

decrease along the test boundary. Porous bed solar air heaters had their Colburn (Jh) factor, a heat transmission parameter, modified. The functional Reynolds number range is defined as 194–591. At mass flow rate of 0.055 kg/s, the overall efficiency was improved by 21 percent. In air heaters with a wire screen, heat dissipation was reduced as a result of improved heat transmission. Furthermore, there was little to no difference in the wire screen matrices in terms of pressure drop in the duct. At full flow, the pressure dropped by only 17 Pa. For optimum thermal performance and minimum pressure loss, a mass flow rate of 0.02-0.055 kg/s was found to be optimal.

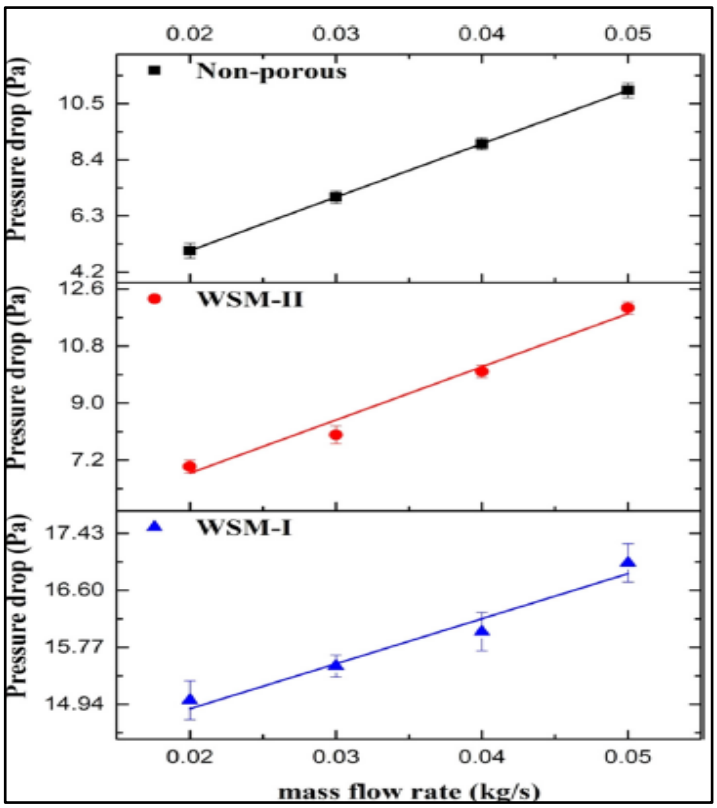

Figure 2.9. Pressure drop across the length of the duct.

Shakaib et al. (2016) [25] carried out a CFD study to identify turbulent flow of fluid, The heat distribution patterns in a solar air heater's rectilinear ribbed channels . The results showed considerable impact of Re number, height of ribs, and pitch on turbulent diffusion and heat convection. When heat flux is specified at the bottom wall, the temperature values raises sharply close to the ribs stagnant zones, and the heat transfer coefficients are less at these locations. On the other hand, when heat flux is defined at the top wall, the change in heat transfer coefficient is relatively margin.

`

Because of the study, the channel, which contains ribs of 3mm and pitch 40mm, are identified appropriate owing due to increased heat transfer rates. It is recommended in the future research to further analyze both heat transfer and fluid flow at different ribs' height, pitch and Reynolds number.

Bhupendra Gupta et al. (2018) [26] conducted an experiment to ameliorate a solar air collector in terms of the thermal performance. The absorber plate of the investigated solar air heater has hollow rectangular shaped (turbulators) attached to it. The results of experiments have been compared with the performance of conventional solar air heater without turbulators. It turned up that was an improvement regarding thermal efficiency of SAH by 11.4% with 0.012 kg/s as the rate of air mass flow. The maximum increase in air temperature was recorder 16.2°C with rectangular bodies be compared to 10.2°C without turbulators. Consequently, an improvement with respect to the effectiveness of a redesigned solar air heater has been obtained. In addition, CFD simulation based on (ANSYS) has been implemented and also validated by the experimental results.

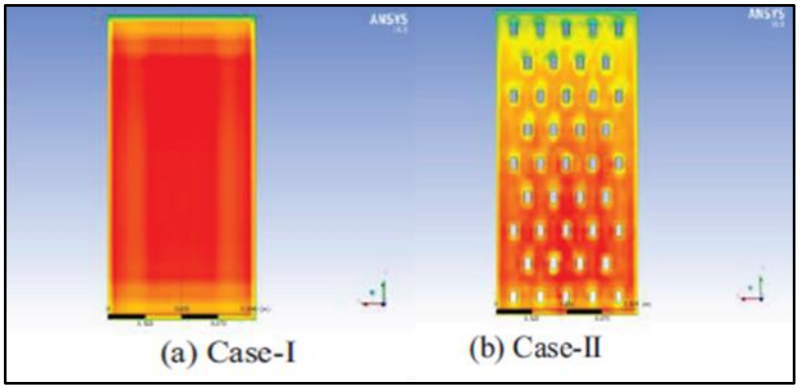

Figure 2.10. Temperature contour of absorber plate for a) case-1 b) case-11.

Pandey et al. (2020) [27] performed numerical and experimental analysis to study solar air heaters which are equipped holes in the absorber plates with arc shaped roughness elements. Heat transfer (Nu) plus friction factor (f) of the SAHs were also analyzed in this research, ANSYS software was employed to simulate the airflow over a rectangular channel. On the surface, a heating source of 1000 W/m^2 was placed. to simulate the irradiance of the sun. Twenty-seven combinations of roughened duct were examined depending on the ANSYS also on an experimental work. The results

`

demonstrated that the maximum value of Nu was obtained for roughness element, for which the gap count is two. Moreover, an evaluation was conducted in terms of Thermo-hydraulic performance and that showed highest values for *P/e* and N_g of (16, 2) respectively.

Ansari et al. (2020) [28] invested a controlled environment to examine how changing the flow geometry, in this case the rib shape, impacts the solar air heater's ability to generate heat. There must be a good reason for adding the ribs, as the heat transmission rate within the entrance length is rather significant. In addition to helping the experiments, CFDs are run so that the flow field may be seen in all its glory. Numerical simulation estimates of heat transmission and pressure drop are validated by experimental data. It may be inferred that non-uniform ribs with an rises pitch in the entrance length can give superior thermal performances when applied to relatively short channels. The reason that about the same heat transfer may be attained while experiencing a lower pressure drop. When the ribs are spaced closely together, the flow will go across each consecutive rib, eliminating the need for a reattachment point. The blending is terrible, and the ribs aren't applied well.

Jawad et al. (2020) [29] proposed a suitable for the cold Baghdad city in winters, a solar air heater system. The proposed heater encompasses aluminum chips and tubes packed with nano-sized silicon carbide (Sic) added to paraffin wax to ameliorate its thermo-physical characteristics, The thermal conductivity of the product was elevated by 18.2% through adding 3 wt% of Nano-SiC. The heat capability of the composite material came by 4.5% and their impact on the SAH performance was limited. Tests conducted outdoors approved the compatibility to heat the air in the proposed heater in light of Baghdad's current climate . It was evident that the utilization of the chips increased efficiency of the heater, and boosted the air to heat up, thus the warming load on the composite material tubes was declined early in the day. In addition to this,after being tested, the air heater showed significantly higher temperatures as it ran for at least three hours after dark.

`

Patel et al. (2020) [30] studied a solar air collector. To begin with, the SAH underwent a decreased coefficient of convection heat transfer As a result of the laminar sub-layer formed between the flowing air and the absorber plate.The authors suggested that for the elevation of the heat transfer factor, the laminar sub-layer can be interconnected with the employment of artificial roughness on the absorber plate. Furthermore, the impacts of relative roughness pitch (P/e) and relative roughness height (e/D) were studied considering the Re varying from 6000 to 18000 As various roughness characteristics are considered, , NASA 0040 profile ribs given in the adverse direction with P/e as 5 and e/D as O.O65 were concluded to be the best possible . The parameter of the thermo-hydraulic performance for this study was found to be 2.53 at Reynold Number of 6,000. Eventually, conclusions drawn from the experiments matched the numerical results, and the highest variation had been found to be 4.84%. Furthermore, there was a development of an empirical correlation for the purpose of prediction Nu and f regarding Re and e/D values, and found to be suitable inside $\pm$ 3% of the corresponding experimental values.

Manjunath et al. (2018) [31] introduced the impact of A profile with sinusoidal Absorbing plate for waves on the enhanced heat transfer and corresponding performance of SAH in thermo-hydraulic manner based on 3D - CFD simulation considering the flow Re varying between the range of 4,000 and 24,000. Implications of different design parameters of corrugated absorbent plate for instance dimensionless wavelength and aspect ratio on the thermal hydraulic performance was highlighted. The aspect ratio within the range of 1.5–4.0 whilst the normalized wavelength was ranged between 1.0 and 6.0. It appeared from the research demonstrated that sinusoidal corrugations gives elevated flow disturbances resulting in significant boost in heat transfer. Lastly, a number of conclusions were discussed, for instance, it was found that the reliance on lower values of aspect ratio and dimensionless wavelength resulted in higher thermal efficiency. Furthermore, there was a raise in thermal efficiency about 12.5% in terms of maximum efficiency, the configuration is optimal when its dimensionless wavelength is 1.0 and its aspect ratio is 1.5.

`

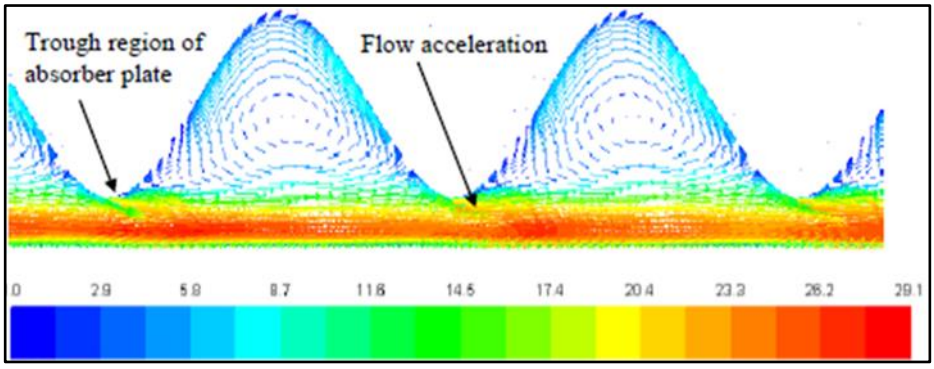

Figure 2.11. Velocity vector plot of air flow over the corrugated plate for the configuration of λ=1 and A.R=1.5.

Al-Damook et al. (2019) [32] investigated influence of flow arrangements on the thermal performance of a SAH. There was a utilization of recovered aluminum cans (RACs) as turbulators along with a double-pass at single duct SAC . They used CFD within Comsol Multiphasic V5.3a to study three models namely, Concurrent (model a), countercurrent (model b), and U-shape (model c). It was evident The U-shaped design was found to increase thermal performance by 5.4% and 6.5%, respectively, in numerical tests , compare to the concurrent and countercurrent flow models. In addition, a practical outdoor experiment was conducted relying on the numerical modeling of flow arrangements. The experimental data is consistent with the design of the double-pass single duct SAC (model C) , and model C-III has a better thermal efficiency of 60.2%, in comparison with those of model C-II, 53.1%, and model C-I, 49.4%.

Gawande et al. (2016) [33] introduced heat transfer of air with forced convection in a SAH with reverse L-shaped ribs in both experimental and numerical manner. Solar air heater thermal efficiency was studied considering design variables for example Reynolds number (3800 ≤ Re ≤ 18,000), roughness pitch relative (7.14≤ P/e ≤ 17.86), heat flux (1000 W/m^2) and constant relative roughness height (e/D = 0.042). a 2D - CFD simulation was implemented along with using ANSYS and RNG k–$\boldsymbol{\varepsilon}$ turbulence model in order to solve turbulence terms in the governing equations. The existence of reverse L-shaped rib showed a considerable effect on heat transfer and friction coefficient attributes in accordance with the alteration in roughness pitch relative (P/e) and Re .THP of 1.9 taking into account supplement of heat transfer

`

equivalent in terms of pumping ability , has been assessed for optimized arrangement of the roughness element (reverse L-shaped rib). The numerical results were compatible with the experimental ones for the range of parameters analyzed. There was a development of correlations for Nu number and friction coefficient as a function of flow parameters and roughness.

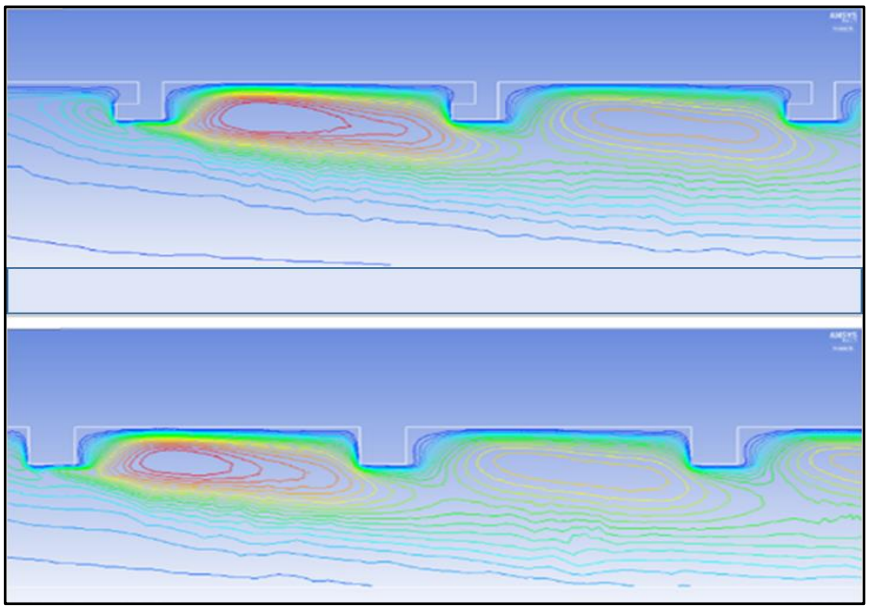

Figure 2.12. Contour plots of turbulence kinetic energy k for reversed L-shaped and square rib roughness.

Doukhi et al. (2019) [34] examined solar collectors by use of a COMSOL Multiphasic-enabled CFD analysis of the system's performance. When it came to physical structures, the SAC model was of the double-pass, single-flow, U-turn variety. Pressure drop and thermal efficiency were used to determine the optimal flow depth and U-turn spacing. The optimal values of performance indicators were found to be (0.01 m) for both the depth of flow and the U-turn spacing. Furthermore, the values for thermal efficiency and pressure drop were 47.25 percent and 93.55 pa, respectively. Depending on the Reynold Number and the ambient temperature, the effect of mean velocity and the influencing variables of mass flow rate on operational metrics was studied, and the results showed a significant improvement in heat transfer and pressure loss efficiency. The thermal efficiency was 57.99 percent and the fan power consumption was 56.36 W when operating at an ambient temperature of 273.15 degrees Celsius and a Reynolds number of 15000. In consequence, solar radiation has

`

grown. That caused the absorber plates and the ambient air to heat up. In order to save time and effort, CFD should be used instead of experimental studies to analyze such study challenges.

Akram et al. (2019) [35] gave a considerable consideration to further improve the performance and thermo-physical characteristics of the heat exchanger fluids of solar collectors with flat plate such as radiative heat transfers and thermal conductivity. Nanofluids were employed. The authors aimed to summarize the studies conducted in the domain of solar flat plate collectors relying on a set of nanofluids. Furthermore, this article discussed the chances for future research in many points. For example, deep study is required for the composition of covalently functionalized nanoparticles seeking improved stability plus thermal performance of their nanofluids, and experiments can be implemented with different kinds of hybrid nanofluids.

Singh et al. (2019) [36] conducted Analyses and studies of designs are performed based on an established SAH numerical model gleaned from experimental data , as that boosts flow rate by exceeding 100% be compared to prevalent flat plate SAH configuration. The combination of bell-shaped designs at SAH inlet has been added to the ram-air impact that transforms dynamic pressure into static pressure thus reflected in an enhanced airflow rate also in excellent heat transfer combined with low hydraulic losses. Incorporating bell-shaped designs at the SAH's input increases the ram-air effect, which transforms dynamic pressure into stationary pressure, and so results in a significant increase in airflow rate and a marked decrease in heat transfer and hydraulic losses. The enhanced flow SAH was calculated to be 33% efficient more than the conventional design. Furthermore, an independent relation for Nusselt number change with Ra numbers and bell mouth ratio of the form $Nu\ (Ra\ cos\vartheta)^m\ (h/R)^n$ was created and compatibility established with the data.

`

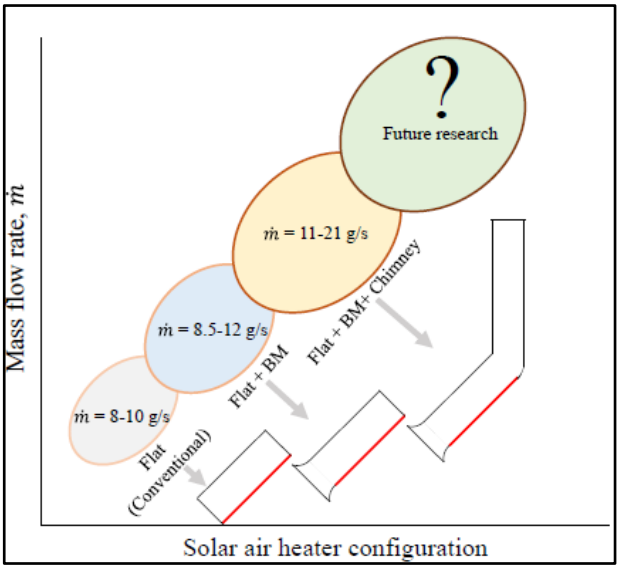

Figure 2.13. Schematic representation of various naturally driven solar air heaters configuration based on their mass flow rates mentioned are for the heat flux 500–1100 W/m^2.

Jia et al. (2021) [37] aims to examine how the quantity of longitudinal baffles affects heat transmission and flow characteristics in spiral solar air heaters (SSAHs). By analyzing velocity gradients at the channel's inlet and outlet, we found that the magnitude of these gradients was proportional to the difference in inlet and outlet sizes and the channel's cross-sectional area. The pressure loss of SSAHs was also exacerbated because of the boundary layer separation phenomena, which induced steep velocity gradients at the turnings. In addition, it was found that the collection efficiency increased with the addition of nearly 2 longitudinal baffles, reached a maximum, and then decreased; this demonstrated that the positive effect of elevating the Qab by adding more baffles did not counteract the negative effect of elevating the QL. The SSAH with two longitudinal baffles was found to be the best option when considering both operational effectiveness and cost effectiveness. To improve the prediction of the collection efficiency and pressure loss of SSAHs with diverse number of longitudinal baffles, the correlations of the pressure loss and Nu of SSAHs were got relying on the least square method.

Sheetal Jain et al. (2019) [38] studied the problem of adding artificial roughness elements on the heated surface of a SAH, as that would pursue heat transfer augmentation. Friction and heat transmission properties of the equilateral triangular

`

passage duct were investigated as a function of the number of Ribs that are broken and angled, having a square cross-section, as that was analyzed relying on computational fluid dynamics. The impact of variables of roughness namely relative gap position plus relative gap width was being studied considering Re varying from (4000 to 18,000). The values of relative gap position (d/w) and relative gap width (g/e) are range from (0.16 to 0.67) and 0.5 to 2 respectively, meanwhile, a constant heat flux is applied on the absorber side, while other surfaces were insulated. The Nu number grew to 2.16 times by utilizing broken ribs compared to the smooth channel at d/w =0.25 and g/e = 1.

Shetty et al. (2021) [39] implemented examination of a SAC using numerical methods with a circular plate with perforations for absorption in order to analyze its effect on the thermo - hydraulic performance because of the eradicating of laminar viscous layer that conversely exists in a conventional solar air heater. The research was conducted for arrangements of the absorber plate with openings of 5, 8, 10, and 12 mm in diameter , and the number of vents is varied as, 24, 36 and 54. The numerical analysis (CFD) was carried out for Re numbers varying from 3000 to 21,000. CFD simulation was assessed in accordance with the experimental results. Thermal efficiency increased by 23.33% and that was obtained considering the configuration with 8 mm diameter vents plus 36 number of vents as compared to the prototype without the absorber plate. The average elevation in thermo-hydraulic efficiency was about 21.78% higher for the aforementioned Contrasted setups to the base model. The highest thermo-hydraulic effectiveness in 72.8 % was recorded. In addition, it was evident that the thermo hydraulic efficiency of the collector was strongly proportional to the elevation in vent diameter. The study concludes that the circular geometry and vented absorber plate resulted in vortex formation leading to an raises in heat transfer caused by turbulence.

`

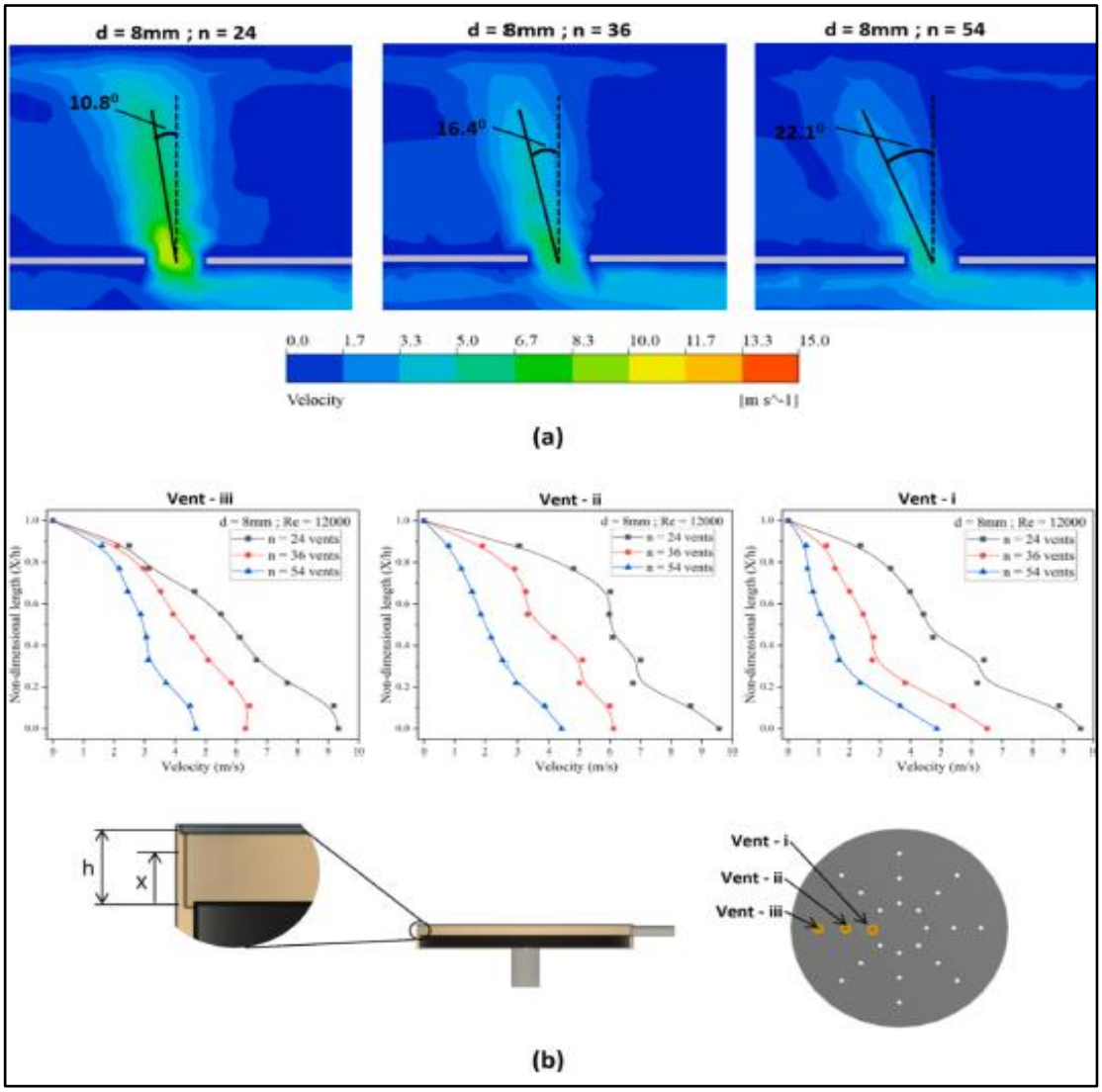

Figure 2.14. (A) Contour plot of velocity jet at the cross section of vents (B) Plots of velocity at different vents for 8 mm diameter configuration.

Kumar et al. (2018) [40] studied the ribbed 3-dimensional solar air collector (SAH) model in numerical method to assess heat transfer and flow through it. The numerical analysis was based on finite - volume scheme and a group of flow governing equations was solved to identify the heat transfer and flow field across the SAH. For deeper analysis, rib chamfer height ratio (e'/e) along with rib aspect ratio (e/w) two creative parameters were discussed and considered in addition with the commonly used roughness parameters. Eventually, there was an adequate compatibility in Nusselt number (Nu) with friction factor (f) as that was evident by comparing the predicted results with the experimental ones. The developed generalized equation for Nu and f showed deviations in percentages studied to be acceptable.

`

Sharma et al. (2021) [41] made a review for CFD analysis on SAH to boost the heat transfer. As, powerful computers as well as mathematical model are used to perform “computational fluid dynamics (CFD) simulation”. The simulation made from CFD is capable of predicting the transfer of momentum, heat and mass in several processes of heat transfer and fluid flow. This work constitutes of reviews of various researchers made in relation of enhancing the performances of the solar air collector. From this review, it was evident that the CFD analysis will be helpful and provide various approaches and opportunities the quality of in order to the drying performance of solar air heater. New concepts are adapted by few of the researchers for increasing the transferring rate of heat in the duct of the SAC.

Pashchenko.et al. (2019) [42] demonstrated the results of their study of the thermodynamic and aerodynamic properties of SAH. They built a computer model using ANSYS fluent and was validated in light of experimental evidence. The conclusions were as follows, the operating efficiency of SAH was the highest at the end of autumn, where the slope of the absorbent surface with respect to the horizontal is 60 degrees. In addition to this, the dependence of the air heating value of the solar heater during daylight hours was identified by the actual and virtual tests. Furthermore, the effect of the transverse ribs on the heat exchange between the air and the light-absorbing surface and the air was demonstrated. Finally, a curvilinear shaping of the temperature circumference generated close to the ribs when zones of reverse current and vortices coalesced.

`

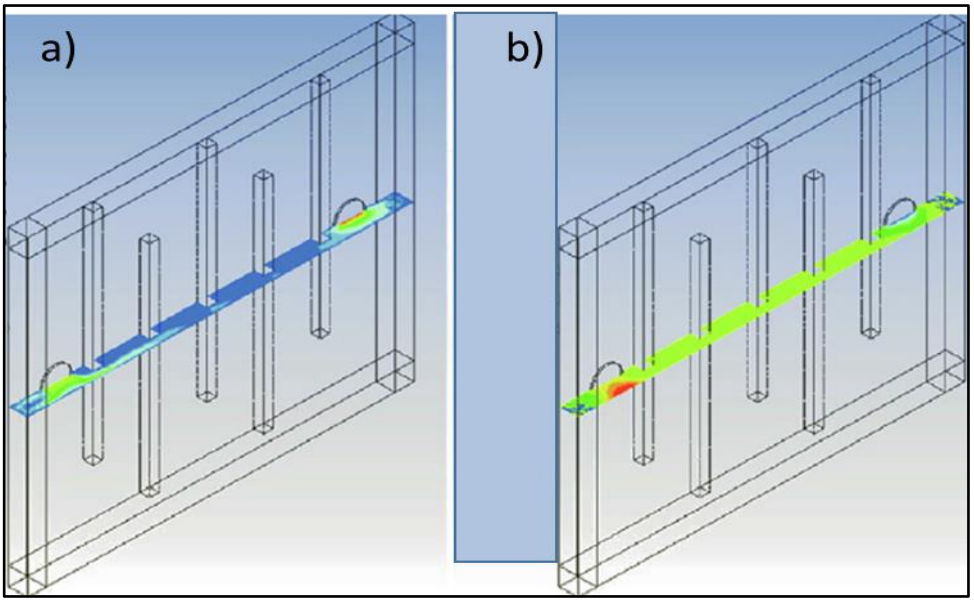

Figure 2.15. Contours of a) air velocities b)static pressure in the SAH.

Mathur et al. (2016) [43] studied the optimization of a lone pass fin SAH for improved thermal performance depending with respect to CFD technology (Fluent 6.3 with Gambit 2.3). Four important characteristic were taken into account ,which are mass flow rate, number of fins, fin height and length. The turbulent DTRM and RNG ($K-\varepsilon$) model was utilized and the results of the simulation were validated with the findings from the March 2012 experiment. According to the simulation outcomes, the SAH should possess four fins, i.e., as in the existing SAH but the height and fin length should rise from (40 to 50 cm) and from 4 cm to 6cm respectively to achieve better performance. In the improved SAH, the immediate efficiency and useful heat gain boosted by 8.35 % and 8.24 % respectively considering the air mass flow rate of 0.024 kg/s compared to the SAH. For future work, the studied can be adjusted using the recommended dimensions depending on this optimization study. The need for more research, UDF PROFILE can be used to characterize materials thus their values alter relative to temperature.

An evaluation of the thermal efficiency of a double-glazed, single-pass SAH encompassing of an absorption plate with longitudinal fins on its upper surface and equipped with phase change material (PCM) in its lower surface was deeply studied by Josyula, et al. (2018) [44]. The PCM utilized was paraffin wax (Rubitherm RT42). , and the key idea of the proposed SAH design is to use it over the night hours. The

`

purpose of this study was to examine how mass flow rate and fin number affected thermal performance under transient conditions. a computational analysis for heat transfer and fluid dynamics utilizing an implicit methodology was created. The maximum output air temperature of the fin-type SAH is achieved by storing the latent heat at (40, 37 and 35°C) for mass flow rates of (0.01, 0.015 and 0.02 kg/s), respectively. Furthermore, the usability of the system for (14, 12 and 10 hours) after sunset had been predicted at relevant mass flow rates. It is predicted that daily average thermal efficiency would peak at 62.4%. at a mass flow rate of 0.02 kg/sec, making it a more expensive option than the other designs under consideration for the study.

Chand et al. (2019) [45] presented The artificially roughened SAH with rectangular duct was analyzed using 2-D CFD to determine the optimal placement of rectangular, triangular, and circular vortex generators on the absorber plate to maximize heat transmission. To analyze the flow in the solar air heater duct equipped with vortex generators, we employed the finite element method using the SIMPLE algorithm as a foundation and ANSYS FLUENT 16.0 as a solver. The average Nu number was studied as it changed in response to a change in Reynolds number from (3800 to18, 000), while the heat flow was held at $1100 W/m^2$. Overall, the average Nusselt number grew drastically throughout all Re number bands. in all the geometries, but most noticeably in the triangle vortex generator with essentially no pressure drop at all, as was determined by the researchers. At a Re number of 18,000, the average Nusselt number in a triangle vortex generator was 3.848 times larger than the average Nusselt number in a smooth duct. It is determined that the duct equipped with a triangular vortex generator performs best at a Reynolds number of 3800 from the standpoint of thermo-hydraulic performance and the enhancement ratio of the Nusselt number.

`

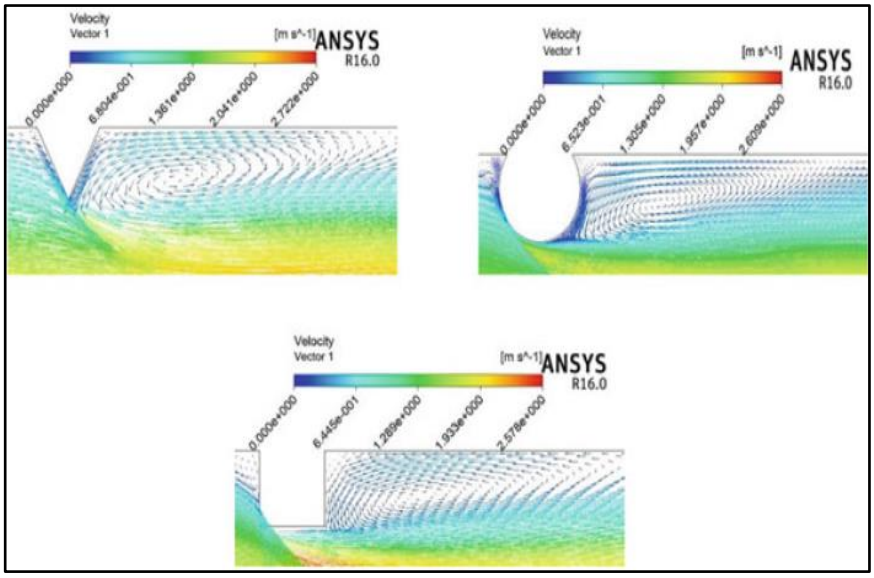

Figure 2.16. Contour of velocity vector shows the vortices formed by the different vortex generators.

Heat transfer improvement by installing investigation on the use of elliptical ribs on the absorber plate by creating CFD code using ANSYS FLUENT 12.1 software by Kumar et al. (2017) [46]. The simulations were implemented on 2-D simulation CFD model and in order to study the impact of relative roughness height, relative roughness width, and relative roughness pitch on friction factor and heat transfer. The considered Reynolds number varied from (4,000 to 15,000) and turbulence has been modeled by using Reynolds-average Navier-Stokes (RANS). The mathematical modeling was then approved and compared with the available outcomes. It was evident that Nusselt number value raised by elevating relative roughness height but it dropped with the increase of relative roughness pitch and relative roughness width. Furthermore, the rib width made a big difference on heat transfer enhancement, with the maximum Nu number being observed for very minor width of roughness (i.e., 0.5) across the investigated ranged from 0.5 mm to 2.0 mm.

Vivekanandan et al. (2020) [47] studied the flow is not completely developed within the SAH's casing; guiding vanes were installed within the duct's trapezoidal form to improve things, but they were not able to do so. Next, flow-restricting devices are installed within the duct to create a mature flow. Experiments have been conducted to compare the SAH with and without flow restrictors and guiding vanes. Through the solar air heater's housing, we measured the speed of the airflow. The solar air heater

`

has undergone CFD analysis to verify the experimental findings. The numerical solutions were consistent with the measured values.

Sivakumar et al. (2019) [48] In this study, we evaluated the performance of a pin-fin absorbent plate used in a forced convection SAH to that of a conventional flat absorbent plate. Experiments were conducted during February and March 2018 in Coimbatore, India. They used for performance comparisons several parameters for instance outlet air temperature, thermal hydraulic efficiency, energy efficiency and external energy efficiency. The results demonstrated that the pin fin adsorption plate possessed a higher air temperature of 17 °C in comparison with the flat plate absorber. The forced convection SAH energy efficiency using pin fin absorption plate was 3% to 12% higher be compared to flat plate absorption with 2 % to 11 % higher energy effectiveness. The results emphasized that forced convection SAH using a pin-finned absorption plate possessed a large performance enhancement regarding the thermodynamic performance with minimal pressure drop along the duct of air collector. Further research studies are needed with respect to improvement of fin pitch and dimensions.

The work of investigated the thermal performance of a new solar air heater with metallic corrugated encapsulation in cold zone buildings. Zheng et al. (2017) [49]. They devolved Mathematical models checked the thermal performance of the collector and the experiments confirmed the results. Hydraulic analysis was carried out experimentally to investigate the pressure drops of airflow in corrugated packing. The effects of operational and structured parameters, such as for example collector dimensions and sun radiation intensity, inlet air temperature ambient air temperature, and velocity were analyzed to ameliorate the thermal performance of the collector. The results indicated that the corrugated Using a solar air collector with metal packaging is preferable. For investment in rural constructions of cold places as it is advantageous due to its substantial region of heat exchange, enhanced heat transfer coefficient and adequate economic performance.

Kumar et al. (2018) [50] presented a CFD computational simulation of heat transfer augmentation in a rectangular channel duct of a solar air collector with square rib

`

roughness on the absorber plate. The effect of the Reynolds Number on the Nu number for the rib roughness of the square-shaped cross-sectional wires was examined and its relative evaluation was plotted. The two-dimensional computational analysis have been used the ANSYS FLUENT 16.2 software for the simulation with the SIMPLE airflow algorithm to visualize the characteristics and distribution of the fluid flowing through the channel considering Reynolds numbers ranging from 3800-18000. The model considered for evaluating smooth canal with square rib roughness was in excellent concordance between experimental findings and established theoretical frameworks. The result obtained through this investigation showed that the Reynolds number has a significant impact on the Nusselt number. and that it increases with the increase of the Reynolds number for the investigation range of parameters.

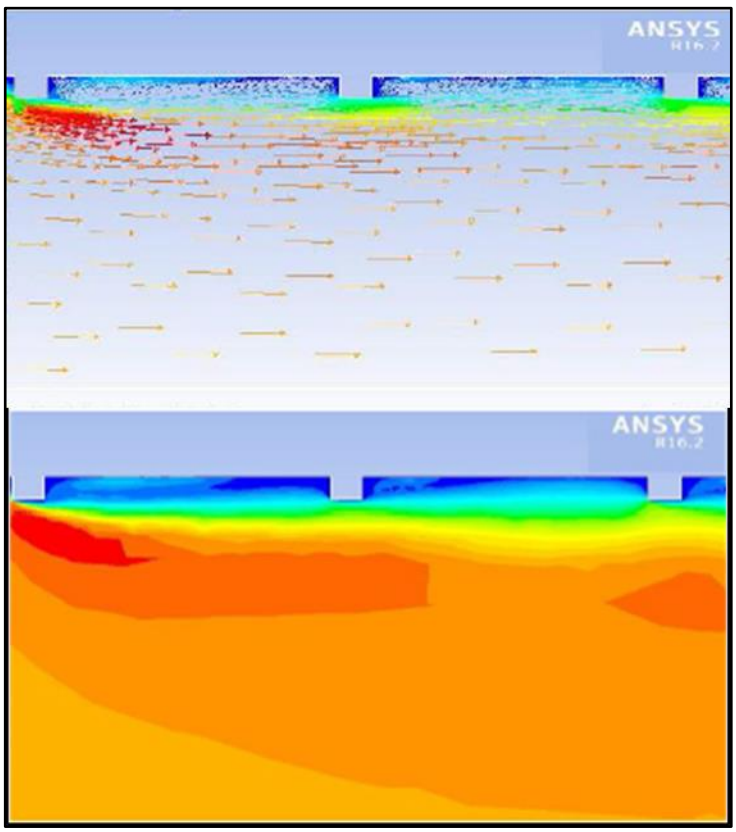

Figure 2.17. Contour of velocity magnitude.

Maithani et al. (2015) [51] researched the effectiveness of a solar air heating duct with coarse V-ribs and symmetrical gaps for heating efficiency. Increased friction from the rougher surface increases the pressure drop as the rougher absorbent plate transfers more heat. Experimental analysis employing V-ribs with consistent gaps revealed the

`

absorber plate's improved heat transfer. High relative roughness (e/D) of 0.0433, moderate relative roughness (P/e) of 10, and a steep angle of attack () of 60 degrees characterize this channel. The gap width was changed from 1-5 g/e and the gap count was changed from 1-5 Ng. Compared to a smooth channel, the maximum values for the Nusselt number and the friction coefficient were 2.59 and 2.87 respectively. The highest value of the thermo-hydraulic performance coefficient was found with a relative gap width of 4 and a number of gaps of 3.

Zhang et al. (2019) [52] in their paper Seeking to raise a solar air collector's thermodynamic efficiency, this research looked at three different approaches: (1) modifying the collector plate with ribs, fins, or grids to reorganize airflow in the laminar sub-layer; (2) employing an air impingement jet to support Heat is transferred from the air to the absorption plate by convection. by reorganizing the air flow near the absorption plate; and (3) switching to a double-duct manifold. The fundamental contribution of this review is a new understanding of the connections between different optimization techniques and a unified approach to rearranging airflow. This review reviewed and analyzed papers on various optimization strategies, offering a new angle from which to evaluate the interconnections between these approaches and aiding researchers in doing so.

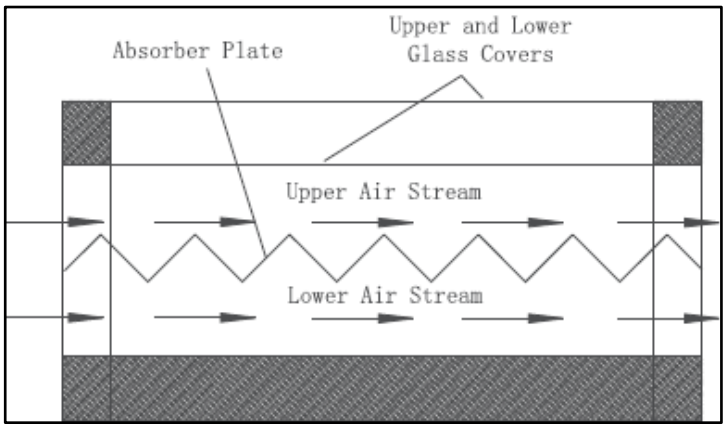

Figure 2.18. Schematic diagram of Double-pass corrugated V-shaped solar air collector.

Jayaraj et al. (2019) [53] attempted in their work attempted to maintain the thermal effectiveness of a Double- pass SAH system (DPSAHS) through thermal retardation

`

of phase materials (PCM). Meanwhile, this study investigated the function of metal macro-encapsulation in terms of storing and reusing heat of PCM embedded within DPASHS. The goals were to deeply study the impact of encapsulation geometry used for storage and to examine whether separate units provide faster charging and unloading of organic paraffin wax (PCM). In the proposed work, the average efficiencies of encapsulation were 47.2% and 67%, respectively, and they were found for rectangular and cylindrical macro encapsulates equipped with DPSAHS. Moreover, they presented a performance comparison of DP-SAHS whether there is storage or not. The total cost analysis showed that with a slight margin in building cost, the time of operation of DP-SAHS was ameliorated.

Binguang Jia et al. (2019) [54] proposed a new sort of solar air collector relying on the helical shape of the spoilers other than the serpentine shape. They investigated experimentally many aspects such as the function of helical solar air heaters (SSAH), including heat gathering efficiency, variances in inlet and outlet temperature, radiation, and air volume. Based on evaluation test, the temperature variation midway between intake and discharge was related to the radiation linearly, and the heat collection efficiency was affected by the quadratic function relationship to the radiation of constant flux. Eventually, SSAH heat loss coefficient was calculated by natural temperature and found to be $5.69 W/m^2.k - 1$. Compared with conventional and serpentine SAH, this type of solar air heater possessed enhanced heat collecting efficiency.

Kottayat et al. (2020) [55] presented Solar air heater duct with a triangular cross-section (SAH) and it was considered by way of the implication of a solar dryer (ITSD). They investigated the thermal-hydraulic performance of the SAH triangular duct with tilted ribs for variable rib tilt ($30^\circ < \alpha < 75^\circ$) in turbulent flow system ($5x10^3 < \mathrm{Re} < 17.5x10^3$) based on the computational study. The studied SAH have been designed including a rib configuration providing maximum thermo-hydraulic performance. In addition, Similar SAH designs were compared to the proposed SAH. . It was shown from the results that the polygonal triangular canal ($\alpha = 45^\circ$) has 17% higher efficiency in comparison with the other types and 79% when compared to smooth SAH. Furthermore, it was evident that the ribs in the triangular duct SAH enhanced an

`

elevation in temperature even in the duct core. The excellence of the polygonal triangle SAH was emphasized by analyzing the drying attributes of okra and two different types of bananas, namely Nendran and Robusta, as maximum temperature was gained in the proposed SAH outlet.

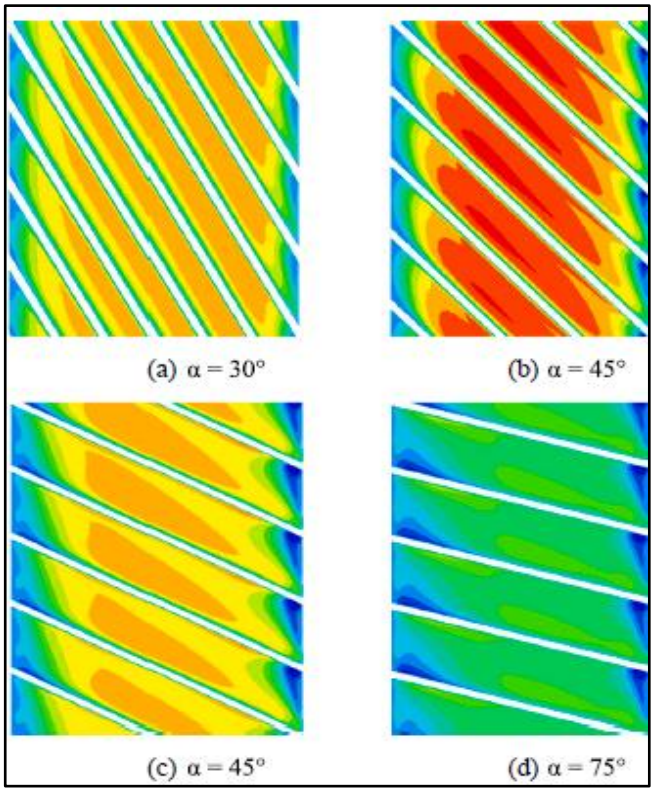

Figure 2.19. Velocity contour indicating secondary flow strength in the inter rib regions for Re = 10000.

Ong et al. (1995) [56] Through the use of a mathematical model and method of solution, the authors anticipate single-pass solar air collectors' thermal efficiency. By eliminating or providing a top glass cover over a plane absorber plate or by providing a bottom plate under the absorber plate, and then circulating air through one or both of the air channels so generated, we investigated four typical types of flat-plate solar air collector systems.

It was presumed that the surface temperatures of the walls next to the air currents would be constant. , whereas the air temperatures varied in a straight line down the collector. The solar collector was assumed sufficiently short in the mathematical model for the assumptions to be valid; the thermal network analysis method was used to

`

derive a set of simultaneous equations for the average temperature of the walls and air streams, assuming a steady state heat transfer. When calculating average temperatures, a matrix inversion technique was utilized in conjunction with a regular subroutine program instead of solving the simultaneous equations directly. The heat transfer coefficients have been estimated using an approximation of the mean temperatures required to account for the temperature dependence of the coefficients. Following this, an iterative method was used to determine the collector's average temperature. Differences between the estimated and calculated averages were examined. The process was iterated until the temperature gap between successive means was smaller than 0.8°C. After that, a second collector section of the same length was attached to the terminal of the first collector. It was expected that the incoming temperature was the same as the outgoing temperature from the first portion. Mean temperatures were calculated using an iterative process again in the following section. Additional pieces were added until the collector's total length was known. This method can be used to predict the average wall and air stream temperatures for a collector of arbitrary length. Despite the fact that just four typical single-pass flat-plate solar collectors are discussed in this article, the solution technique might be expanded to accommodate the vast majority of alternative collector designs.

`

PART 3

THEORETICAL BACKGROUND AND MATHEMATICAL MODEL

In this part, the governing mathematical equations will be presented, as well as the theoretical aspect of the solar heater and its physical properties, including the type of heat loads. Convection, radiation, conduction and their representation by mathematical equations.

3.1. PHYSICAL MODEL

A one-way solar heater will be used for ductwork where the air is pulsating, to calculate the heat and pressure distribution equations on the absorber surface, and to add some improvements to the solar heater, Where the air duct will be considered forced using certain equations, then the thermal loads will be calculated theoretically using the energy and momentum equations. There are five types of thermal loads in the duct:

1) Radiation between glass and sky.
2) Convection between glass and sky.
3) Radiation between glass and absorber.
4) Convection between glass and fluid.
5) Convection between absorber and fluid

We consider the airway symmetrical, using only 2D- equations in the X- and Y-axis direction. The mathematical model accommodates two main parts; the first part is Navier stocks equations that consist (momentum equations, continuity equations and thermal energy equation) and (k-e) equations.

`

And the second part is the subroutines as in the present work there are three subroutines for front glass, absorber plate and air gap where energy equation was solved. The aim of both parts (main program combined with the subroutines) is to calculate the temperature distribution, Nusselt number values, TPF values and friction factor values within solar collector. Solar air collector has a physical model as demonstrate in Figure 3.1 with the dimensions (2 *1 * 0.04) m in length, width and height.

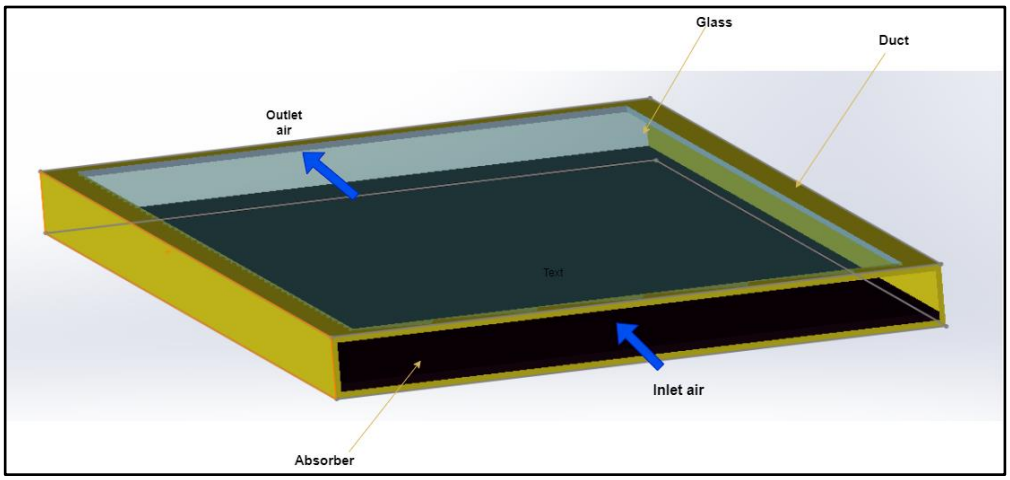

Figure 3.1. Solar air collector.

3.2. SOLAR AIR COLLECTOR

A traditional solar air collector heater is made up of a flat plate with an absorber plate, a clear cover system on top, and insulation on the bottom and sides. Everything is contained within a metal box. . The working fluid is air, and the path through which it flows varies depending on the kind of air heater. The components of an air heater are constructed from the same sorts of components as those of a liquid flat plate collector. Like liquid flat-plate collectors, the transmission of solar light via the cover system and subsequent absorption in the absorber plate may be accounted for by formulae. On maximize collection, a selective coating might be applied to the absorber plate.

3.2.1. Solar Air Components

There are three main components of the solar air collector :

`

1) **Absorber plate:** High heat conductivity is required of the absorber plate, suitable tensile and compressive strength, and be resistant to corrosion. Copper is widely used due of its extraordinarily high conductivity and corrosion resistance. Steel, aluminum, Galvanized Iron (GI) sheets, and metal ions and a wide range of thermoplastics are also used to make collectors. Depending on the type of solar air collector, the standard technique for producing To use a metal sheet as an absorber plate (such as Copper or aluminum) and insulate the non-flow surface. Solar energy absorbed by this metal sheet heats it, and some of the heat is transferred to the surrounding air. This hot air is employed for practical purposes.
2) **Cover plate:** An equally important part of a solar air collector is the cover plate or plates through which the sun energy must be transferred. The following are some of the uses for cover plates:

    1) In order to transmit the maximum amount of solar energy to the absorber plate.
    2) Reduce environmental impact by reducing absorber plate loss.
    3) As a measure against direct weathering, the absorber plate must be covered. .

Toughness, lasting, non-digestibility, and solar energy transmission are the most significant requirements for cover plate materials. Collectors favorite cover material is glass. Tempered glass is more durable than other types of glass and can withstand thermal cycling. When choosing glass for cover plates, its mechanical strength must be high enough to withstand the highest wind and snow loads predicted. , Mechanical strength is commensurate to square of the thickness of the glass; The minimum acceptable thickness of a cover plate is 0.33cm.

Glass cover plate thermal shock is also taken into account. . A number of distinct procedures causes it .Heating and cooling on a daily basis, for example, produced by variations in sunlight intensity on the collectors at that time of day in the morning and ensuing reduction in the afternoon. Again, as clouds move overhead, the temperature of glass may rapidly change, perhaps by 50 degrees in just a few minutes. . The central

`

portion of the collectors is heated more than the edges; this causes thermal stress, which can cause glass covers to break [57].

3) **Insulation:** Insulation prevents loss of heat due to the absorber plate owing to conduction or convection. Rock wool or glass wool are common insulating materials. Depending on the design, Insulate the underside and/or sides of the absorber plate. . A key benchmark for among the requirements for something to be considered an insulator are that it is resistant to heat. .

3.3. ASSUMPTION

In this study we have assumed:

1) the flow is pulsating. .
2) a two-dimensional flow.
3) The collector is designed to account for turbulent flow.
4) All properties have been measured at ambient temperature.
5) Using Heat transferred by forced convection.
6) Body forces are negligible.
7) The temperature of the incoming air is the same as the surrounding air.
8) Incompressible flow.
9) Taking as Unsteady state.
10) Newton's law.

3.4. GOVERNING EQUATIONS

3.4.1. Navier Stocks Equations [58].

I. Continuity equation:

$$\frac{\partial \rho}{\partial t} + \frac{\partial}{\partial \mathrm{x}} \rho \mathrm{u} + \frac{\partial}{\partial \mathrm{y}} \rho \mathrm{v} = 0 \qquad (3.1)$$

`

Where **t** represented time, u and v are components of the fluid velocity in the x and y directions respectively.

II. Momentum equation in X-direction:

$$\rho\frac{\partial u}{\partial t}+\rho U\frac{\partial u}{\partial x}+\rho V\frac{\partial u}{\partial y}=-\frac{\partial P}{\partial x}+\frac{\partial}{\partial x}\left[(\mu+\mu_t)\left(2\frac{\partial u}{\partial x}\right)\right]+\frac{\partial}{\partial y}\left[(\mu+\mu_t)\left(\frac{\partial u}{\partial y}+\frac{\partial v}{\partial x}\right)\right] \qquad (3.2)$$

Whenever p is pressure, μ the fluid viscosity and μ_t the eddy or turbulent viscosity.

III. **Momentum equation in the y-direction:**

$$\rho\frac{\partial v}{\partial t}+\rho U\frac{\partial v}{\partial x}+\rho V\frac{\partial v}{\partial y}=-\frac{\partial P}{\partial y}+\frac{\partial}{\partial x}\left[(\mu+\mu_t)\left(\frac{\partial v}{\partial x}+\frac{\partial u}{\partial y}\right)\right]+\frac{\partial}{\partial y}\left[(\mu+\mu_t)\left(\frac{\partial v}{\partial y}+\frac{\partial v}{\partial y}\right)\right] \qquad (3.3)$$

IV. **Equation of thermal energy:**

$$\rho\frac{\partial T}{\partial t}+\rho U\frac{\partial T}{\partial x}+\rho V\frac{\partial T}{\partial y}=\frac{\partial}{\partial x}\left[\left(\frac{\mu}{p_r}+\frac{\mu_t}{\sigma_T}\right)\left(\frac{\partial T}{\partial x}\right)\right]+\frac{\partial}{\partial y}\left[\left(\frac{\mu}{p_r}+\frac{\mu_t}{\sigma_T}\right)\left(\frac{\partial T}{\partial y}\right)\right] \qquad (3.4)$$

Where T is the temperature of the fluid at a certain location. , σ_T is the turbulent prandtl number temperature Pr is the fluid prandtl number.

3.4.2. The Standard (K-$\mathcal{E}$) Model

In turbulent flow, the numerical simulation is executed using (K-$\mathcal{E}$) turbulence model [59]. This model contains two equations, turbulence dissipation rate ($\mathcal{E}$) and turbulence kinetic energy (k). the equations are thusly:

I. Turbulent kinetic energy (k) equation:

$$\rho\frac{\partial K}{\partial t}+\rho U\frac{\partial K}{\partial X}+\rho V\frac{\partial K}{\partial Y}=\frac{\partial}{\partial X}\left[\left(\mu+\frac{\mu_t}{\sigma_k}\right)\left(\frac{\partial K}{\partial X}\right)\right]+\frac{\partial}{\partial Y}\left[\left(\mu+\frac{\mu_t}{\sigma_k}\right)\left(\frac{\partial K}{\partial Y}\right)\right]+D+P\kappa-\rho\varepsilon \qquad (3.5)$$

`

K is the turbulent kinetic energy, σ_k is the turbulent prandtl number for k and ε is the rate of energy dissipation, D represented a term which arises when low Reynolds turbulent model are implemented.

II. Equation of turbulent dissipation ($\mathcal{E}$):

$$\rho\frac{\partial\varepsilon}{\partial\tau}+\rho U\frac{\partial\varepsilon}{\partial x}+\rho V\frac{\partial\varepsilon}{\partial y}=\frac{\partial}{\partial x}\left[\left(\mu+\frac{\mu_t}{\sigma_\varepsilon}\right)\left(\frac{\partial\varepsilon}{\partial x}\right)\right]+\frac{\partial}{\partial y}\left[\left(\mu+\frac{\mu_t}{\sigma_\varepsilon}\right)\left(\frac{\partial\varepsilon}{\partial y}\right)\right]+\ C_{\varepsilon 1}f_1\frac{\varepsilon}{k}-C_{\varepsilon_2}f_2\,\rho\frac{\varepsilon^2}{k}+E \qquad (3.6)$$

When E is a term that occurs when low Reynolds number turbulence models are used. σ_ε Is the turbulent Prandtl number for $\mathcal{E}$. Where μt=turbulent viscosity.

$$\mu_t=\ f_\mu\rho C_\mu\frac{K^2}{\varepsilon} \qquad (3.7)$$

P_k Is the generation of turbulence energy due to mean velocity gradients, ρ ε is its mean destruction, Member P_k written as:

$$P_K=\mu_t\left[2\left(\frac{\partial U}{\partial X}\right)^2+2\left(\frac{\partial V}{\partial Y}\right)^2+\left(\frac{\partial U}{\partial Y}+\frac{\partial V}{\partial X}\right)^2+\left(\frac{\partial V}{\partial Z}+\frac{\partial W}{\partial Y}\right)^2 \qquad (3.8)$$

III. Modification for low Reynolds number

Low Reynolds number K-$\mathcal{E}$ model of Jones and Launder (1972) [60]. The following values are experimental constants used in the standard k-ε model. Cμ=0.09, $C_{\mathcal{E}1}$=1.44, $C_{\mathcal{E}2}$=1.92, σ_T=0.9, σ_k=1.0, σ_ε=1.3, fμ=f1=f2=1.0.

$$f\mu=exp\left[\frac{-2.5}{1+\frac{Re_t}{50}}\right], f1=1.0\,, f2=1-0.3exp\left(-{Re_t}^2\right) \qquad (3.9)$$

$$D=-2\mu\left[\left\{\frac{\partial\sqrt{k}}{\partial x}\right\}^2+\left\{\frac{\partial\sqrt{k}}{\partial y}\right\}^2\right], E=2\mu\frac{\mu_t}{\rho}\left[\left\{\frac{\partial^2 u}{\partial y^2}\right\}^2+\left\{\frac{\partial^2 v}{\partial x^2}\right\}^2\right] \qquad (3.10)$$

`

3.5. SUBROUTINE EQUATIONS

3.5.1 Equation of the Glass Cover:

Because of the thickness of the cover. It is fair to expect a consistent temperature through it. Furthermore, by taking into account glass's invariable characteristics, the governing equation possible to obtain from an energy balance in a variable thickness volume c and area (pz). Heat is transferred into the glass via convection between it and the surrounding environment, in addition to atmospheric radiation and absorber-generated heat. Figure 3.2.

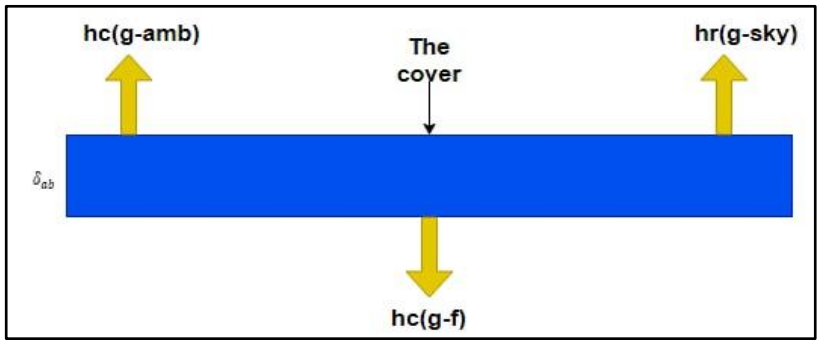

Figure 3.2. 1-D Heat transfer in the cover.

Then equation can be written as:

$$\rho_g\, Cp_g\, V_g.\frac{\partial T_g}{\partial t} = \alpha_g.I - hc(g-amb)Ag\left(T_g - T_{amb}\right) - hr(g-sky).Ag\left(T_g - Tsky\right) - hr(g-abs).A_g\left(T_g - T_{abs}\right) - hc(g-flow).A_g\left(T_g - T_f\right) \quad (3.11)$$

Where ρ_g is density of glass, Cp_g specific heat of glass, V_g volume of glass, α_g is absorption coefficient, T temperature, h_r is radiation heat transfer factor,h_c convection heat transfer coefficient.

3.5.2. The Absorber Equation.

Applying the absorber zone's heat-energy balance , Figure (3.3), and considering the solar irradiance on the absorber zone in the solar collector control volume, the radiation

`

between the absorber and the glass cover, the conduction between the absorber and the insulation zone, and convective heat transmission occurs in conjunction with the motion of the fluid. , the following relationship is obtained:

$$\rho_{ab}.\ Cp_{ab}.V_{ab}.\frac{\partial T_{ab}}{\partial t} = \alpha_{ab}.T_g.I - hr(g-abs).A_{ab}(T_{ab}-T_g) - hc(ab-flow).A_{ab}(T_{ab}-T_f) \quad (3.12)$$

ρ_{ab} Is density of absorber, Cp_{ab} is specific heat of absorber, t time.

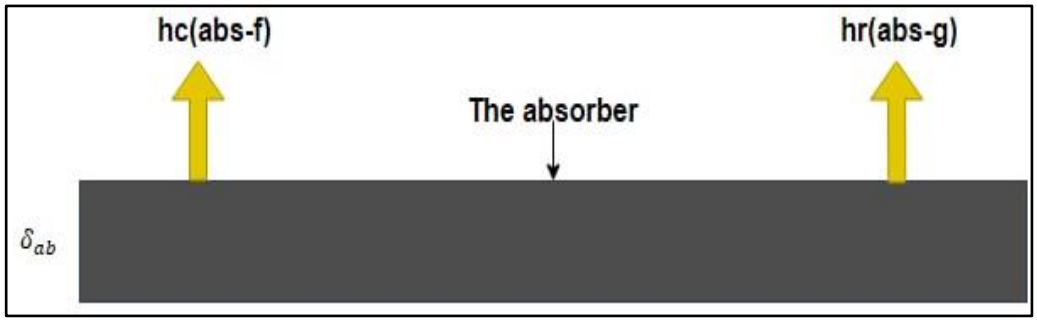

Figure 3.3. 1D heat transfer in the absorber.

3.5.3. The Air Gap Equation

By assessing the space between the solar collector's glass and the air gap control volume and taking into account the transient thermo physical properties of the air, heat transfers into the air gaper by convection between it and the glass on the top side and the absorber on the other side Figure 3.4.

$$c_a\ (T_a)\ \rho_a\ (T_a)\ V_a\ \frac{dT_a}{dt} = [\text{hc}\ (T_g - T_a) + \text{hr}\ (T_{abs} - T_a)]\ \text{p}\ \boldsymbol{\Delta}\text{z} \quad (3.13)$$

`

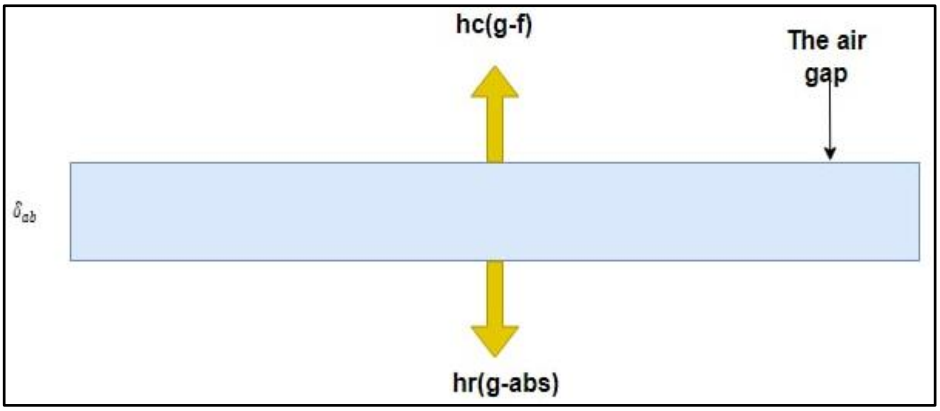

Figure 3.4. 1D heat transfer through air gap.

3.6. THE HEAT TRANSFER COEFFICIENT CALCULATION

I. The radiation heat transfer coefficient between glass and sky.

We can calculate hr from equation, Duffie and Beckmann (2006) [61].

$$\text{hr (g-sky)} = \sigma.\mathcal{E}_g(T_g{}^2 + T_{sky}{}^2).(T_g + T_{sky}) \tag{3.14}$$

Where σ Stefan – Boltzmann constant, emissivity of glass.

We can calculate T_{sky} from Swanbank's formula.

$$T_{sky} = 0.0552\, T_{amb}{}^{1.5} \tag{3.15}$$

The final formula becomes:

$$\text{hr (g-sky)} = \frac{\sigma.\mathcal{E}_g\ (T_g+T_{sky})(T_g{}^2+T_{sky}{}^2)(T_g-T_{sky})}{(T_g-T_{amb})} \tag{3.16}$$

II. The radiation heat transfer coefficient between glass and absorber.

$$\text{hr (g-abs)} = \sigma\ \frac{T_g{}^2+T_{ab}{}^2).(T_g+T_{ab})}{(\frac{1-\mathcal{E}_g}{\mathcal{E}g}+\frac{1-\varepsilon_{ab}}{\varepsilon_{ab}}+1)} \tag{3.17}$$

`

III. The experimental convection heat transfer coefficient between the glass and surrounding

hc (g-amb)= 2.8+3.3 V for V≤ 5 m/s (3.18)

hc (g-amb)= 5.67+3.86 V for V> 5 m/s (3.19)

3.7.THERMAL PERFORMANCE FACTOR (TPF) CALCULATIO

$$\text{TPF} = \frac{(Nu_p / Nu_0)}{(f_p / f_0)^{\frac{1}{3}}} \quad (3.20)$$

at first we must find local nusselt number from equation:

$$\text{Nu} = \frac{h D_h}{K_f} \quad (3.21)$$

where,

$$\text{h} = k_f \frac{\partial T}{\partial y} / (T_s - T_F) \quad (3.22)$$

then we should calculate local friction factor from equation :

$$f = \frac{2\Delta P}{\rho U_{in}^2} * \frac{D_h}{L_x} \quad (3.23)$$

when **Δ**P is pressure dropped ,U_{in} inlet velocity

Then equations of average nusselt number and average friction factor can be writeen as:

$$\text{Nu}^- = \frac{1}{L} \int_0^L Nu\, dx \quad (3.24)$$

$$f^- = \frac{1}{L} \int_0^L f\, dx \quad (3.25)$$

3.8. BOUNDARY CONDITIONS

At the cover of collector, glass on the front side and lower absorber surface and the sides edge walls, these (U=V=W=0) no slip condition.

So

`

$$K=0 \quad , \frac{\partial \varepsilon}{\partial Y} = 0 \tag{3.26}$$

3.8.1. Inlet Boundary Conditions

$$\text{At } x=0 \quad , T=Tin=T_{amb} \ , \quad V=0$$

$$U= U_0 \ (1+A\sin \ (2\boldsymbol{\pi} \ f_p \ t) \tag{3.27}$$

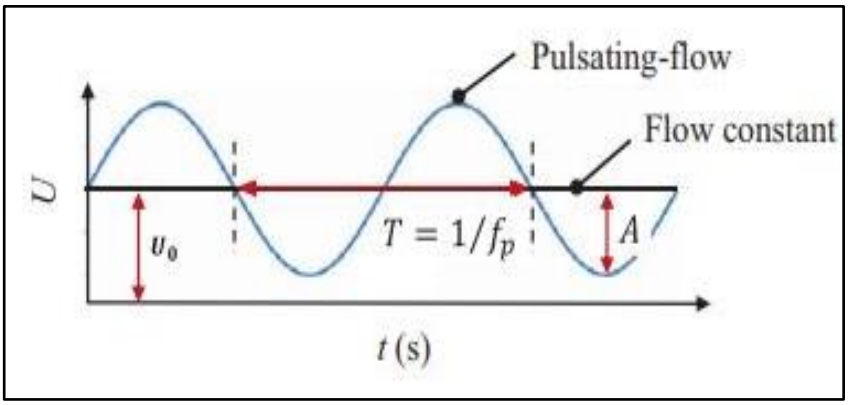

Wherever A is the dimensionless pulsating amplitude and f_p the pulsating frequency .subsequently the non-dimensional St Strouhal number is used to show the pulsating flow field.

Where

$$St = \frac{f_p D_h}{U_o} \tag{3.28}$$

The reference velocity magnitude Uo was calculated from hydraulic diameter and Reynolds number defined as:

$$U_0 = \frac{Re.v}{D_h} \tag{3.29}$$

Where Dh is calculated as:

`

$$Dh = \frac{4HW}{2(H+W)} \tag{3.30}$$

For (K-$\mathcal{E}$) we used these equations.

$$K=0.0013U^2{}_{in} \tag{3.31}$$

$$\boldsymbol{\varepsilon}=\frac{C_D\, K_{in}^{3/2}}{0.03\, h_i} \tag{3.32}$$

3.8.2.Outlet Boundary Conditions.

I. In the duct outlet section, fully developed flow included the set normal gradients to be zero, which can also be expressed as:

$$\frac{\partial u}{\partial x} = 0 \ , \ \frac{\partial v}{\partial x} = 0 \ , \frac{\partial T}{\partial x} = 0 \ , \frac{\partial k}{\partial x} = 0 \ \ , \frac{\partial \mathcal{E}}{\partial x} = 0 \tag{3.33}$$

II. Calculation of glass temperature T_g from equation (3.11)

III. Calculation of absorber temperature (T_{abs}) from equation (3.12)

`

PART 4

COMPUTATIONAL MODELING AND NUMERICAL ANALYSIS

4.1. INTRODUCTION

This part examines and analyzes the thermal distribution performance of a solar air heater duct with glass on one side using numerical analysis of PDEs (Partial Differential Equations). Using FORTRAN 90 , CFD programing ,and Tecplot 9.0 . Two-dimensional forced convection turbulent flow in a solar air heater collector was solved using a Finite-Volume scheme (SIMPLE) based mathematical model and formulation.The governing differential equations were discretized using the finite volume technique after being integrated across a control volume. Heat transfer and fluid movement in the system will be characterized using (mass, momentum, and thermal energy conservation), which is the foundation of the governing equations.

4.2. COMPUTATIONAL FLUID DYNAMICS (CFD)

Dynamic fluid computation CFD is one of the most recent methods for analyzing engineering problems in two steps. First, step, all fluid domains have been subdivided divided into manageable portions or components known as grids (or meshes). Second step, the governing equations for describing the physical and phenomena that required modeling using elements must be chosen. The numerical finite volume method is used in this analysis to solve non-linear partial differential equations [62].

`

4.2.1. The computational Grid

To solve finite volume equations, the computing domain structure-wise into a large number of tiny control volumes. By generating a volume of influence at any point on the grid, the governing equations are converted to algebraic equations. The faces of control volumes between adjacent grid points in the center were used in this analysis. The goal is to collect data on the base dependent variables at all network scale [65].

Differential equations are found by constructing control around each grid level and reducing them to algebraic equality. The goal, as shown in Figure 4-1, is to measure the base dependent variables at all network scales. Differential equations are found by constructing control around each grid level and then reducing them to algebraiequality.

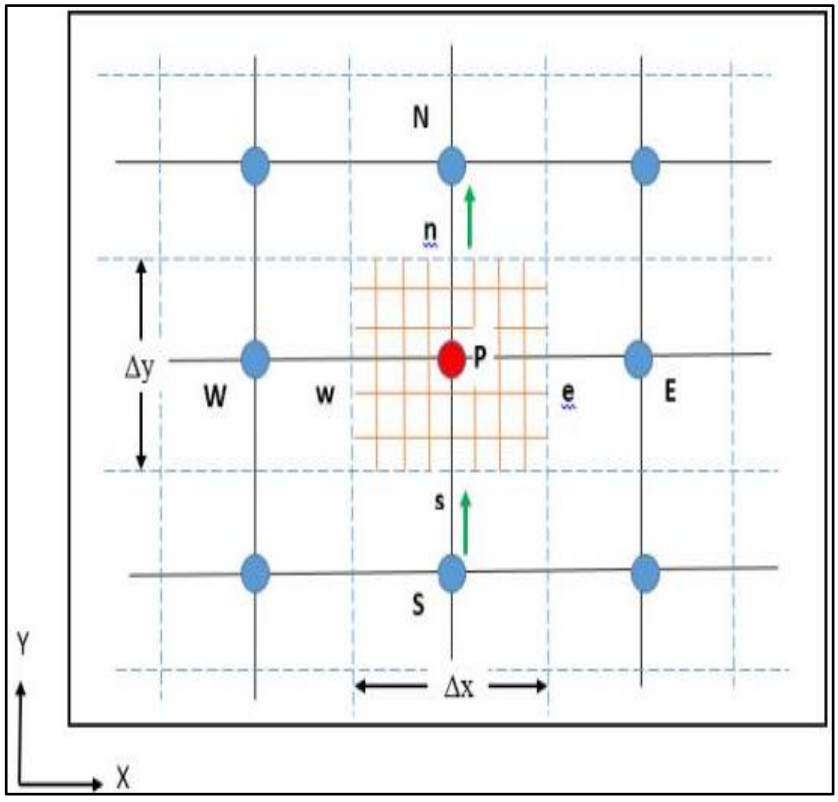

Figure 4.1. 2D Grid and control volume

`

.

4.2.2. Staggered Grid

To properly describe pressure in the momentum equation parameterization, the concept of velocity has to be established. Away from the regular grid of scalar coordinates using a staggered grid technique to predict the velocity modules. Scalar variables are preserved at central mesh nodes ,whereas velocity modules are reserved at staggered mesh [62]. Figures (4-2) show the staggered grid of pressure and temperature at the cell center, besides velocities at the cell faces. As a result, this grid arrangement has two advantages. Firstly, calculating pressure gradients is simple because it is located between velocities that affect and drive them. Second, the velocities are available for predicting flows of convection via the limit of the (C.Vs) around the mesh nodal as shown in Figure 4.3.

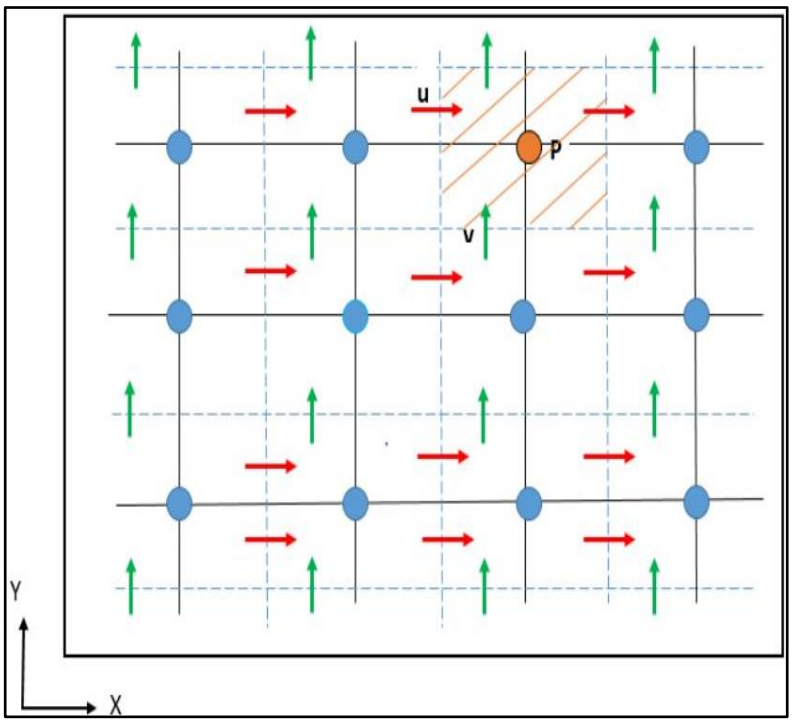

Figure 4.2. Staggered grid for velocity vector.

`

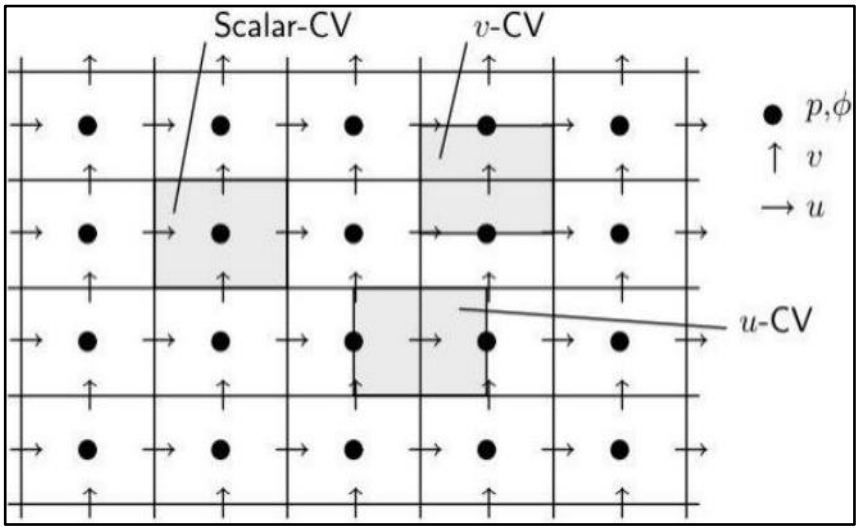

Figure 4.3. Staggered arrangement of variables and CVs.

4.3. THE FINITE – VOLUME SCHEME

Numerical methods include the Finite Volume Method (FVM) for converting partial differential equations depicting conservation laws over discrete volumes into discrete algebraic equations over finite volumes (or elements or cells).

The discretization of the geometric domain is the initial action required to solve the problem according to the finite element or finite difference method, which is discretized into finite volumes or interference elements in the FVM. The partial differential equations are then parameterized transformed into algebraic equations by integrating them across each discrete element. After that, the system of algebraic equations is solved the values of the dependent variable for all the constituents [64].

Nowadays, FEM and FVM are the most commonly used models. While FEM is most commonly used in structural mechanics, FVM is most commonly used in flow mechanics this is related to the significance of these two. Application areas in combination with the corresponding discretization technique [65].

4.3.1. One Dimensional- Discretization Grid Equation.

For the basic situation, the finite – volume procedure is defined as long as a first step in the discretization of a solution to a complete differential equation. Consider the following equation:

`

$$\frac{\partial}{\partial_X}(\rho U\lambda) = \frac{\partial}{\partial_x}[\Gamma\ \frac{\partial_\lambda}{\partial x}] \tag{4.1}$$

The grid in Figure 4.4 can be used to derive an equivalent discretized equation [66]. The control volume surfaces are represented by the intermittent lines in this figure. Assume the volume of control is equal to x. The equation's integration yields

$$(\rho U\lambda)_e - (\rho U\lambda)_w = [\Gamma\frac{\partial\lambda}{\partial x}]_e - [\Gamma\frac{\partial\lambda}{\partial x}]_w \tag{4.2}$$

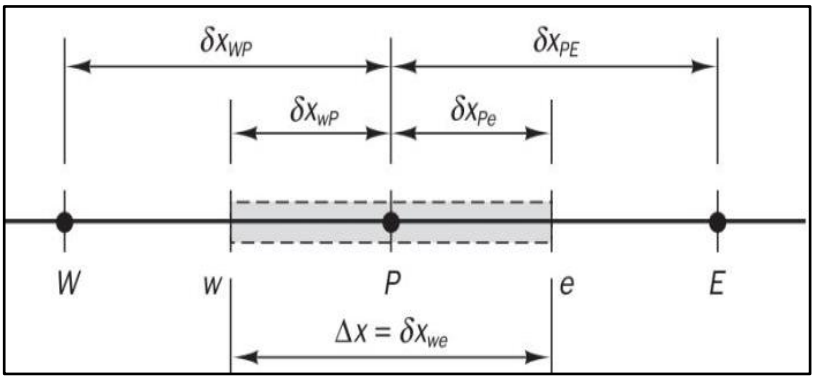

Figure 4.4. One dimensional field of grid point.

To parameterize this equation moreover, different scheme requirement must be met

I. Central- Differencing Method:

Use the central divergence technique and assume regular grid intermission the $\boldsymbol{\lambda}$ value provided by:

$$\left.\begin{aligned} \lambda e = \quad & 0.5\ (\lambda_E + \lambda_P) \\ \lambda_w = \quad & 0.5\ (\lambda_w + \lambda_p) \end{aligned}\right\} \tag{4.3}$$

Substitute $\boldsymbol{\lambda}$e and $\boldsymbol{\lambda}$w in Eq. (4.2)

$$0.5\ (\rho U)_e(\lambda_E + \lambda_P) - 0.5(\rho U)_w(\lambda_W + \lambda_P) = \frac{\Gamma_e}{\delta x_e}(\lambda_E - \lambda_P) - \frac{\Gamma_w}{\delta x_w}(\lambda_P - \lambda_w) \tag{4.4}$$

By following patankers recommendation **[67]** the diffusion coefficient can be expressed by:

`

$$\left.\begin{aligned} \Gamma_e &= \left[\frac{1-f_e}{\Gamma_p}+\frac{f_e}{\Gamma_E}\right]^{-1} \\ \Gamma_w &= \left[\frac{1-f_w}{\Gamma_p}+\frac{f_w}{\Gamma_W}\right]^{-1} \end{aligned}\right\} \tag{4.5}$$

Where$fe = \delta x_{e+}/\delta x_e$,$f_w = \delta x_{w+}/\delta x_w$

From the continuity equation,

$$\int \frac{\partial}{\partial x}(\rho U)dx = 0 \tag{4.6}$$

$\rho U = const$

Express,

F=ρU (term of convection)

D=$\Gamma/\delta x$ (term of diffusion)

Replacing into Eq. (4.4) becomes,

$$a_p\lambda_{\boldsymbol{p}} = a_E\lambda_E + a_W\lambda_W \tag{4.7}$$

Where,

$$\left.\begin{aligned} a_E &= D_e - 0.5F_e \\ a_W &= D_w - 0.5F_w \\ a_p &= a_E + a_W + F_e - F_w = a_E + a_W \end{aligned}\right\} \tag{4.8}$$

II. Up wind differencing scheme

The velocity is checked, and the value of the scalar variable is assigned based on its direction, i.e.

$$\left.\begin{aligned} \lambda_e &= \lambda_p \quad For\ F_e > 0 \\ \lambda_e &= \lambda_E \quad For\ F_e < 0 \end{aligned}\right\} \tag{4.9}$$

Through the use of symbolism $\langle A, B\rangle$ to indicate which of A or B is larger

`

$$F_e\,\lambda_e = \lambda_p\langle F_e, 0\rangle - \lambda_E\langle -F_e, 0\rangle \tag{4.10}$$

By using the upwind scheme, the coefficient of Eq.(4.8) become,

$$\left.\begin{aligned} a_E &= D_e + \langle -F_e, 0\rangle \\ a_W &= D_w + \langle F_w, 0\rangle \\ a_p &= a_E + a_W + F_e - F_w = a_E + a_W \end{aligned}\right\} \tag{4.11}$$

4.3.2. Basic Rules for Convergence

Basic guidelines for calculating control volumes should be followed for optimal results.

- Volume-control face-plate homogeneity .
- Coefficients must have positive values. .
- Aggregate of adjacent factors may be equal to (a_p).

4.3.3. Modified Scheme

a) The values of the convection and diffusion coefficients at the scheme epicenter are:

$a_E = D_e - \ O.5F_e$

$a_W = D_W - 0.5F_w$

For $a_E, and\ a_W > 0$

$|F| < 2\ D$

The solution is valid only for if $\frac{\rho U\delta}{\Gamma}$ Peclet number is given by $p_e =$

(When very small Reynolds number) -2≤ $p_e \leq 2$

To the upwind scheme,

$a_E = D_e + \langle -F_e, o\rangle$

$a_W = D_w + \langle F_w, o\rangle$

`

This technique only works effectively at high Reynolds numbers, and the incorrect diffusion is a major drawback.

(b) Hybrid schemes

At small Re values, this implementation is similar to the central procedure, while at large Re values, it is similar to the upwind method. If on the other hand, the diffusion term is nullified, the coefficient in Eq. (4.7) becomes:

$$\left.\begin{aligned} a_E &= \langle o, D_e - 0.5|F_e|\rangle + \langle -F_e, o\rangle \\ a_W &= \langle o, D_W - 0.5|F_w|\rangle + \langle F_w, o\rangle \\ a_p &= a_E + a_W + F_e - F_W = a_E + a_W \end{aligned}\right\} \quad (4.12)$$

Because the hybrid technique can provide a sensible balancing of thrift and accuracy (time for computing), it is employed for the following auguring in the current analysis.

4.3.4. Two - Dimensional Discretization.

An equation of transport in its most general form can be written as,

$$\frac{\partial}{\partial xi}(J_i) = S_\lambda \quad (4.13)$$

Where

$$J_i = \rho U_i \lambda - \Gamma_\lambda \frac{\partial \lambda}{\partial x_i} \quad (4.14)$$

J_i Denotes all diffusion and convection fluxes. The source term's linear expression can be written as,

$$S_\lambda = b\lambda_p + c \quad (4.15)$$

Integrate using the control volume in figures (4-2) and (4-3) to get:

`

$$J_e - J_w + J_n - J_s = (b\lambda_p + c)\Delta V \tag{4.16}$$

Where, **Δ**V=**Δ**x **Δ**y

Integrate the continuity to get,

$$F_e - F_w + F_n - F_s = 0 \tag{4.17}$$

F is shorthand for the air velocity at the control face intersection. . The discretization of two- dimensional equation is contains the following text:

$$\sum_i a_i - b)_{\lambda_p} = \sum_i a_i\lambda_i + C \tag{4.18}$$

Where,

$$\sum_i a_i = a_p = a_E + a_W + a_N + a_S$$
$$\sum_i a_i\lambda_i = a_E\lambda_E + a_W\lambda_W + a_N\lambda_N + a_S\lambda_S$$

$$\left.\begin{aligned} b &= S_p\Delta V \\ C &= S_u\Delta V \end{aligned}\right\} \tag{4.19}$$

S_p And S_u are factors that can be calculated using a finite difference convergence of (S_λ). To resolve this, use any scheme to get the magnitude of (a_i) by using the upwind technique while:

$$\left.\begin{aligned} a_E &= D_e + \langle O, -F_e\rangle \\ a_W &= D_W + \langle F_w, O\rangle \\ a_N &= D_n + \langle O, -F_n\rangle \\ a_S &= D_s + \langle F_s, O\rangle \end{aligned}\right\} \tag{4.20}$$

In scientific notation, the terms convective and diffusive fluxes are represented as,

`

$$\left.\begin{array}{l} F_e = (\rho U)_e \Delta y \Delta z \, , D_e = \Gamma_e \Delta y \Delta z / \delta x_e \\ F_w = (\rho U)_w \Delta y \Delta z \, , D_w = \Gamma_w \Delta y \Delta z / \delta x_w \\ F_s = (\rho V)_s \Delta x \Delta z \, , D_s = \Gamma_s \Delta x \Delta z / \delta y_s \\ F_n = (\rho V)_n \Delta x \Delta z \, , D_n = \Gamma_n \Delta x \Delta z / \delta y_n \end{array}\right\} \quad (4.21)$$

All the coefficient in Eq (4.20) and (4.21) In order to resolve (U, V, W, T, K and $\boldsymbol{\mathcal{E}}$)

4.4. PARAMETERIZATION EQUATION SOLUTION

4.4.1. Parameterization Mode of Pressure - Linked

A connection must be made between the velocity and pressure fields to satisfy the continuity condition. SIMPLE (Semi-Implicit-Methods for Pressure-Linked Equation) has been used to accomplish this [68]. The discretized equations forU_e, V_n, and W_t. at points (e, n, and t) ,after extracting the pressure terms from the sourcing terms coefficient Su are as follow:

$$\left.\begin{array}{l} a_e U_e = \sum_i a_i U_i + c + \left(P_p - P_E\right) \Delta y \Delta z \\ a_n V_n = \sum_i a_i V_i + c + (P_p - P_N) \Delta x \Delta z \end{array}\right\} \quad (4.22)$$

In the event that the grid pressures are accurate, , the terms in Eq. (4.22) can all be fulfilled mass. As a result, At the outset, the magnitudes of the pressure and the velocity are assessed. , and continuity has not yet reached satiety. As a result , pressure modification is required to find a solution.The (SIMPLE algorithm) presuppose,

$$\left.\begin{array}{l} P = P' + P^* \\ U = U' + U^* \\ V = V' + V^* \end{array}\right\} \quad (4.23)$$

Where a star indicates a predicted value and the magnitude of the alteration required maintaining continuity. The following are the discretization of the guessed variables:

$$\left.\begin{array}{l} a_e U_e^* = \sum_i a_i U_i^* + c + (P_p^* - P_E^*) \Delta y \Delta z \\ a_n V_n^* = \sum_i a_i V_i^* + c + (P_p^* - P_N^*) \Delta x \Delta z \end{array}\right\} \quad (4.24)$$

`

When Eq (4.22) is subtracted from Eq (4.24) the result is,

$$\left.\begin{aligned} a_e U'_e &= \sum_i a_i U'_i + c + \left(P'_p - P'_E\right)\Delta y \Delta z \\ a_n V'_n &= \sum_i a_i V'_i + c + \left(P'_p - P'_N\right)\Delta x \Delta z \end{aligned}\right\} \quad (4.25)$$

For computational convenience, $\sum aiUi'$ $\sum aiVi'$ and $\sum aiWi'$ are set to zero [68] will get,

$$\left.\begin{aligned} U_e &= U_e^* + \Delta y \Delta z / a_e (P'_p - P'_E) \\ V_n &= V'_n + \Delta x \Delta z / a_n (P'_p - P'_N) \end{aligned}\right\} \quad (4.26)$$

Continuity can be achieved by substituting the aforementioned equations. ,

$$\sum_i a_i P'_p = \sum_i a_i P'_i + \text{c} \quad (4.27)$$

Where

$\sum_i a_i = a_E + a_W + a_N + a_S$

$\sum_{\boldsymbol{i}} a_{\boldsymbol{i}} P'_{\boldsymbol{p}} = \boldsymbol{a_E} P'_E + a_W P'_W + a_N P'_N + a_S P'_S$

$a_E = (\rho_e / a_e)(\Delta y \Delta z)^2 \quad \& \; a_W = (\rho_w / a_w)(\Delta y \Delta z)^2$

$a_N = (\rho_n / a_n)(\Delta x \Delta z)^2 \quad \& \; a_S = (\rho_s / a_s)(\Delta x \Delta z)^2$

$\text{C} = F_w^* - F_e^* + F_s^* - F_n^*$

$F_e^* = (\rho U^*)_e \Delta y \Delta z \quad \& \; F_w^* = (\rho U^*)_w \Delta y \Delta z$

$F_n^* = (\rho V^*)_n \Delta x \Delta z \quad \& \; F_s^* = (\rho V^*)_s \Delta x \Delta z$

The SIMPLE method is briefly described as:

1) Assume appropriate initial conditions.
2) Estimate the probability that P^*
3) Resolve the momentum Eq. (4.24) to get U^* , V^* W^* .
4) Find the P' from Eq. (4.27)
5) Add P' to P^* to obtain pressure field.
6) Velocity components U, V *and* W have been calculated from Eq. (4.26).
7) Using the general Eq. (4.18to find the factors affecting the answer for (U, V, W, T, k, and $\boldsymbol{\mathcal{E}}$).

`

8) Make the current pressure P the predicted pressure P*., retrace your steps (3) and reiterate the process until the convergence is satisfied.

In order to keep everything on the same path caused by a non-linear solution, it is critical to under–relaxation the solution by:

$$\lambda_p^r = R\lambda_p(1-\alpha)\lambda_p^0 \quad (4.28)$$

Where

λ_p^r = New under –relaxed value of λ_p

λ_p = Magnitude of anterior iteration.

λ_p^0= acquired value.

R= reduction in the factor of relaxation ($0< \alpha \leq 1$)

For(R= 0.5) of the (U, V, W, K and $\boldsymbol{\varepsilon}$), while (R=1) for temperature (T) and pressure (P).

4.4.2. ACCURACY

In terms of solution precision, we have based on the "Convergence Criterion," which is satisfied by satisfying one of the following [67]:

1) The accepted residual value.
2) Accepted value variance in two subsequent iterations.

Because it includes residual source assurance after any iteration, the aforementioned approach is preferred. The solution is declared convergent when the maximum remain for variable is lower than the convergence criterion. On nodal (n), the convergence variable ($\boldsymbol{\lambda}$) is as follows:

$$\frac{|\lambda_n - \lambda_{n-1}|}{\lambda_n} \leq \boldsymbol{\varepsilon}$$

We choose $\boldsymbol{\varepsilon}$= 5 x 10^{-3}

`

The remain source is considered the balance of mass on the control volume in the pressure correction equation.

4.5. SUBROUTINES CALCULATION (MOMENTUM EQUATION)

The discretized formulation of the momentum equations is represented The SIMPLE method is briefly described as resented by the subroutines CALCU and CALCV. The momentum equation in the x direction is as follows:

$$\rho\frac{\partial u}{\partial t}+\rho u\frac{\partial u}{\partial x}+\rho v\frac{\partial u}{\partial y}=-\frac{\partial p}{\partial x}+\sqrt{\frac{Pr}{Ra}}\frac{\partial}{\partial x}\left[(\mu+\mu_t)\frac{\partial u}{\partial x}\right]+\sqrt{\frac{Pr}{Ra}}\frac{\partial}{\partial y}\left[(\mu+\mu_t)\frac{\partial u}{\partial y}\right]+\sqrt{\frac{Pr}{Ra}}\frac{\partial}{\partial x}\left[(\mu+\mu_t)\left(\frac{\partial u}{\partial x}+\frac{\partial v}{\partial y}\right)\right] \quad (4.29)$$

For an incompressible fluid since the density does not change with time the term:

$$\sqrt{\frac{Pr}{Ra}}\frac{\partial}{\partial x}\left[(\mu+\mu_t)\left(\frac{\partial u}{\partial x}+\frac{\partial v}{\partial y}\right)\right] \quad (4.30)$$

4.6. PROGRAM FLOW CHART

Detailed problem-solving steps are depicted in Figure 4.5, which is a flowchart. In this section, a mathematical model is presented and developed. As the name suggests, this type is employed for flat plate. A solar collector with just one cover glass and a parallel channel configuration. Any flat solar collector with a single glass cover can be used as-is because all relevant physical dimensions can be entered as input;

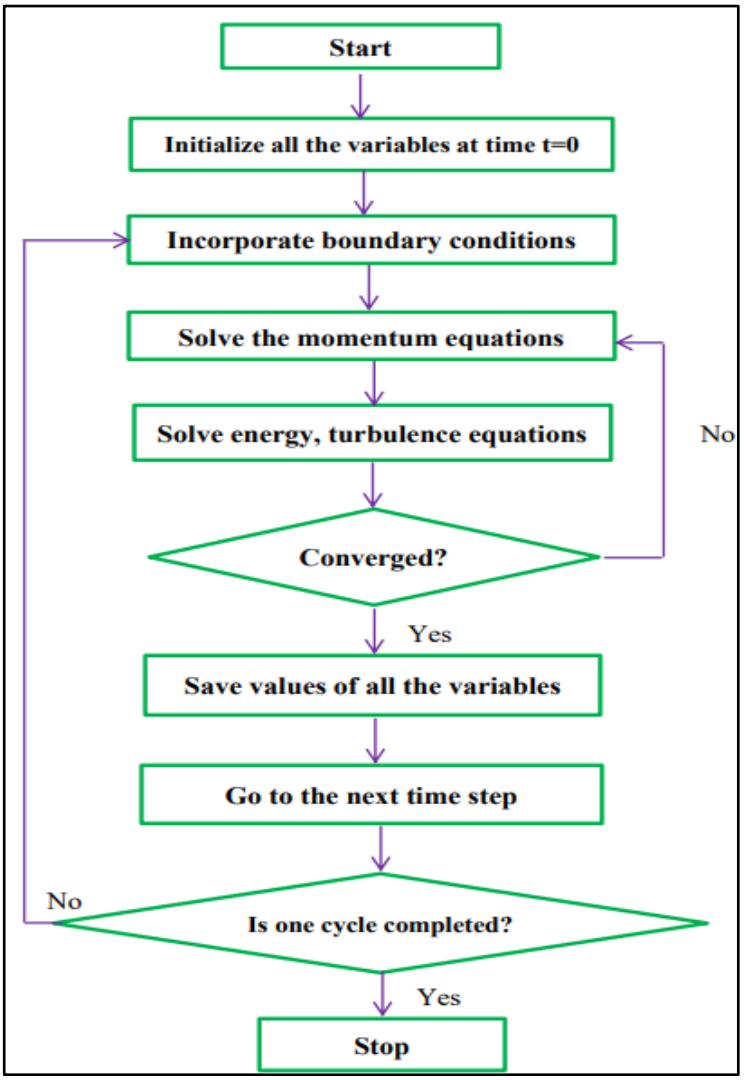

Figure 4.5. Flow chart of the numerical Algorithm.

`

PART 5

RESULTS AND DISCUSSION

5.1. INTRODUCTION

This part presented the improved results of the thermal behavior, through the single-pass solar air collector .the numerical analysis was studied in certain conditions through the attached Table 5.1 depending on Iraq's climatic conditions at 10 may at 12pm, by taking a different values for the pulsating wave, through changing the amplitude (Amp) and frequency (F) values, the results were obtained from FORTRAN 90 code and CFD software, using finite-volume scheme to derive the Navier stocks equations.

Then we can note the improvements that were made in channel, during the values of the thermal performance factor (TPF), the values of average Nusselt number (Nu^{-}), the value of the friction factor (f).and by adopting specific values of Reynolds number (7500, 10000, 12500, 15000).

Table 5.1. Boundary conditions.

Boundary conditions	Values
Solar irradiance	550 W/m^2
Ambient temperature	30 ^{o}C
Ambient velocity	5.4 m/s

5.2. THE EFFECT OF CHANGING THE AMPLITUDE VALUE (AMP)

In this case four different values of the wave amplitude (Amp) were taken as (0.0, 0.25, 0.5, and 0.75). The frequency value is fixed (St=0.2), by taking four values of Reynolds

`

number, considering that the time is one hour for the peak, the thermal and numerical analysis were studied and clarified through the attached drawing.

5.2.1. Effect of Changing the Amplitude Value on the Average Nusselt Number

It was observed in this case that when the value of the amplitude increases, the value of the average Nusselt number improves, and since the relationship is direct between Re and Nu, the valu e of Nusselt number improves and search within the range (44-98) with the value of Reynolds (15000).

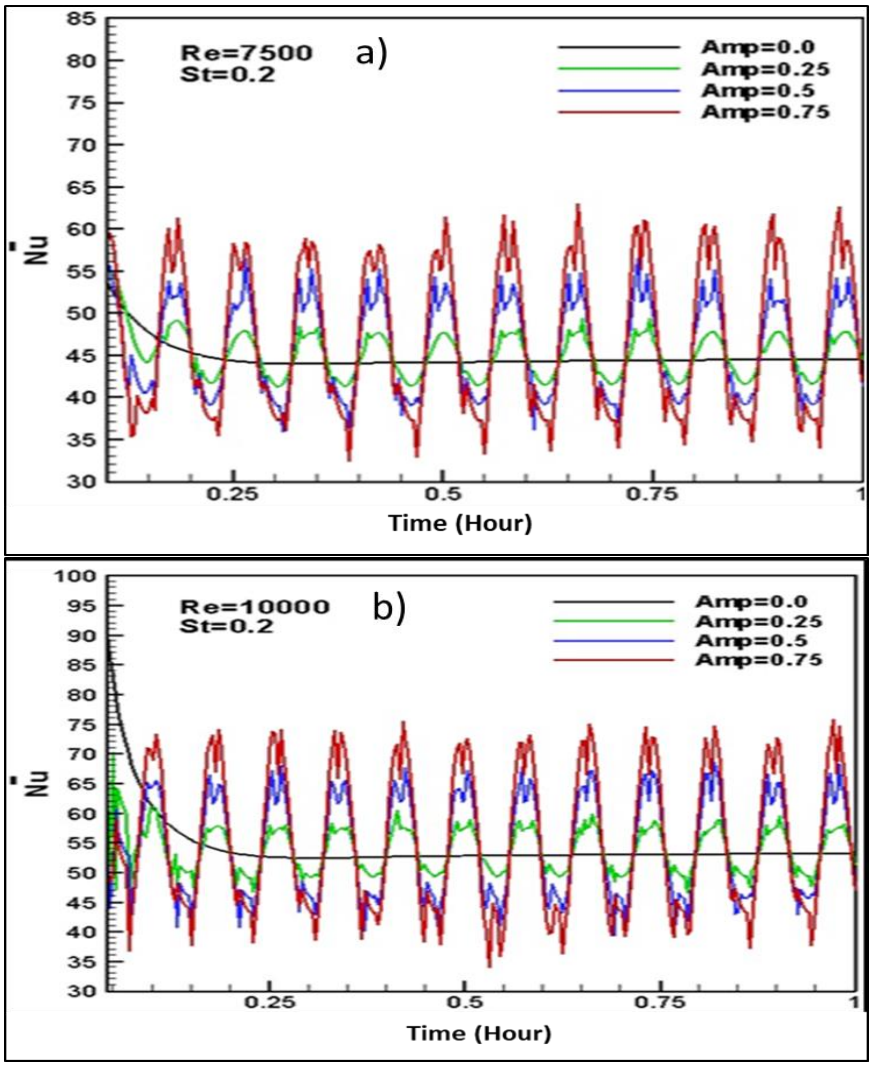

`

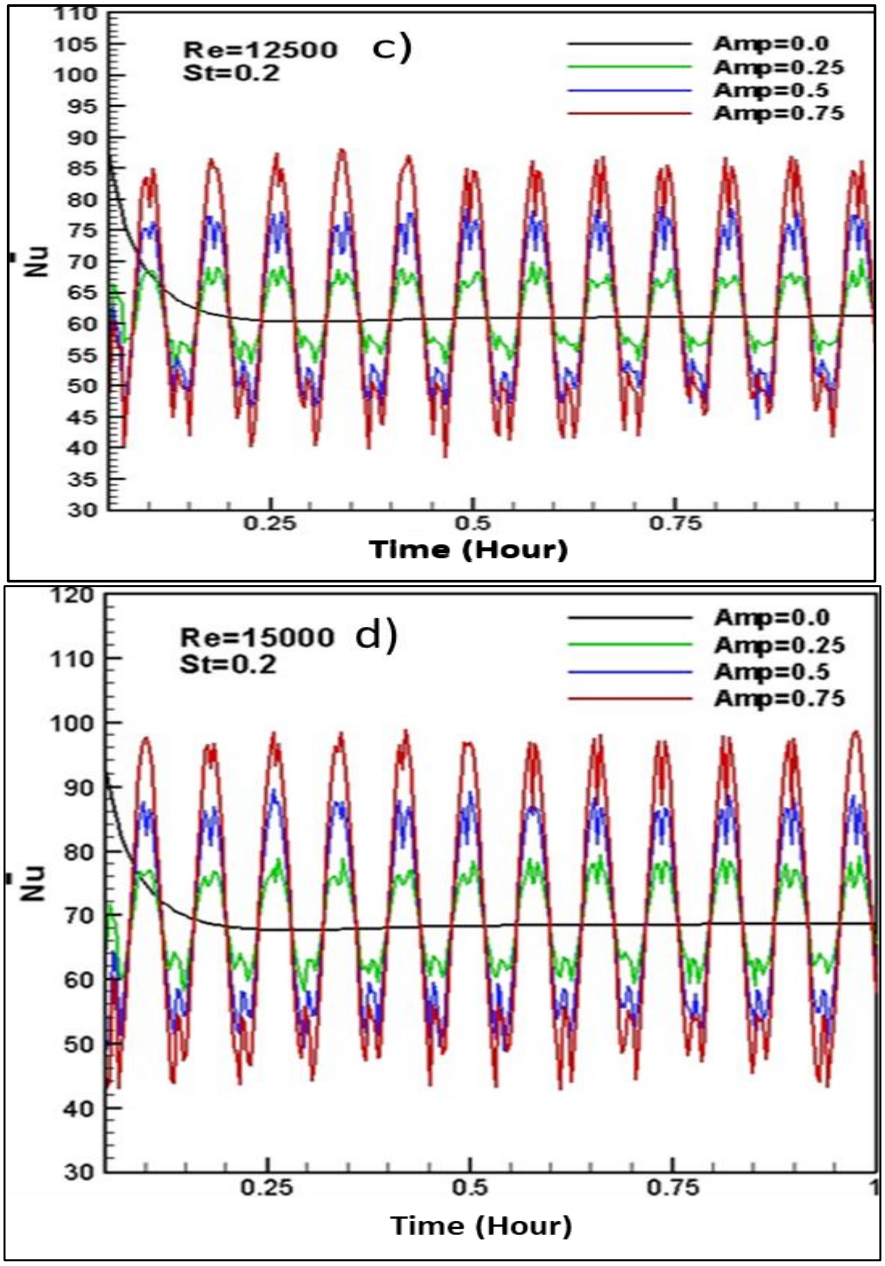

Figure 5.1. Variation average Nusselt number with time at various amplitude and Reynolds number. a) Re =7500 b) Re =10000 c) Re=12500 d) 15000.

Table 5.2. Extent of Nusselt numbers values relative to Reynolds number.

Reynolds number	Average Nusselt number
7500	32-62
10000	33-75
12500	38-88
15000	44-98

`

5.2.2. Effect of Changing Amplitude on Thermal Performance Factor (TPF)

The thermal performance factor is a measure of thermal efficiency of the solar air collector, whereas this factor approaches (TPF≥1), the system performance becomes more effective, based on the results in figure (5-2), by changing the amplitude values and stabilizing the frequency value (St),it was found that by increasing the amplitude ,the value of the thermal performance factor increases expressly with the increase of the Reynolds number ,where it was found that the highest value of TPF at Re =15000, the Table 5.3 shows below the extent of the TPF at the peak and the bottom of amplitude.

Table 5.3. Extent of TPF values relative to Reynolds.

Reynolds number	**TPF**
7500	(0.3-2.1)
10000	(0.4-2.6)
12500	(0.5-3)
15000	(0.5-3.5)

Figure 5.2. Variation of TPF with time at various amplitude and Reynolds number.

`

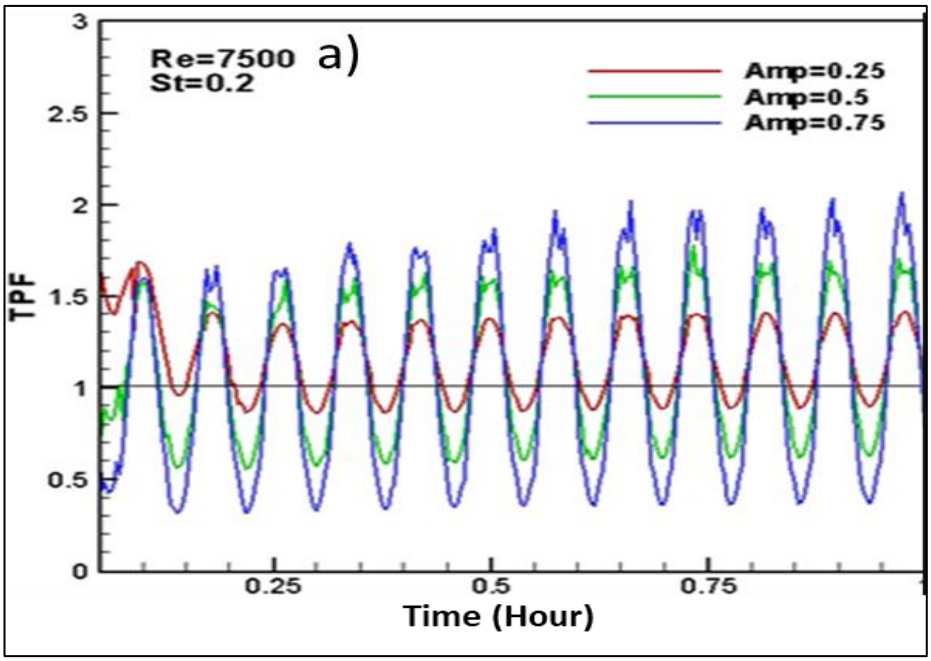
Re=7500
St=0.2
a)
Amp=0.25
Amp=0.5
Amp=0.75
TPF
Time (Hour)
0
0.5
1
1.5
2
2.5
3
0.25
0.5
0.75

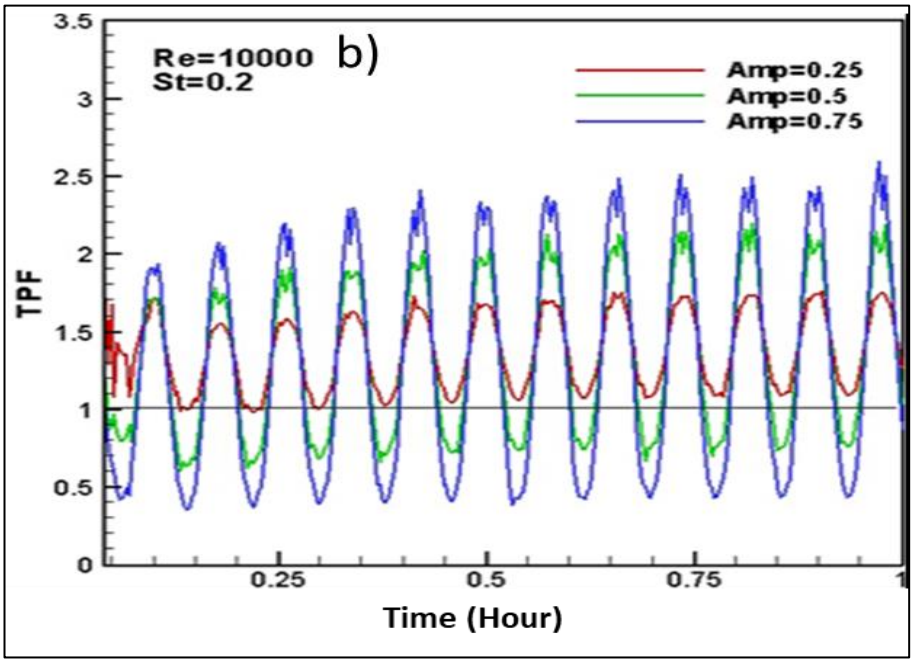
Re=10000
St=0.2
b)
Amp=0.25
Amp=0.5
Amp=0.75
TPF
Time (Hour)
0
0.5
1
1.5
2
2.5
3
3.5
0.25
0.5
0.75

`

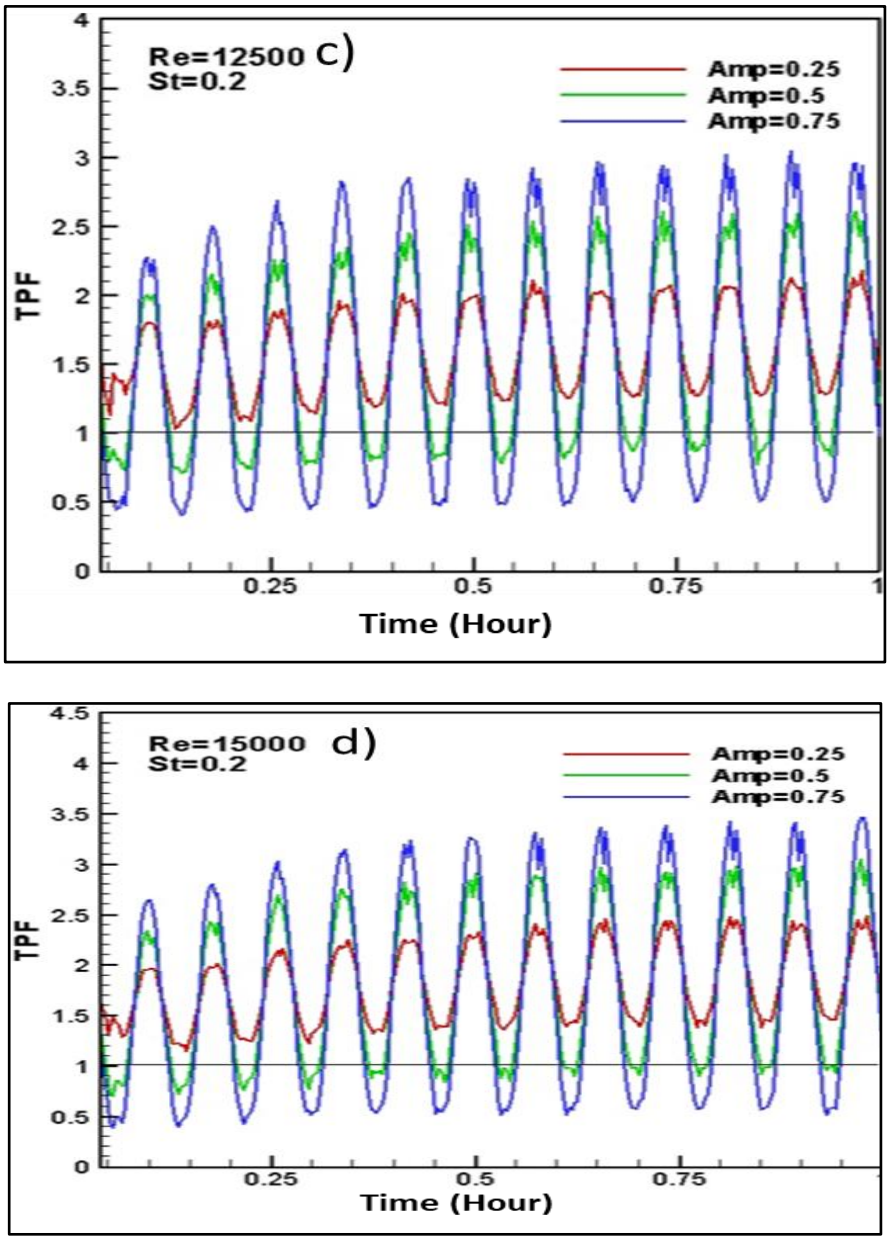

Figures 5.2. Variation of TPF with time at various amplitude and Reynolds number: (a) Re =7500, (b) Re =10000,(c) Re=12500 and (d) Re=15000

5.2.3. Effect of Changing Amplitude on Friction Coefficient (*f*)

The coefficient of friction is one of the important criteria in the heat transfer, as it negatively affects the heat transfer in the air flow when it is value increases, and the coefficient of friction is affected by several variables such as Reynolds number and nusselt number ,as it has an inverse relationship with both of Reynolds and nusselt number, so researcher try to reduce the value of friction factor by increasing Reynolds

`

number, and since our research revolves around the pulsating flow ,the effect of the coefficient of friction must be found at variable values of amplitude and with stability of the frequency values ,as it was observed that increasing the values of amplitude leads to an increase the values of friction factor ,but the value of friction coefficient begins to decrease when increasing Reynolds number at the same amplitude ,so we found that the best value was obtained at Re=15000, figure (5-3) below shows the values of the coefficient of friction and it is effect through changing the values of amplitude.

Table 5.4. Extent of friction factor values related to Reynolds number.

Reynolds number	**Friction coefficient**
7500	(0.04 – 1.2)
10000	(0.04 – 1.12)
12500	(0.04 – 1.04)
15000	(0.04 – 0.88)

Figure 5.4 Variation of friction coefficient with time at various amplitude and Reynolds number.

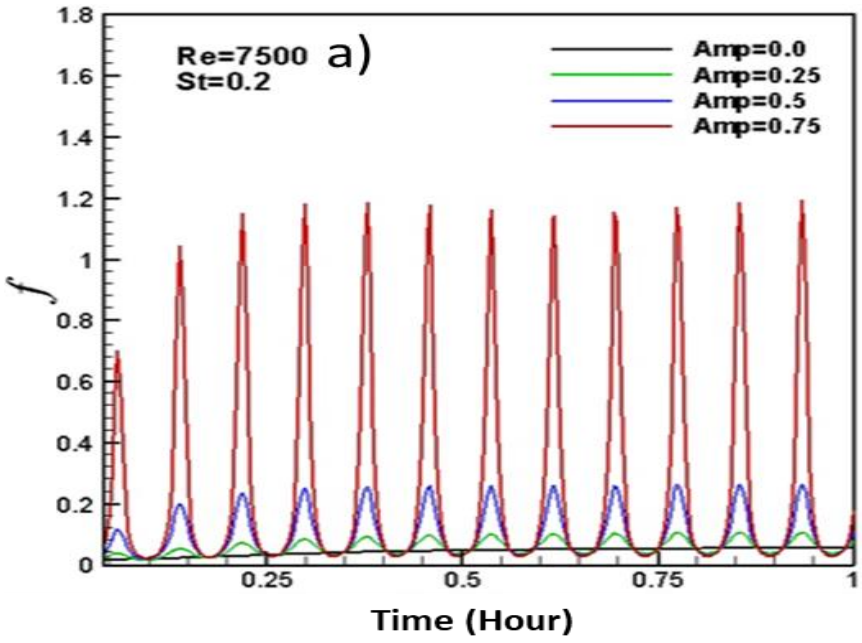

`

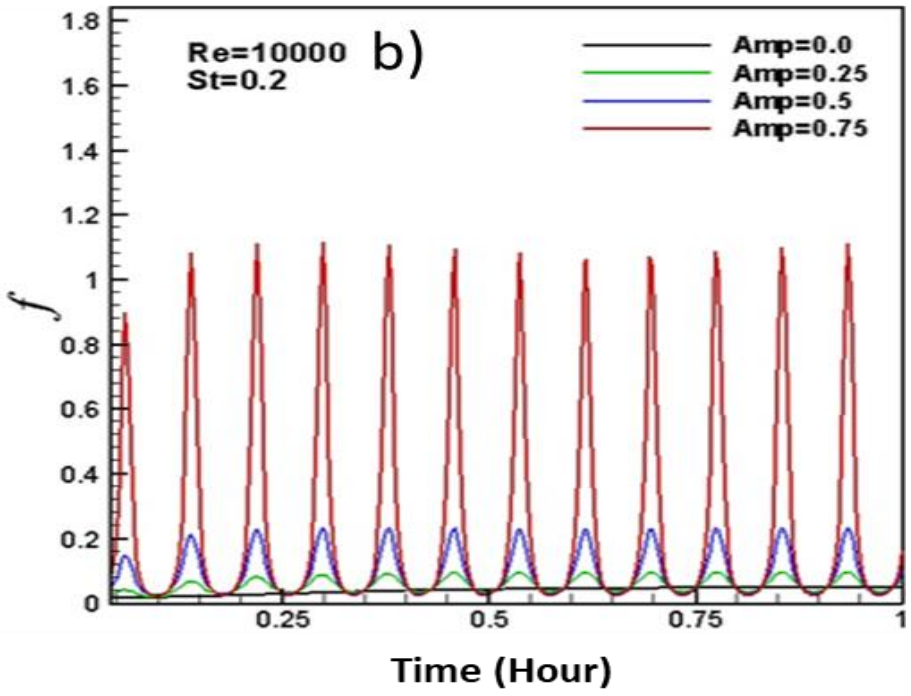
Re=10000
St=0.2
b)
Amp=0.0
Amp=0.25
Amp=0.5
Amp=0.75
f
Time (Hour)

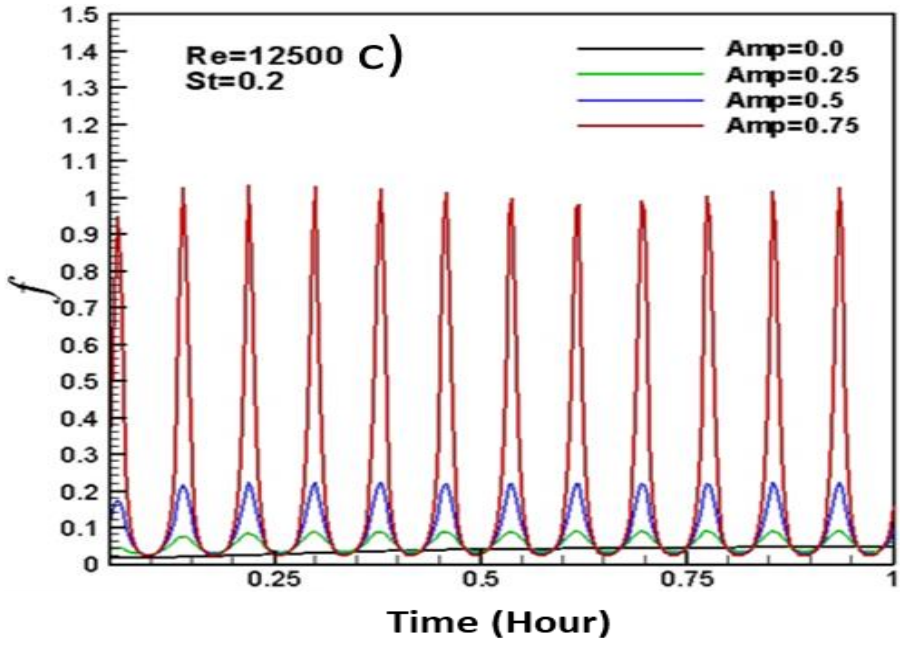
Re=12500
St=0.2
c)
Amp=0.0
Amp=0.25
Amp=0.5
Amp=0.75
f
Time (Hour)

`

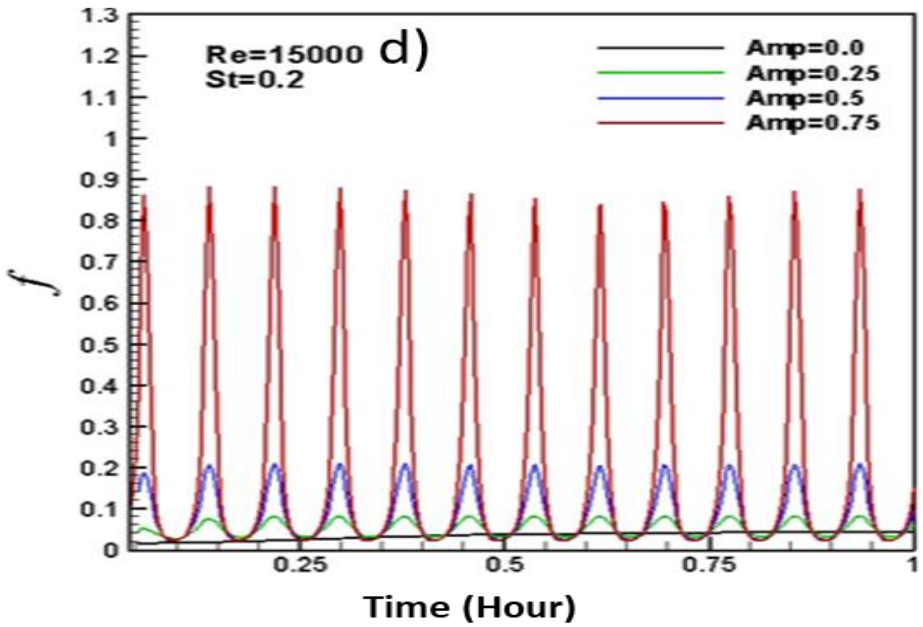

Figure 5.3. Variation of friction coefficient with time at various amplitude and Reynolds number: (a) Re=7500 , (b) Re=10000 , (c) Re=12500, and (d) Re=15000.

5.2.4. The Effect of Changing the Amplitude on Temperature Distribution

Through Figure 5.4 below, we show the effect of changing amplitude values with constant frequency on the distribution of temperatures in the solar collector channel within a full hour ,we observed that the absorber temperature improves with an increase ranging from (20-30 °C), as well as improved air temperature passing through the channel from (10-20 °C), but we conclude that increasing the value of Reynolds number adversely affects the temperatures, the more the Reynolds number value the lower the curve of wave for both absorber and fluid.

`

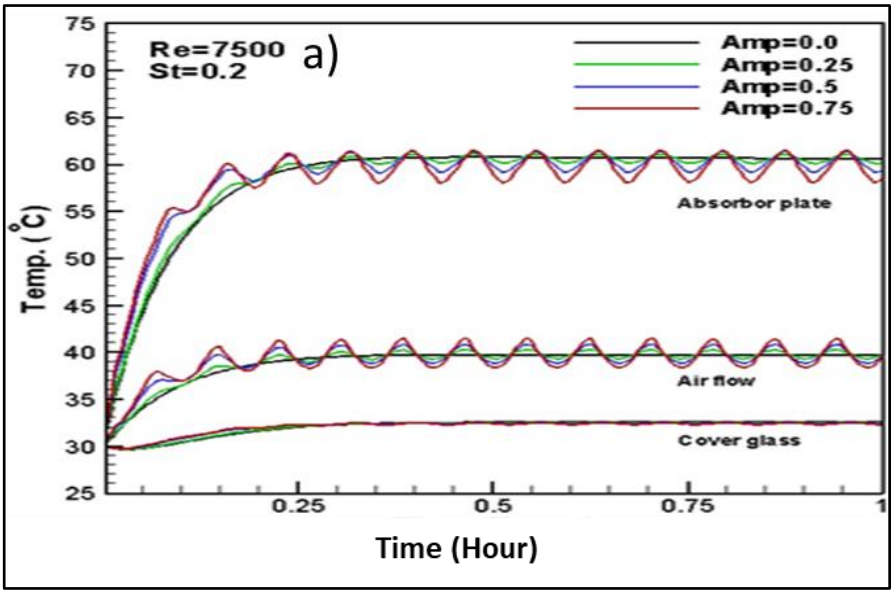
Re=7500
St=0.2
a)
Amp=0.0
Amp=0.25
Amp=0.5
Amp=0.75
Absorbor plate
Air flow
Cover glass
Temp.(°C)
Time (Hour)

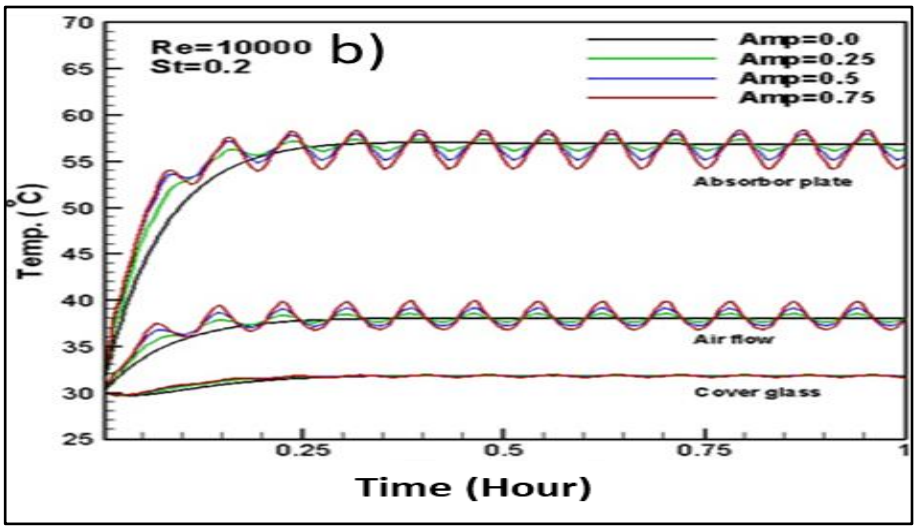
Re=10000
St=0.2
b)
Amp=0.0
Amp=0.25
Amp=0.5
Amp=0.75
Absorbor plate
Air flow
Cover glass
Temp.(°C)
Time (Hour)

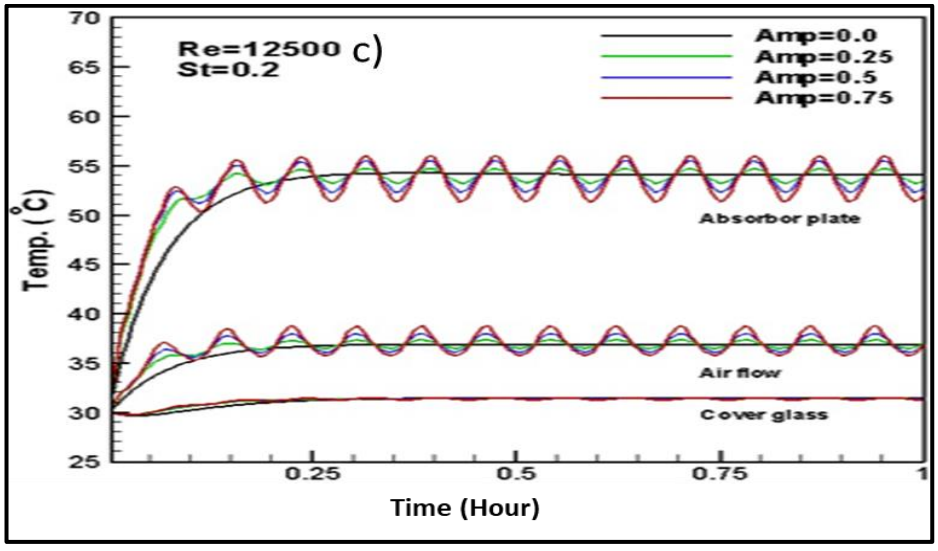
Re=12500
St=0.2
c)
Amp=0.0
Amp=0.25
Amp=0.5
Amp=0.75
Absorbor plate
Air flow
Cover glass
Temp.(°C)
Time (Hour)

`

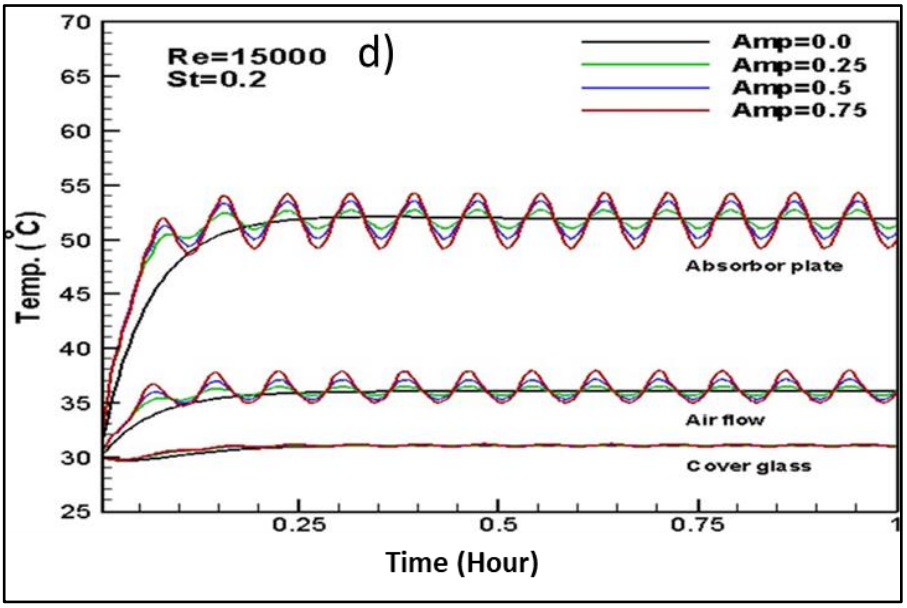

Figure 5.4. Variation of temperature distribution in absorber and airflow with different amplitude, at (a) Re=7500 ,(b) Re=10000 , (c) Re=12500 ,and (d) Re=15000.

5.3. INFLUENCE OF CHANGING FREQUENCY VALUES

Through this part we studied the effect of changing frequency values on heat transfer properties during the solar collector channel where four frequency values were taken (0.2, 0.4, 0.6, and 0.8)respectively ,where we fixed amplitude value at (0.5) , where prediction show that the frequency value has an obvious effect on the air flow of the friction coefficient and thermal performance of the solar collector ,the impact of Reynolds number changing values has also been show to play a significant role in temperature distribution.as well as reducing the value of losses to the system, since flow is turbulent the more Reynolds the higher the solar heater performance improves significantly at certain values of amplitude .

5.3.1. Influence of Friction Coefficient by Changing Pulse Frequency Values

From Figure 5.5 below, it was found the effect of changing the values of the pulse frequency is much better than the change of the values of the pulse amplitude with respect of coefficient friction , where good proportions were obtained by increasing the value of (St), and since the flow is turbulent, then by increasing the Reynolds

`

number values, the value of the coefficient friction improves by significant amount and is observed at the highest value of Reynolds (15000),the attached table(5-5)shows the values of the friction coefficient obtained for the highest and lowest crest of the wave.

Table 5.5. Friction coefficient ratios obtained at Reynolds number are different.

Reynolds number	Friction factor
7500	(0.03 – 0.26)
10000	(0.03 – 0.25)
12500	(0.025 – 0.22)
15000	(0.025 – 0.21)

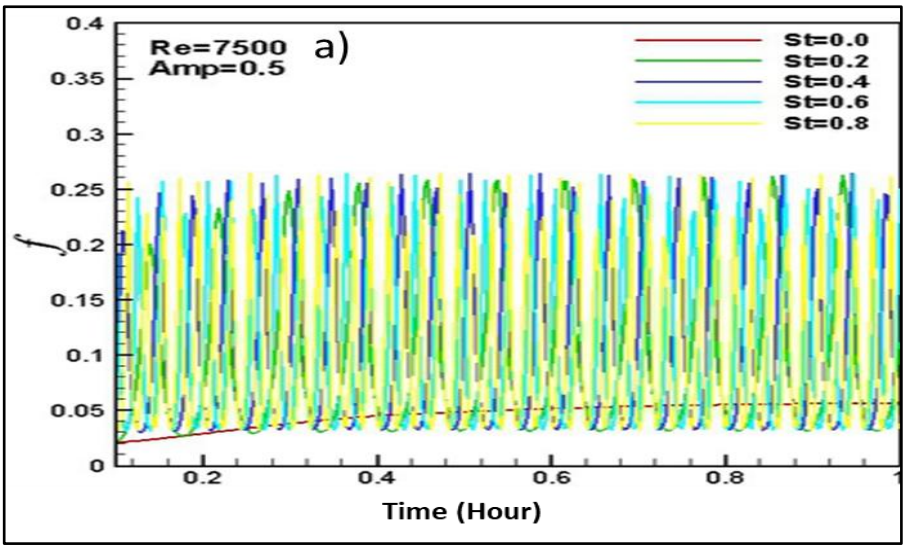

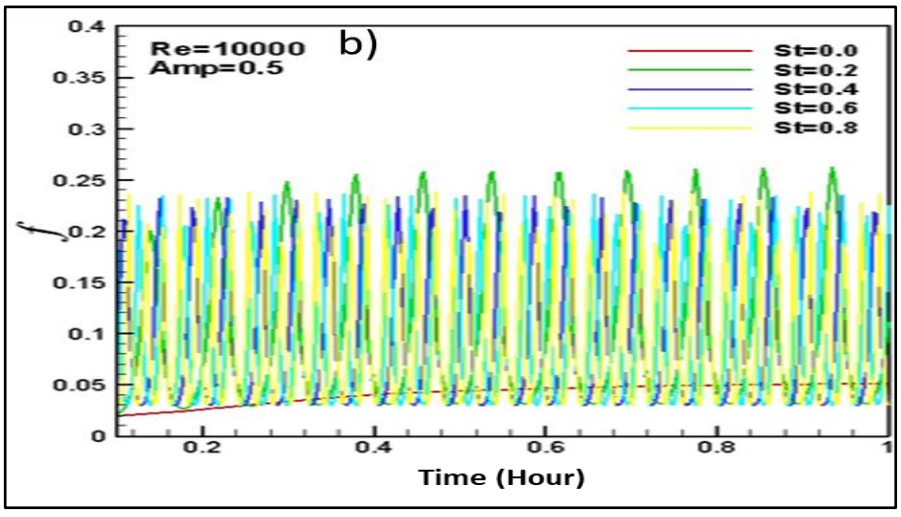

`

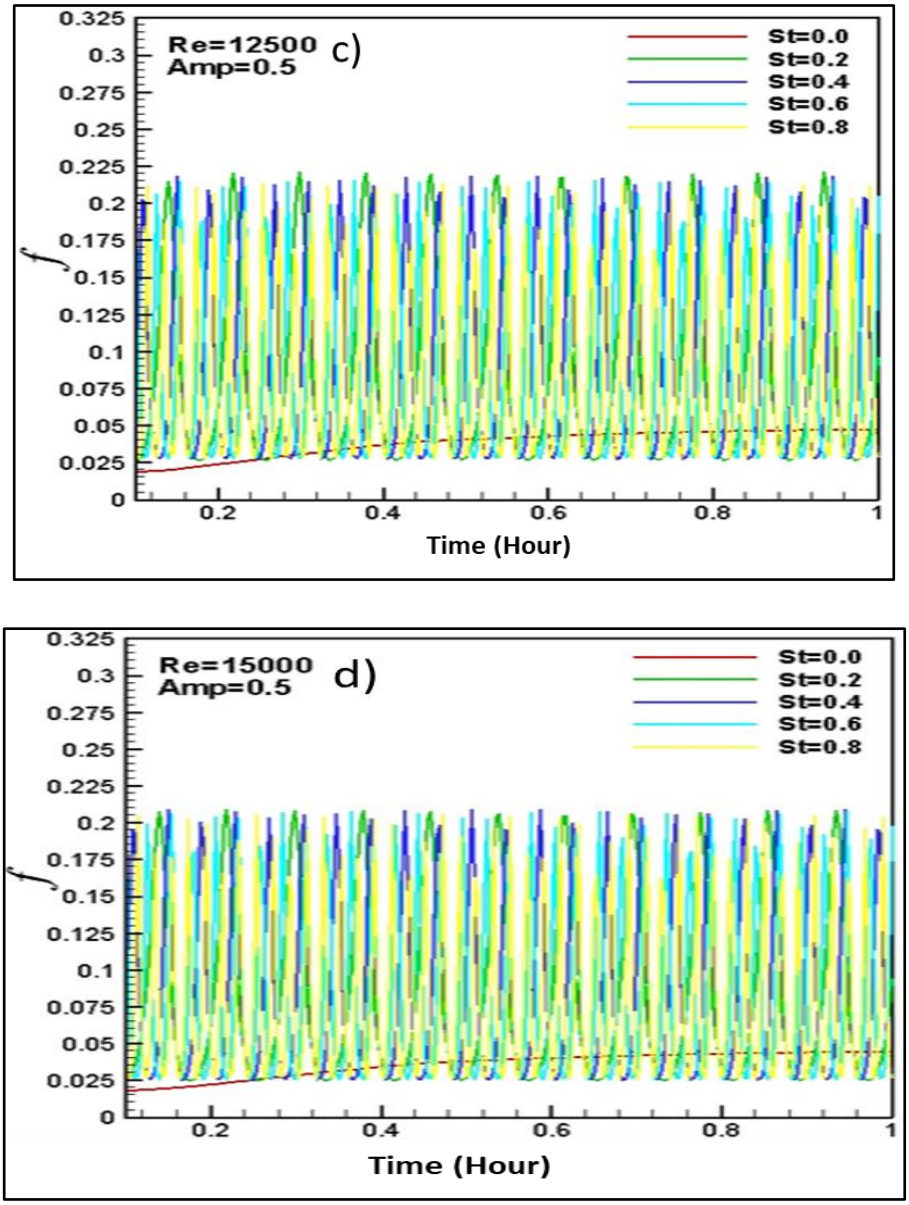

Figure 5.5. Variation friction factor with time at different frequency,at (a)Re=7500, (b)Re=10000 , (c)Re=12500 , and (d)Re=15000

5.3.2. Influence of Average Nusselt Number by Changing Pulse Frequency Values

Nusselt number is an important factor in heat transfer in solar heater, helping to promote heat transfer by convection load, because the correlation with the heat transfer coefficient , wherever the value of nusselt number has improved the heat transfer coefficient has promote, and since nusselt number is considered to be a function of Reynolds number the higher Re the better the value of Nu , in figure(5-6) below it we

`

didn’t get the highest Nu but we got the best range at the bottom and the peak of wave, the attached Table 5.6 shows the range of the obtained nusselt number.

Table 5.6. Range of nusselt number related to Reynolds number.

Reynolds number	Nusselt number
7500	(34 – 56)
10000	(36 – 68)
12500	(44 – 78)
15000	(48 – 88)

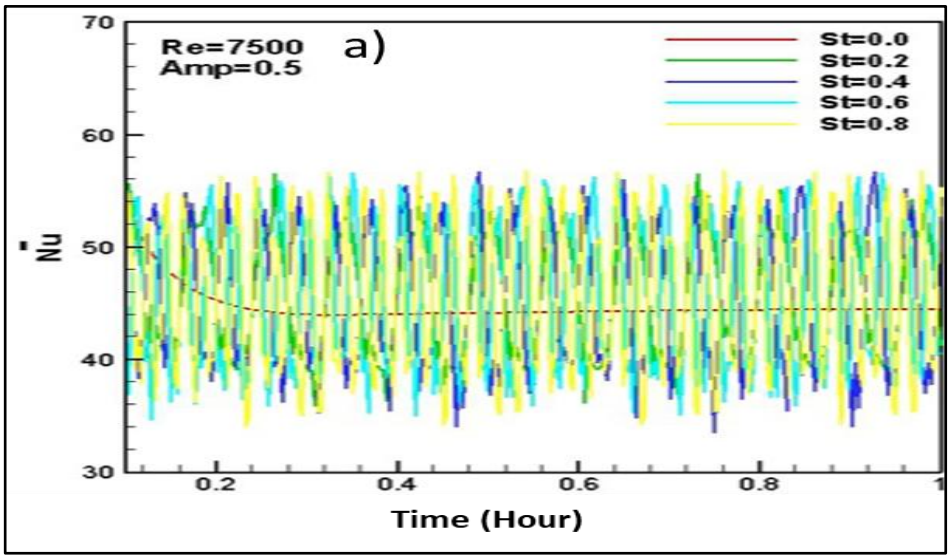

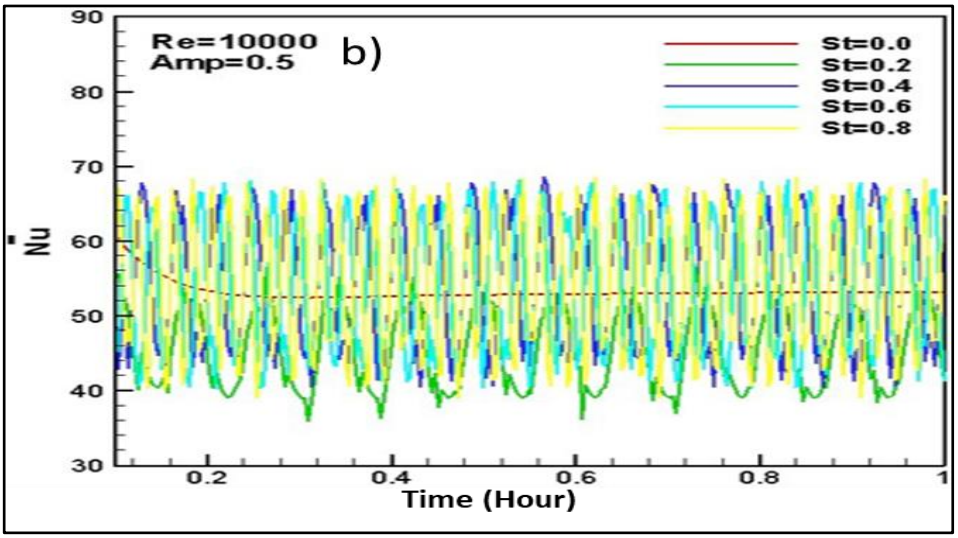

`

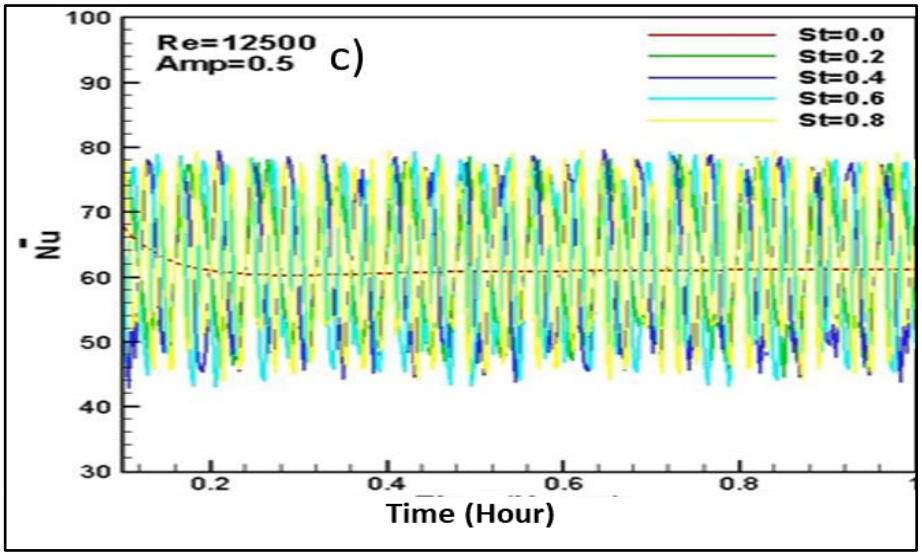

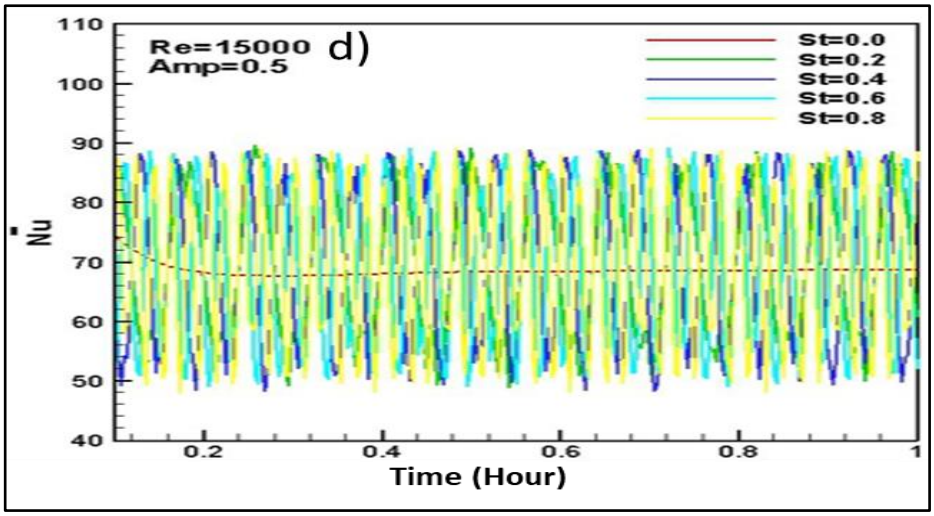

Figures 5.6. Variation nusselt number with time at different frequency, with (a)Re=7500 , (b)Re=10000 , (c)Re=12500, and (d)Re=15000.

5.3.3. Influence of Thermal Performance Factor by Changing Frequency Values

Thermal performance factor is an significant factor to measure the power of a solar heater , when the amount of heat gained increases the value of the thermal performance factor increases to approach (1) , the attached figure(5-7) shows the impact of the value of the pulsating frequency change on the performance factor, as the predictions proved that there is a significant improvement in the value of the performance factor ,where there is an appreciable difference between the previous case, we observed an raise in the waveband height to approach more than 1 when the time period raises, and since the raise in Reynolds number is positively reflected on the increase in the mean of

`

thermal performance value, we observe the best value at highest Reynolds number , Table 5.7 shows rates of thermal performance values.

Table 5.7. Range of thermal performance factor related to Reynolds number.

Reynolds number	TPF
7500	(0.5 – 1.8)
10000	(0.6 – 2.3)
12500	(0.7 – 2.6)
15000	(0.8 – 3)

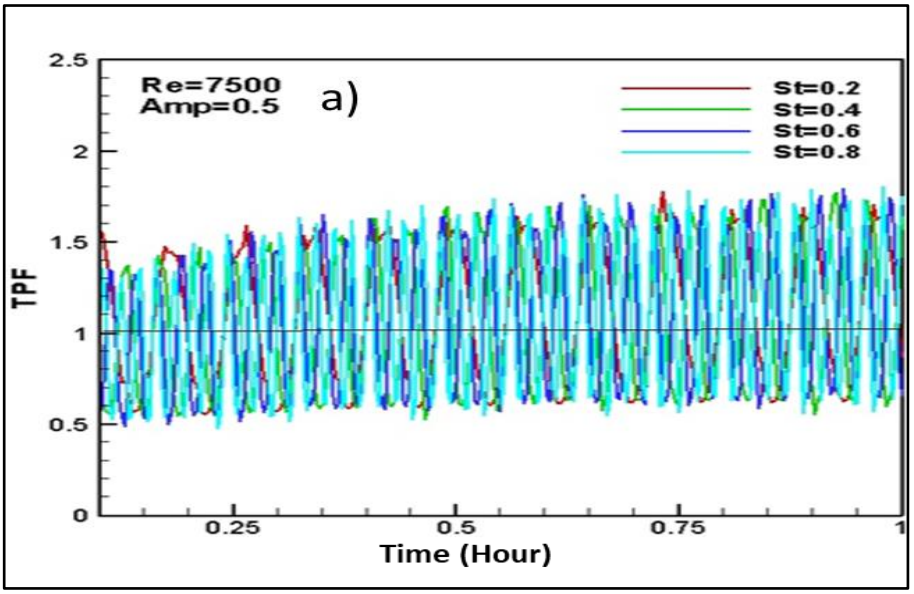

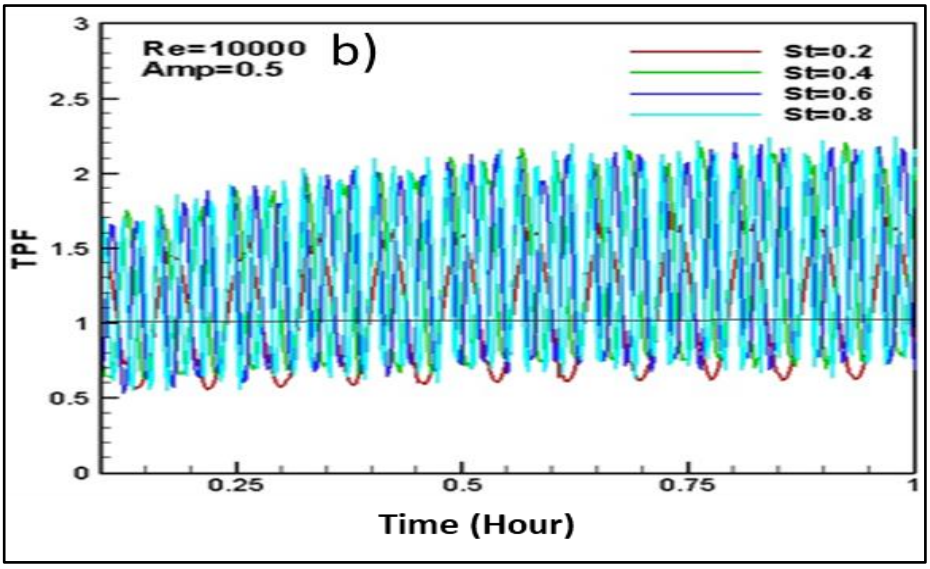

`

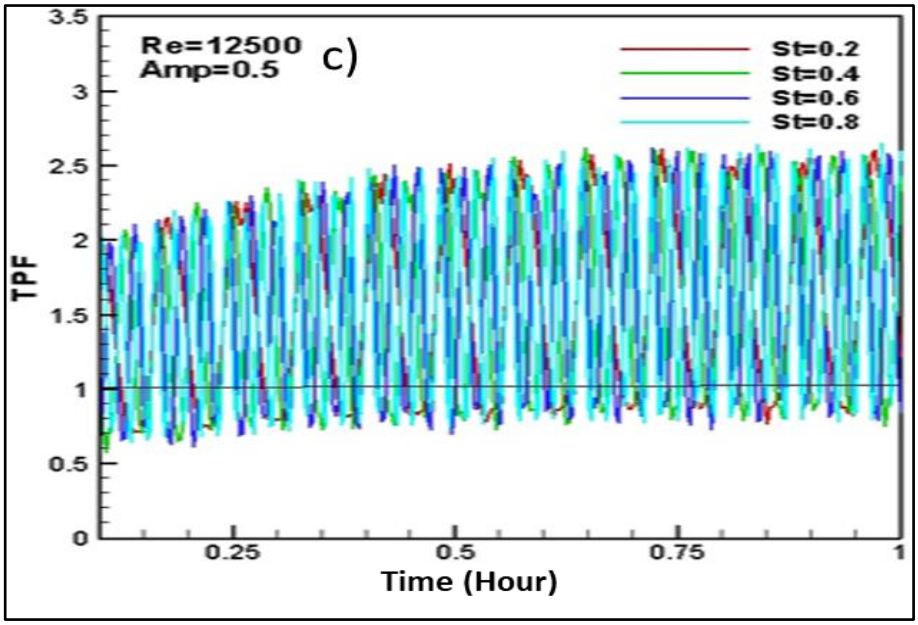

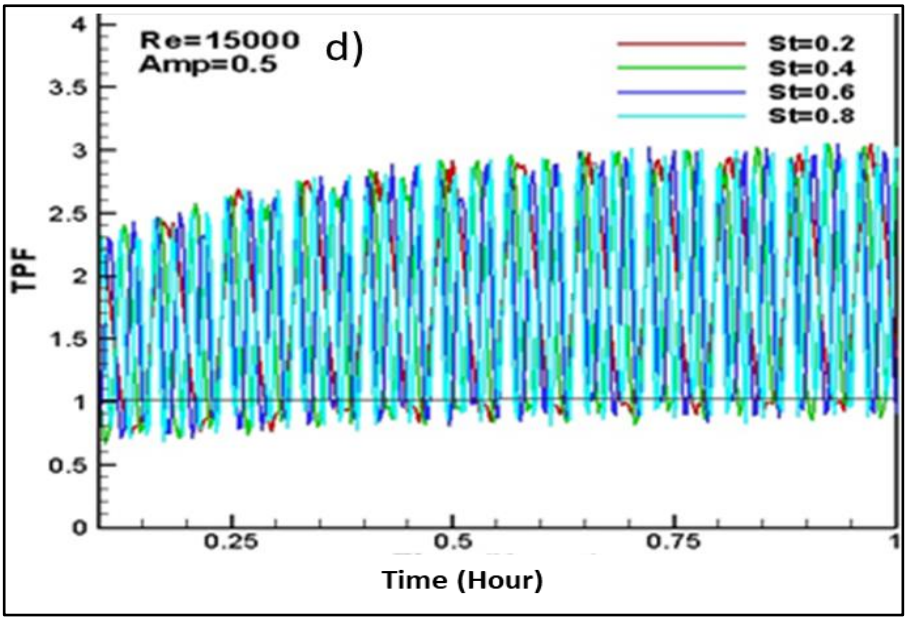

Figures 5.7. Variation TPF with time at different frequency values,when (a)Re=7500, (b)Re=10000 , (c)Re=12500 ,and (d)Re=15000.

5.3.4. Influence of Temperature Distribution by Changing Frequency Values

As expected, the absorbing temperature records the highest value along the running time, as much as possible can reach through glass and lose a little heat as possible up to the atmosphere and down through the back of solar channel, and into heat transfer retained to pass flow. The purpose of the cover is to accept as much solar radiation as possible and reduce upward heat loss to the lowest possible value, it therefore works

`

efficiently that purpose ,temperature variation of air gap area due to convection and radiation ,change has been shown not to be at a very high level at the highest frequency value ,it has also been observed that increasing the Reynolds number results in a decrease in temperature value ,in this case reducing flow rate is better at certain frequency values. As shown in Figure 5.8.

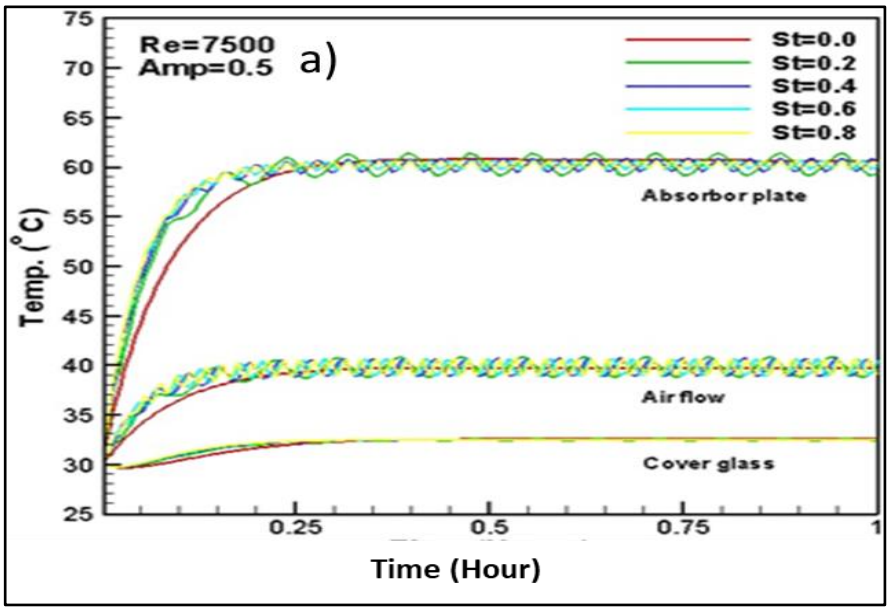

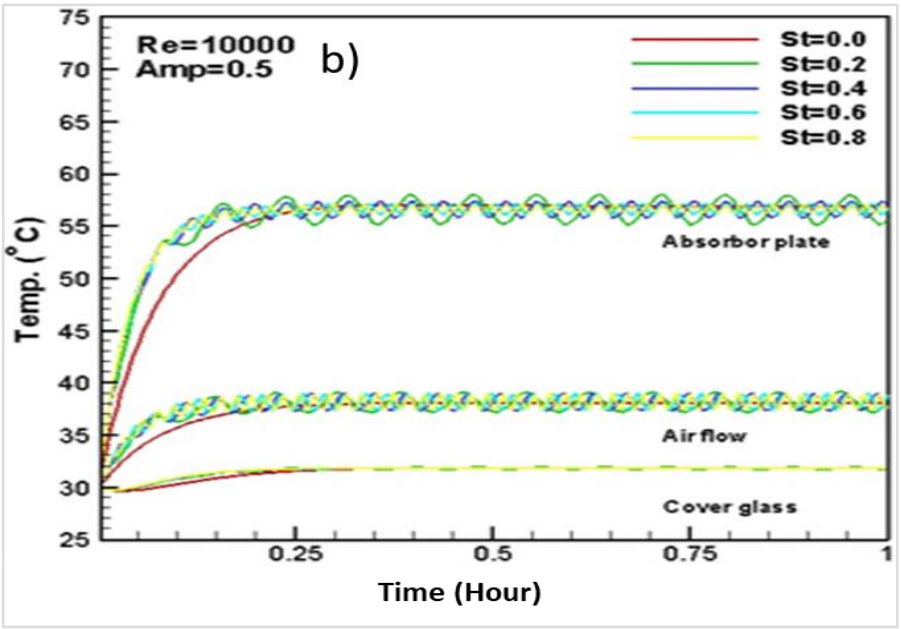

`

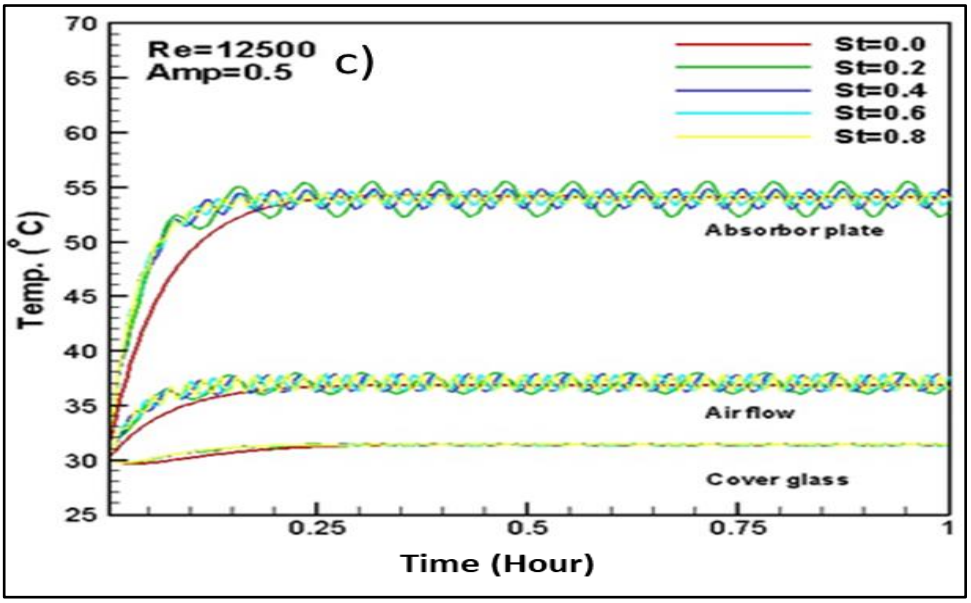

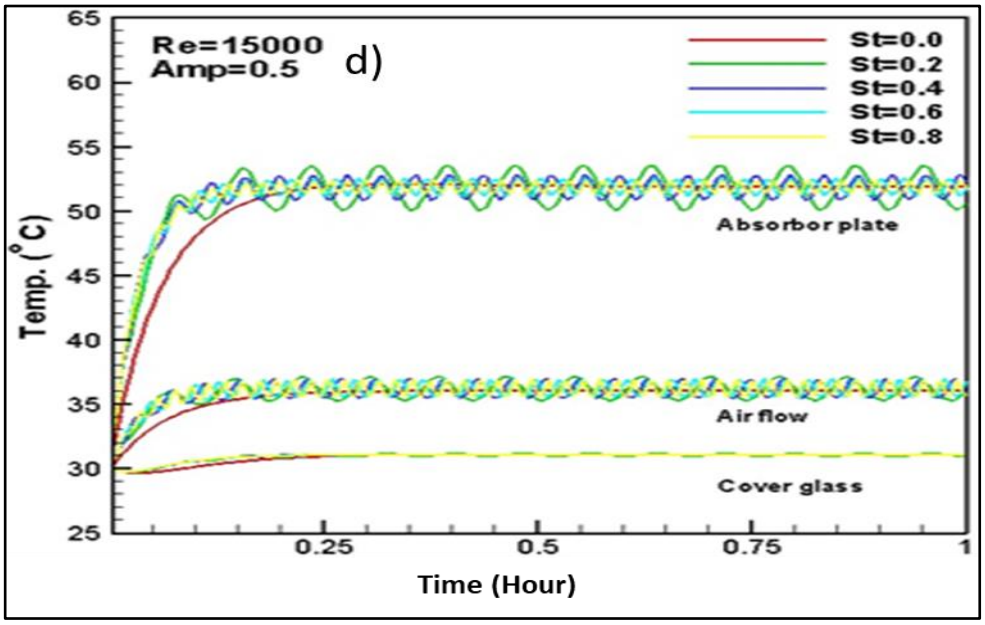

Figure 5.8. Variation in temperature distribution with different frequency values.at (a)Re=7500 , (b)Re=10000 , (c)Re=12500 ,and (d)Re=15000.

`

5.4. CFD CONTOURS AND VELOCITY VECTORS

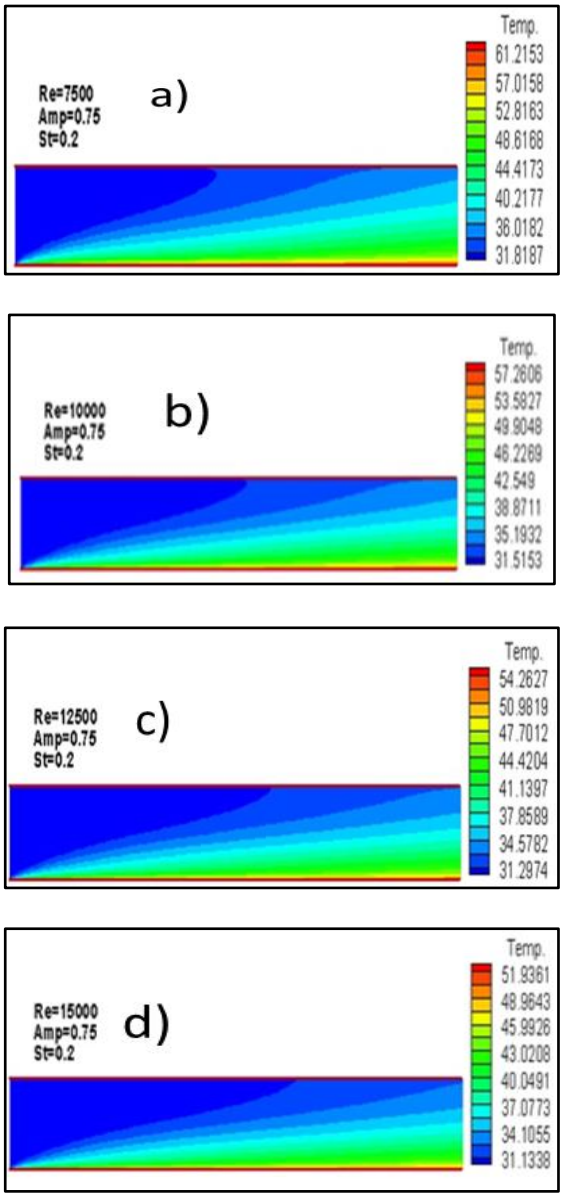

Figure 5.9. Temperature distributions with different Reynolds number.

`

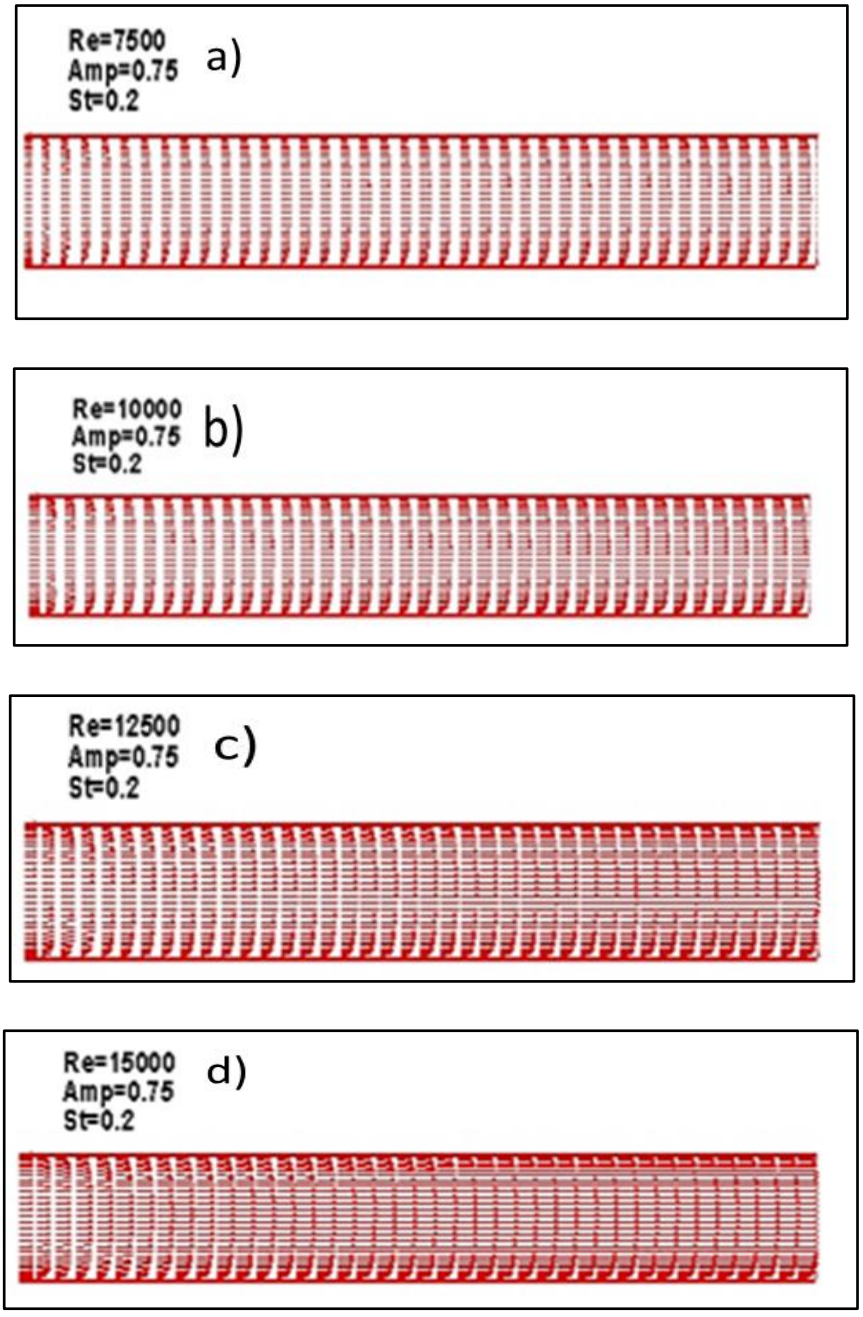

Figure 5.10. Velocity vector with different Reynolds number.

5.5. COMPARISON WITH ANOTHER STUDY

This research was compared with previous research by Elshafei [69] through the variation of the nusselt number values, where Elshafei took several; frequencies at the Reynolds value of (16800), the values of nusselt number is shown to increase at the entrance of the duct and then taken in parallel to the stable value, through Figure 5.11 there has been a marked improvement in nusselt number.

`

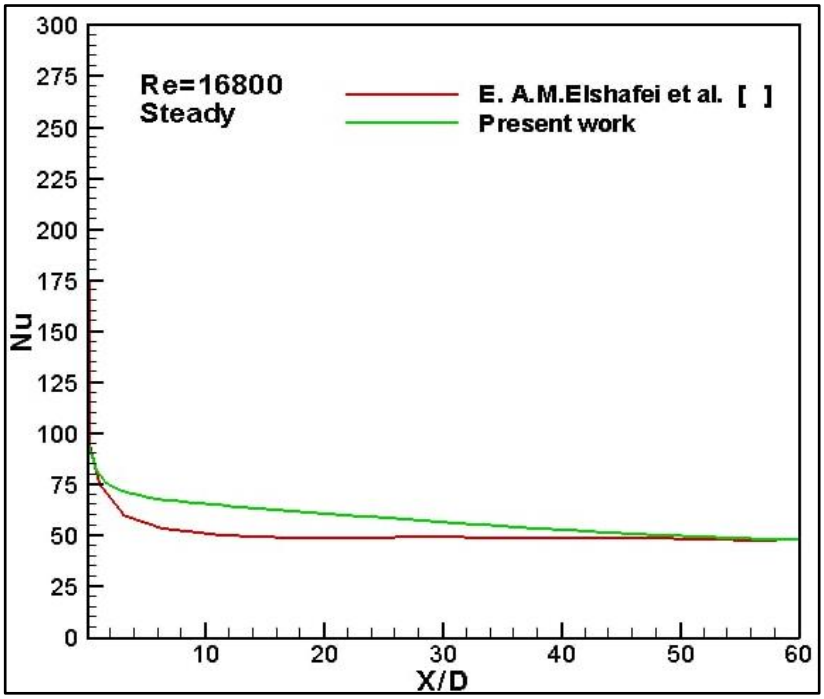

Figure 5.11. Distribution average nusselt number at different frequency with Re=16800.

`

PART 6

CONCLUSION

On the basis of the results obtained in this study, the following conclusion can be drawn:

- A detailed mathematical derivation for the flat-plate solar collector cross section (cover, air gap, absorber, and working fluid) was presented.
- All the thermo-physical properties of the air gap, the absorber plate, and the working fluid are computed in time dependent mode.
- A mathematical model was created to derive the Navier stock equation using finite-volume scheme, based on FORTRAN90 Code and CFD software.
- Increased frequency value when amplitude is proven has a positive effect on nusselt number value, as it has been observed that the area of improvement increases by increasing frequency value at constant amplitude, and since nusselt number raises when flow rate rises we get the highest value at Reynolds (15000).
- Through the results extracted, the friction factor is influenced by a change in frequency and amplitude values, from which it is concluded that when reducing the amplitude value and raising the frequency value we get the best friction factor ratio at (St=0.8).
- From this study, it was concluded that the thermal performance factor has a significant role in the characteristics of heat transfer during the solar collector, as the thermal performance becomes TPF≥ 1, the systems performance improves well, having the best ration of the TPF when increasing frequency value and stabilizing the amplitude value.
- Comparison between the present study and previous study showed a good agreement and a slight difference between the mentioned results.

`

REFERENCES

1. Smil, V., "General energetics: energy in the biosphere and civilization", ***Wiley,*** New York, 67-89 (1991).

2. Hassain, A., Arif, S. M., & Aslam, M., "Emerging renewable nergy technologies: state of the art", ***Renewable and Sustainable Review,*** 7(1): 12-28 (2017).

3. Rajaseenivasan, T., Srinivasan, S., & Srithar, K., "Comprehensive study on solar air heater with circular and V-type turbulators attached on absorber plate", ***Energy,*** 8(8): 863-873 (2015).

4. Tyagi, V. V., Panwar, N. L., Rahim, N. A., & Kothari, R., "Review on solar air heating system with and without thermal energy storage system", ***Renewable and Sustainable Energy Reviews,*** 16(4): 2289-2303 (2012).

5. Alkilani, M. M., Sopian, K., Alghoul, M. A., Sohif, M., & Ruslan, M. H., "Review of solar air collectors with thermal storage units", ***Renewable and Sustainable Energy Reviews,*** *15*(3): 1476-1490 (2011).

6. Chamoli, S., Chauhan, R., Thakur, N. S., & Saini, J. S., "A review of the performance of double pass solar air heater", ***Renewable and Sustainable Energy Reviews,*** 16(1): 481-492 (2012).

7. Hoang, T. T., Dinh, C. T., & Plourde, F., "Large eddy simulation of the turbulence heat and mass transfer of pulsating flow in a V-sharp corrugated channel", ***International Journal of Heat and Mass Transfer,*** *16(6):* 120-720 (2021).

8. Nerkar, S. G., Rudrapati, R., Biradar, N. S., & Kolhe, K. P., "Numerical Analysis of Pulsating Flow in 2D Channel", ***ISSN,*** 1(2): 19-26 (2015).

9. Nandi, T. K., Bhattacharyya, S., Das, S. G., Banerjee, A., & Chattopadhyay, H., "Thermohydraulic transport characteristics in wavy microchannel under pulsating inlet flow condition", ***Chemical Engineering Transactions,*** 6(2): 271-276 (2017).

10. Akdag, U., Akcay, S., & Demiral, D., "Heat transfer enhancement with laminar pulsating nanofluid flow in a wavy channel", ***International Communications in Heat and Mass Transfer,*** 5(9): 17-23 (2014).

`

11. Chattopadhyay, H., Durst, F., & Ray, S., "Analysis of heat transfer in simultaneously developing pulsating laminar flow in a pipe with constant wall temperature", ***International Communications in Heat and Mass Transfer,*** 33(4): 475-481 (2006).

12. Hemida, H. N., Sabry, M. N., Abdel-Rahim, A., & Mansour, H., "Theoretical analysis of heat transfer in laminar pulsating flow", ***International Journal of Heat and Mass Transfer,*** 45(8): 1767-1780 (2002).

13. He, S., & Jackson, J. D., "An experimental study of pulsating turbulent flow in a pipe", ***European Journal of Mechanics-B/Fluids,*** 28(2): 309-320 (2009).

14. Li, G., Zheng, Y., Yang, H., & Xu, Y., "Numerical investigation of heat transfer and fluid flow around the rectangular flat plane confined by a cylinder under pulsating flow", ***Journal of Applied Fluid Mechanics,*** *9*(4): 1569-1577 (2016).

15. Nandi, T. K., & Chattopadhyay, H., "Numerical investigations of simultaneously developing flow in wavy microchannels under pulsating inlet flow condition", ***International Communications in Heat and Mass Transfer,*** 4(7): 27-31 (2013).

16. Wang, X., & Zhang, N., "Numerical analysis of heat transfer in pulsating turbulent flow in a pipe", ***International Journal of Heat and Mass Transfer,*** 48(20): 3957-3970 (2005).

17. Wang, Y., He, Y. L., Yang, W. W., & Cheng, Z. D., "Numerical analysis of flow resistance and heat transfer in a channel with delta winglets under laminar pulsating flow", ***International Journal of Heat and Mass Transfer,*** 8(2): 51-65 (2015).

18. Yu, J. C., Li, Z. X., & Zhao, T. S., "An analytical study of pulsating laminar heat convection in a circular tube with constant heat flux", ***International Journal of Heat and Mass Transfer,*** 47(24): 5297-5301 (2004).

19. Zohir, A. E., Habib, M. A., Attya, A. M., & Eid, A. I., "An experimental investigation of heat transfers to pulsating pipe air flow with different amplitudes", ***Heat and Mass Transfer,*** *42*(7): 625-635 (2006).

20. Korpale, V. S., Deshmukh, S. P., Mathpati, C. S., & Dalvi, V. H., "Numerical simulations and optimization of solar air heaters", ***Applied Thermal Engineering,*** 18(20): 115744 (2020).

21. Singh, A. P., & Singh, O. P., "Curved vs. flat solar air heater: Performance evaluation under diverse environmental conditions", ***Renewable Energy,*** 14(5): 2056-2073 (2020).

22. Shetty, S. P., Madhwesh, N., & Karanth, K. V., "Numerical analysis of a solar air heater with circular perforated absorber plate", ***Solar Energy***, 21(5): 416-433 (2021).

`

23. Masoumi, A. P., Tajalli-Ardekani, E., & Golneshan, A. A., "Investigation on performance of an asphalt solar collector: CFD analysis, experimental validation and neural network modeling", ***Solar Energy***, 20(7): 703-719 (2020).

24. Rajarajeswari, K., Alok, P., & Sreekumar, A., "Simulation and experimental investigation of fluid flow in porous and non-porous solar air heaters", ***Solar Energy,*** 17(1): 258-270 (2018).

25. Qureshi, M. H., & Shakaib, M., "A CFD (Computational Fluid Dynamics) Based Thermal Performance of Solar Air Heater with Rib-Roughened Channels", ***In ASME International Mechanical Engineering Congress and Exposition,*** 50(6): 10-098 (2016).

26. Gupta, B., Kumar, A., Kushwaha, R., & Shukla, A. P., "Experimental and CFD Analysis of Solar Air Heater with Rectangular Shaped Hollow Bodies", ***In 2018 2nd International Conference on Green Energy and Applications***, Singapore, 69-73 (2018).

27. Pandey, N. K., Bajpai, V. K., Sharma, A., & Yadav, S., "CFD and thermo-hydraulic analysis of multiple arc roughened absorber plate with gaps used in solar air heaters", ***International Journal of Ambient Energy,*** *43*(1): 3275-3281 (2022).

28. Ansari, M., & Bazargan, M., "Experimental and numerical investigation on irregular spacing of the ribs in the entry length of a solar air heater channel", ***Science and Technology for the Built Environment,*** 26(9): 1231-1240 (2020).

29. Jawad, Q. A., Mahdy, A. M., Khuder, A. H., & Chaichan, M. T., "Improve the performance of a solar air heater by adding aluminum chip, paraffin wax, and nano-SiC", ***Case Studies in Thermal Engineering,*** *1(9):* 100-622 (2020).

30. Patel, Y. M., Jain, S. V., & Lakhera, V. J., "Thermo-hydraulic performance analysis of a solar air heater roughened with reverse NACA profile ribs", ***Applied Thermal Engineering,*** *17(10):* 114-940 (2020).

31. Karimi, A., Al-Rashed, A. A., Afrand, M., Mahian, O., Wongwises, S., & Shahsavar, A., "The effects of tape insert material on the flow and heat transfer in a nanofluid-based double tube heat exchanger: two-phase mixture model", ***International Journal of Mechanical Sciences,*** 15(6): 397-409 (2019).

32. Al-Damook, M., Obaid, Z. A. H., Al Qubeissi, M., Dixon-Hardy, D., Cottom, J., & Heggs, P. J., "CFD modeling and performance evaluation of multipass solar air heaters", ***Numerical Heat Transfer, Part A: Applications,*** 76(6): 438-464 (2019).

33. Gawande, V. B., Dhoble, A. S., Zodpe, D. B., & Chamoli, S., "Experimental and CFD investigation of convection heat transfer in solar air heater with reverse L-shaped ribs", ***Solar Energy,*** 13(11): 275-295 (2016).

`

34. Doukhi, A., Heggs, P., & Aldamook, M., "MSc. advanced chemical engineering", ***Research Gate,*** 4(6): 345-674 (2019).

35. Gu, M., Xu, X., Liu, X., Qiu, L., & Zhang, R., "Preparation and characterization of GdTaO4: Eu3+ sol-gel luminescence thin films", ***Journal of Sol-Gel Science and Technology,*** 35(3): 193-196 (2005).

36. Singh, A. P., Kumar, A., & Singh, O. P., "Designs for high flow natural convection solar air heaters", ***Solar Energy,*** 19(3): 724-737 (2019).

37. Jia, B., Liu, F., Li, X., Qu, A., & Cai, Q., "Influence on thermal performance of spiral solar air heater with longitudinal baffles", ***Solar Energy,*** *22(5):* 969-977 (2021).

38. Jain, S. K., Agrawal, G. D., Misra, R., Verma, P., Rathore, S., & Jamuwa, D. K., "Performance investigation of a triangular solar air heater duct having broken inclined roughness using computational fluid dynamics", ***Journal of Solar Energy Engineering,*** 141(6): 61-88 (2019).

39. Shetty, S. P., Madhwesh, N., & Karanth, K. V., "Numerical analysis of a solar air heater with circular perforated absorber plate", ***Solar Energy,*** 21(5): 416-433 (2021).

40. Kumar, R., Kumar, A., & Goel, V., "Simulation of flow and heat transfer in triangular cross-sectional solar-assisted air heater", ***Journal of Solar Energy Engineering,*** 141(1): (2019).

41. Mayank, S. E, & Meen, P. M., "CFD Analysis on Solar Air Heater to Enhance the Heat Transfer - A Review". ***International Journal of Science Management & Engineering Research (IJSMER),*** 56(6): 2455-6203 (2021).

42. Pashchenko, D. I., "CFD modeling of operating processes of a solar air heater in ANSYS Fluent", ***Journal of Engineering Physics and Thermophysics***, *92*(1): 73-79 (2019).

43. Mathur, A., & Agrawal, G. D., "Thermal performance investigation and optimisation of fin type solar air heater-a CFD approach", ***Progress in Computational Fluid Dynamics, an International Journal,*** *16*(1): 58-65 (2016).

44. Josyula, T., Singh, S., & Dhiman, P., "Numerical investigation of a solar air heater comprising longitudinally finned absorber plate and thermal energy storage system", ***Journal of Renewable and Sustainable Energy,*** *10*(5): 55-91 (2018).

45. Jacob, S., Yadav, S. S., & Sikarwar, B. S., "Design and simulation of isolation room for a hospital", ***Springer,*** Singapore, 75-93 (2019).

46. Kumar, R., & Kumar, A., "A parametric study of the 2D model of solar air heater with elliptical rib roughness using CFD", ***Journal of Mechanical Science and Technology,*** *31*(2): 959-964 (2017).

`

47. Vivekanandan, M., Jagadeesh, D., Natarajan, A., Mohan, N., & Dineshkumar, M., "Experimental and CFD investigation of fully developed flow solar air heater", ***Materials Today: Proceedings,*** 3(7): 2158-2163 (2021).

48. Sivakumar, S., Siva, K., & Mohanraj, M., "Experimental thermodynamic analysis of a forced convection solar air heater using absorber plate with pin-fins", ***Journal of Thermal Analysis and Calorimetry,*** 136(1): 39-47 (2019).

49. Zheng, W., Zhang, H., You, S., & Fu, Y., "Experimental investigation of the transpired solar air collectors and metal corrugated packing solar air collectors", ***Energies,*** 10(3): 302 (2017).

50. Kumar, A., & Layek, A., "Computational heat transfer analysis of a solar air heater having square rib roughness on the absorber plate", ***Energies,*** 34(34): 132-234 (2018).

51. Maithani, R., & Saini, J. S., "Performance evaluation of solar air heater having V-ribs with symmetrical gaps in a rectangular duct of solar air heater", ***International Journal of Ambient Energy***, 38(4): 400-410 (2017).

52. Hu, J., & Zhang, G., "Performance improvement of solar air collector based on airflow reorganization: A review", ***Applied Thermal Engineering,*** 15(5): 592-611 (2019).

53. Raj, A. K., Srinivas, M., & Jayaraj, S., "A cost-effective method to improve the performance of solar air heaters using discrete macro-encapsulated PCM capsules for drying applications", ***Applied Thermal Engineering,*** 14(6): 910-920 (2019).

54. Jia, B., Liu, F., & Wang, D., "Experimental study on the performance of spiral solar air heater", ***Solar Energy,*** 18(2): 16-21 (2019).

55. Kottayat, N. Kumar, S., Yadav, A. K. & Anish, S." Computational and experimental studies on the development of an energy-efficient drier using ribbed triangular duct solar air heater", ***Elsevier,*** Germany, 120-134 (2013).

56. Ong, K. S., "Thermal performance of solar air heaters: mathematical model and solution procedure", ***Solar Energy,*** 55(2): 93-109 (1995).

57. Shankar, G. B., & Kishore, P. S., "Performance analysis of a conventional air heater", ***International Journal of Research-Granthaalayah***, *5*(4):678-788 (2017).

58. Holman, J. P. "Heat Transfer (McGraw-Hill Series in Mechanical Engineering)," ***The McGraw-Hill Companies,*** USA, 56-88 2010.

59. Launder, B. E., & Spalding, D. B., "The numerical computation of turbulent flows", ***In Numerical prediction of flow, heat transfer, turbulence and combustion***, 6(7): 96-116 (1983).

`

60. Jones, W. P., & Launder, B. E., "The prediction of laminarization with a two-equation model of turbulence", ***International Journal of Heat and Mass Transfer,*** 15(2): 301-314 (1972).

61. Duffie, J. A., & Beckman, W. A., "Solar engineering of thermal processes", ***John Wiley & Sons,*** Texas, 78-99 (2013).

62. Versteeg, H. K., & Malalasekera, W., "An introduction to computational fluid dynamics: the finite volume method", ***Pearson Education,*** USA, 56-77 (2007).

63. Lomax, H., Pulliam, T. H., & Zingg, D. W., "Fundamentals of computational fluid dynamics", ***Springer Science & Business Media,*** Germany, 45-66 (2013).

64. Darwish, M., & Moukalled, F., "The finite volume method in computational fluid dynamics: an advanced introduction with OpenFOAM and Matlab", ***Springer,*** Germany 56-78 (2021).

65. Schäfer, M., "Computational engineering: Introduction to numerical methods", **Springer,** Berlin, 34-45 (2006).

66. Adeloye, M. Y., Kotoye, A. A., Idris, O. Y., & Egbedele, I. A., "Construction of a temperature controlled fan using a microprocessor", ***American Journal of Engineering Research (AJER),*** 6(9): 324-328 (2017).

67. Patankar, S., "Numerical Heat Transfer and Fluid Flow", ***CRC Press,*** Germany, 23-56 (1980).

68. Onbasioglu, S. U., & Onbaşıoğlu, H., "On enhancement of heat transfer with ribs", ***Applied Thermal Engineering,*** 24(1): 43-57 (2004).

69. E. A. M. Elshafei, M. Safwat Mohamed., & M. Sakr., "NUMERICAL STUDY OF HEAT TRANSFER IN PULSATING TURBULENT AIR FLOW", Thermal Issues in Emerging Technologies, ThETA 1, Cairo, Egypt, Jan 3-6th 2007.

`

RESUME

Alaa Raad Radie NEDAWI was born in Baghdad and he graduated primary, elementary, and high school in this city, after that, he started the higher diploma at University of Technology-Baghdad College of Engineering, Department of mechanical Engineering in 2015. Then in 2020, he started at Karabuk University Mechanical Engineering to complete his M. Sc. education.